

DOKUZ EYLÜL UNIVERSITY
GRADUATE SCHOOL OF NATURAL AND APPLIED SCIENCES

MONTE CARLO STUDY OF
COMPENSATION AND CRITICAL TEMPERATURES
IN FERRIMAGNETIC MIXED ISING SYSTEMS

by

Ebru KIŞ ÇAM

June, 2012

İZMİR

**MONTE CARLO STUDY OF
COMPENSATION AND CRITICAL TEMPERATURES
IN FERRIMAGNETIC MIXED ISING SYSTEMS**

**A Thesis Submitted to the
Graduate School of Natural and Applied Sciences of Dokuz Eylül University
In Partial Fulfillment of the Requirements for the Degree
of Doctor of Philosophy in
Physics**

by

Ebru KIŞ ÇAM

June, 2012

İZMİR


Ph.D. THESIS EXAMINATION RESULT FORM

We have read the thesis entitled “MONTE CARLO STUDY OF COMPENSATION AND CRITICAL TEMPERATURES IN FERRIMAGNETIC MIXED ISING SYSTEMS” completed by **EBRU KIŞ ÇAM** under supervision of **PROF. DR. HAMZA POLAT** and **ASSOC. PROF. DR. EKREM AYDINER** (Co-Supervisor) and we certify that in our opinion it is fully adequate, in scope and in quality, as a thesis for the degree of Doctor of Philosophy.



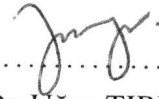
Prof. Dr. Hamza POLAT

Supervisor



Assoc. Prof. Dr. Ekrem AYDINER

Co-Supervisor



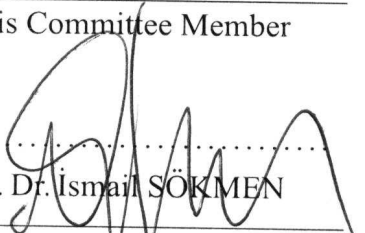
Prof. Dr. Uğur TIRNAKLI

Thesis Committee Member



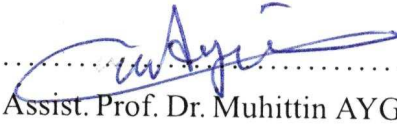
Assoc. Prof. Dr. Gökhan BİLHAN

Thesis Committee Member



Prof. Dr. İsmail SÖKMEN

Examining Committee Member



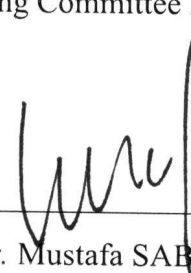
Assist. Prof. Dr. Muhittin AYGÜN

Examining Committee Member



Prof. Dr. Halil YARANERİ

Examining Committee Member



Prof. Dr. Mustafa SABUNCU
Director Graduate School of Natural and Applied Sciences

ACKNOWLEDGEMENTS

I would like to express my gratitude to my advisor Prof. Dr. Hamza POLAT, support and guidance through the duration of this work.

I would next like to thank my co-advisor, Assoc. Prof. Ekrem AYDINER, for his guidance and discussions he has had with me throughout my Ph.D study and, for his patience, motivation, understanding, advise and knowledge.

My friends and colleagues including Dr. Meltem GÖNÜLOL, Dr. Nazli BOZ YURDAŞAN, Dr. Sinem ERDEN GÜLEBAĞLAN and Dr. Aylin YILDIZ have helped me in various ways. I thank them all very much.

I am very grateful to my mother Gülşen KIŞ and sister Ayşe ÖZTÜRK, for their understanding, supporting and encouragement.

Finally, I wish to specially to thank my loving husband Uğur ÇAM who has been with me at all times. I always feel your encouragement, love and kindness. Next I would like to thank my kids, Zeynep and Yusuf for giving me unlimited happiness.

Ebru KIŞ ÇAM

MONTE CARLO STUDY OF COMPENSATION AND CRITICAL TEMPERATURES IN FERRIMAGNETIC MIXED ISING SYSTEMS

ABSTRACT

In this thesis, three different mixed Ising model is studied by using Monte Carlo simulation method. Since real ferrimagnets have fairly complicated structures, mixed Ising spin models have been used as simple systems that can characterize ferrimagnetic behavior. Magnetic materials have been a very important part of our lives due to numerous technological applications such as memory devices. Especially, ferrimagnetism plays a key role in the physics behind magneto-optical recording. Therefore, in this thesis, three different mixed Ising model have been examined.

In the first study, dependence on site dilution of critical and compensation temperatures of a two dimensional mixed spin-1/2 and spin-1 system has been investigated. The dependence of the thermal and magnetic behaviors on dilution of mixed spin system have been discussed. The results of this study show that dilution plays a significant role on the critical and compensation points of a two dimensional mixed spin-1/2 and spin-1 system. It has been shown that the critical and compensation temperatures of diluted mixed spin system linearly decrease with increasing number of diluted sites. Results of this study indicate that the compensation temperature of the real ferrimagnetic spin systems can be changed by diluting the lattice with non-magnetic atoms, in order to obtain desired compensation temperature.

In the second study, the compensation temperature of the mixed ferro-ferrimagnetic ternary alloy composed of three different Ising spins (spin-3/2, spin-1 and spin-5/2) in the presence of next nearest neighbor interaction between A ions is studied in cubic lattice whose spin values corresponding to the Prussian blue analog of the type in ref. (Okhoshi et al., 1997a) alloy with Ni. By changing concentration p and interaction parameter R , we obtain interesting properties of ferro-ferrimagnetic ternary compound. Results of in this work show that the system has multi-compensation behavior with suitable R , p parameters and next nearest neighbor interaction between A ions value.

In the third study, it has been investigated the effects of single-ion anisotropy on magnetic properties of three dimensional mixed ferro-ferrimagnetic model consist-

ing of three different Ising spins (spin-3/2, spin-2 and spin-5/2) which corresponds to Prussian blue analog in ref. (Okhoshi et al., 1997a) alloy with Fe. It has been found that the critical temperature of this system linearly changes dependent upon the interaction ratio R for any mixing ratio p value, and critical interaction ratio value decreases for increasing D values. In addition, we have demonstrated that the magnetic pole inversion can appear and compensation temperature decreases for increasing external magnetic field dependent upon some values of the Hamiltonian parameters. As a result, we state that single-ion anisotropy can be used as a control parameter like mixing rate p to arrange the critical and compensation temperature of the Prussian blue analog in ref. (Okhoshi et al., 1997a) alloy with Fe.

Keywords: Monte Carlo simulation method, Mixed Ising spin systems, Compensation temperature, Ferro-ferrimagnetic ternary alloys.

FERRİMANİYETİK KARMA ISING SİSTEMLERİNDE KARŞILAMA VE KRİTİK SICAKLIKLARIN MONTE CARLO İNCELEMESİ

ÖZ

Bu tez kapsamında, üç farklı karma spin Ising modeli Monte Carlo simülasyon yöntemi kullanılarak çalışılmıştır. Gerçek ferrimanyetler oldukça kompleks bir yapıya sahip oldukları için karma spin Ising modelleri ferrimanyetik davranışı karakterize edebilen basit bir model olarak kullanılmaktadır. Kayıt cihazları gibi önemli teknolojik uygulamalarından dolayı manyetik malzemeler hayatımızın önemli bir parçasıdır. Özellikle ferrimanyetizma, manyeto-optik kayıtçıların ardındaki fizikte bir anahtar rol oynamaktadır. Bundan dolayı, bu tez kapsamında üç farklı ferrimanyetik karma Ising model çalışılmıştır.

İlk çalışmada, iki boyutlu bir karma spin-1/2 ve spin-1 sisteminin karşılama ve kritik sıcaklıklarının konum seyreltmeye bağlılığı çalışılmıştır. Termal ve manyetik davranışların karma spin sisteminin seyreltilmesine bağlılığı tartışılmıştır. Bu çalışmanın sonuçları seyreltmenin iki boyutlu karma spin-1/2 ve spin-1 sisteminin karşılama ve kritik sıcaklıkları üzerinde önemli bir rol oynadığını göstermektedir. Seyreltilmiş karma spin sisteminin karşılama ve kritik sıcaklıklarının konum seyreltme sayısının artışı ile doğrusal olarak azaldığı gösterilmiştir. Bu çalışmanın sonuçları, istenilen karşılama sıcaklığının elde edilmesi için örgüyü manyetik olmayan atomlar ile seyrelterek gerçek ferrimanyetik spin sistemlerinin karşılama sıcaklığının değiştirilebileceğini göstermektedir.

İkinci çalışmada, üç farklı Ising spininden (spin-3/2, spin-1 ve spin-5/2) oluşan karma ferro-ferrimanyetik ternary alaşımının karşılama sıcaklığı A iyonları arasında ikinci en yakın komşu etkileşmesinin varlığında çalışılmıştır. Buradaki örgü kübik örgüdür ve spin değerleri (Okhoshi et al., 1997a) referansındaki Ni' li Prussian blue analog tipi bileşiğe uygun olarak seçilmiştir. Burada R etkileşim oranı parametresi ve p konsantrasyonu değiştirilerek ilginç özellikler elde edilmiştir. Bu çalışmanın sonucu uygun R , p parametreleri ve A iyonları arasındaki en yakın ikinci komşu etkileşim oranı değeriyle sistemin çoklu-karşılama davranışına sahip olduğunu göstermiştir.

Üçüncü çalışmada, tek-iyon anizotropisinin üç farklı Ising spininden (spin-3/2, spin-2 ve spin-5/2) oluşan (Okhoshi et al., 1997a) referansındaki Fe'li Prussian blue

analog tipi bileşimin manyetik özellikleri üzerine etkisi incelenmiştir. Sistemin kritik sıcaklığının etkileşme oranı R ve karışım oranı p değerine bağlılığının doğrusal olarak değiştiği bulunmuştur. Ayrıca, kritik etkileşme oranı R nin D değerinin artışıyla azaldığı görülmüştür. Başka bir deyişle, modelin kritik ve karşılama sıcaklıklarının D değerinin artışıyla yavaşça arttığı gösterilmiştir. Ek olarak, manyetik kutup terslenmesinin görülebileceği ve karşılama sıcaklığının artan dış manyetik alan değerinin artışıyla azaldığı gösterilmiştir. Sonuç olarak, (Okhoshi et al., 1997a) referansındaki Fe'li Prussian blue analog tipi bileşimin kritik ve karşılama sıcaklıklarını düzenlemek için, tek-iyon anizotropisinin de karışım oranı p gibi bir kontrol parametresi olarak kullanılabilceği gösterildi.

Anahtar sözcükler: Monte Carlo simülasyon yöntemi, Karma Ising spin sistemleri, Karşılama sıcaklığı, Ferro-ferrimagnetic ternary alaşımlar.

CONTENTS

	Page
Ph.D. THESIS EXAMINATION RESULT FORM	ii
ACKNOWLEDGEMENTS	iii
ABSTRACT	iv
ÖZ	vi
CHAPTER ONE - INTRODUCTION	1
CHAPTER TWO - MOLECULE-BASED MAGNETS	3
2.1 Introduction to Magnetism.....	3
2.2 Ferrimagnetism and Compensation Temperature	5
2.3 Magneto-Optical Recording	7
2.4 Exchange Interactions.....	10
2.4.1 Direct Exchange Between Spins.....	10
2.4.2 Hund Rules	11
2.4.3 Anisotropic Exchange (Magnetocrystalline) Interaction	12
2.4.3.1 Crystal Field	13
2.4.3.2 Single-Ion Anisotropy	16
2.5 Molecule-Based Magnets	20
2.5.1 Prussian Blue Analogues	21
CHAPTER THREE - MODEL AND SIMULATION METHOD	24
3.1 Ising Model	24
3.1.1 Historical Background	24
3.1.2 Theoretical Background	26
3.1.3 Statistical Mechanics of Ising Model.....	30
3.2 Monte Carlo Simulation Method	33
3.2.1 History of Monte Carlo Method	33
3.2.2 Random Sequences.....	36
3.2.3 Pseudo-Random Numbers	37
3.2.4 Importance Sampling	38

3.2.5 Markov Chain	40
3.2.6 Metropolis Algorithm	42
CHAPTER FOUR-DEPENDENCE ON DILUTION OF CRITICAL AND COMPENSATION TEMPERATURES OF A TWO DIMENSIONAL MIXED SPIN-1/2 AND SPIN-1 SYSTEM	47
4.1 Introduction.....	47
4.2 Model and Simulation Technique	49
4.3 Results and Discussion.....	51
CHAPTER FIVE-COMPENSATION TEMPERATURE OF 3D MIXED FERRO-FERRIMAGNETIC TERNARY ALLOY	59
5.1 Introduction.....	59
5.2 Model and Its Monte Carlo Simulation	62
5.3 Results and Discussion.....	64
CHAPTER SIX-THE EFFECTS OF SINGLE-ION ANISOTROPY ON MAGNETIC PROPERTIES OF THE PRUSSIAN BLUE ANALOG	72
6.1 Introduction.....	72
6.2 Model and Simulation Method	73
6.3 Monte Carlo Simulation Results	75
CHAPTER EIGHT - CONCLUSION	85
REFERENCES	87

CHAPTER ONE

INTRODUCTION

During the past several decades there has been intensive interest in the experimental and theoretical research of the ferrimagnetic compounds because of their potential device applications in technologically important materials such as high-density magneto-optical recording (Tanaka et al., 1987; Alex et al., 1990). Ferrimagnetic materials have a special temperature point at which the resultant magnetization vanishes below the transition temperature T_c (Néel, 1948), because of the different dependence of the sublattice magnetization on temperature. Because its sublattice magnetizations cancel exactly each other, this point is called compensation point. The occurrence of a compensation point is of highly technological importance, because to change the sign of resultant magnetization require only a small driving field at this point. It has been shown that the coercive field is very strong at the compensation point favoring the creation of small, stable, magnetic domains (Hansen, 1987; Hernando & Kulik, 1994; Multigner et al., 1996). In magneto-optical recording devices the coercivity is changed by local heating of the media with a focused beam. Temperature dependence of the coercivity near the compensation point can be applied to writing and erasing in high-density magneto-optical recording media.

Numerous materials-science laboratories worldwide aim toward the discovery and development of new, improved magnetic materials. One approach being investigated for new magnets is based on molecules as building blocks. Molecule-based magnets present several attributes unavailable in conventional metal/intermetallics and metal-oxide magnets. The past decade has witnessed the discovery of several families of molecule-based magnets (Miller J. S. & Epstein A.J., 2000). Molecule-based magnetic materials have been widely studied, because the design of their properties is easier compared to that of classical magnetic materials such as metal alloys and metal oxides (Kahn, O. 1993). In particular, Prussian blue analogues show various characteristic magnetic properties depending on their transition metal ions (Ferlay, S., et al., 1995; Ohkoshi, S., 1997). These compounds are attractive for the molecular design of magnetic properties because various types metal ions can be incorporated there as a spin center. Thus the magnetic properties can be precisely controlled during the

synthesis process by changing the ratio of incorporated metal ions (spins). Also analytic descriptions of molecular magnetic materials properties have been studied in the mean field approximation, the effective field theory and Monte Carlo simulation method. In general, Monte Carlo simulation method is performed to describe the behavior of these magnetic materials at the critical temperature using mixed Ising spin model. Since real ferrimagnets have fairly complicated structures, mixed Ising spin models have been used as simple systems that can characterize ferrimagnetic behavior.

Therefore in this thesis, different mixed spin systems are examined by using Monte Carlo simulation method. An introduction that consist of literature survey and motivation of this thesis is given in chapter one. Background section which cover the required concepts and techniques are explained in chapter two, three. In chapter four, dependence on site dilution of critical and compensation temperatures of two-dimensional mixed spin system has been investigated and the dependence of the thermal and magnetic behaviors on dilution of mixed spin system has been discussed. In chapter five, we have investigated the dependence of the critical and compensation temperatures of the three dimensional mixed ferro-ferrimagnetic ternary alloy model on concentration and interaction parameters. In chapter six, magnetic properties of another mixed ferro-ferrimagnetic ternary alloy model have been studied in the presence of a single ion anisotropy on a cubic lattice. In the last chapter, it was explained that the results of studies in this thesis.

CHAPTER TWO

MOLECULE-BASED MAGNETS

2.1 Introduction to Magnetism

Magnetism is the response of a material to an applied magnetic field and originates from the movement of charge (i.e., electron spins). The essential component of any magnetic material is the presence of an unpaired electron or more precisely, the spin associated with an unpaired electron. Typically, unpaired electron spins are located in *d* orbital of metals; however unpaired spins in *s* and *p* orbitals for organics (Kahn O., 1987; Miller J. S. et. al., 1988) and *f* orbital for rare earth elements (Kahn, M. L. et. al., 2000) have also been shown to contribute to the magnetism of a material.

Apart from which orbital the electron spins reside there are a variety of ways that they can interact each other. In Figure 2.1 possible spin configurations of various types of magnetic ordering are illustrated at two different time. Electrons occupy atomic or molecular orbitals; and each orbital can contain a maximum of two electrons (one spin up \uparrow and one spin down \downarrow) as described by the Pauli's exclusion principle. If the orbital is filled, it will exhibit diamagnetism, which repels the magnetic field. This applies to most of the things around us such as plastic, wool and water. However, if the orbital contains a single unpaired electron, it will exhibit paramagnetism, which will attract an applied magnetic field. An ideal paramagnetic material has random spins that are uncorrelated. When spins are correlated, magnetic interaction (or coupling) takes place.

Magnetic interactions are common for isolated spins, particularly at low temperature as the thermal energy, kT , is small. When the correlation is strong enough to overcome kT , long range ordering can occur and form a magnet. Conventional magnets, such as iron, have their spins aligned with the earth's magnetic field when they are formed. These spins become "locked" upon cooling and the material becomes a magnet. When all the spins are aligned and locked, they become magnetically ordered (a phenomenon that occurs below the critical temperature, T_c) (Shum, W. W., 2008).

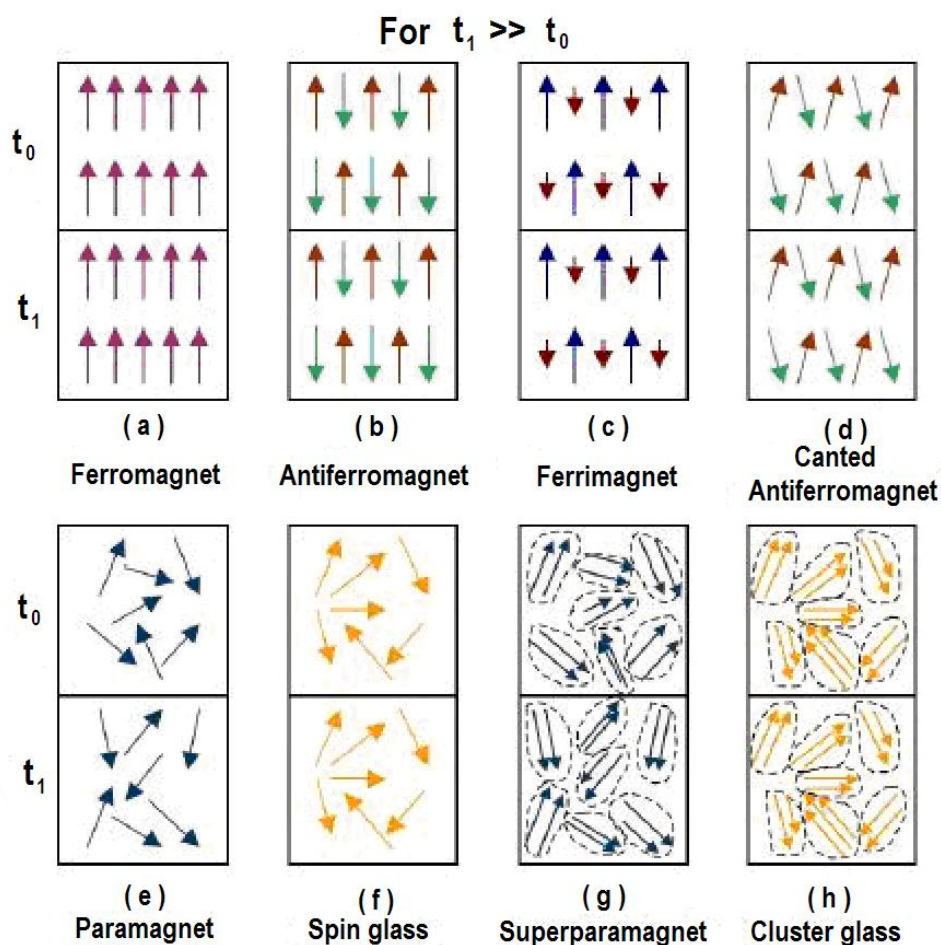


Figure 2.1 Illustration of spin configuration of various magnetic orders at two different instants: t_0 and t_1 (Etzkorn, S. J., 2003).

In situations where strong long-range coupling between electron spin sites occurs there are two main ways the spins will align and be considered magnets. Ferromagnets are formed when the adjacent electron spins within a material align parallel to one another in regions known as domains. In the absence of an applied magnetic field aligned spins within different domains of a ferromagnet may or may not be aligned with one another; however, in an applied field (often small) these domains will align themselves. Antiferromagnets, are formed when the adjacent electron spins within a material align antiparallel to one another and is attributed to a greater degree of orbital overlap where the unpaired electron spins are located. This is a consequence of an effect related to the Pauli Exclusion Principle. As a result of antiparallel arrangement throughout the spin domains the material will have a resulting net magnetic moment of zero.

Finally, when the electron spins in a material with different magnitudes are strongly coupled antiferromagnetically throughout the bulk material then the system is termed a ferrimagnet (for more detail see section 2.2). Because the spins are of unequal magnitude they do not completely compensate one another resulting in a finite net moment observed for the bulk material. Therefore, a ferrimagnet is a special case of an antiferromagnet; however, the material displays behavior much like that of a ferromagnet (Nelson, K. J., 2007).

In addition to ferri- and ferromagnetic behavior, other magnetic-ordering phenomena, such as metamagnetism, canted antiferromagnetism, and spin-glass behavior, may occur. The transformation from an antiferromagnetic state to a high moment state (i.e., the spin alignment depicted in Figure 2.1b being transformed into that depicted in Figure 2.1a by an applied magnetic field) is called metamagnetism. A canted antiferromagnet (or weak ferromagnet) results from the relative canting of antiferromagnetically coupled spins that leads to a net moment (Figure 2.1d). A spin glass occurs when local spatial correlations with neighboring spins exist, but long-range order does not. The spin alignment for a spin glass is that of a paramagnet (Figure 2.1e); however, unlike paramagnets, for which the spin directions vary with time, the spin orientations of a spin glass remain fixed or vary only very slowly with time. Examples of molecule-based magnets exhibiting each of these behaviors have been reported (Miller J. S. & Epstein A.J., 2000).

2.2 Ferrimagnetism and Compensation Temperature

Ferrimagnets consist of several sublattices with inequivalent moments interacting antiferromagnetically. Under certain conditions, the sublattice magnetizations compensate each other, then the resultant magnetization vanishes at a *compensation temperature* T_{comp} below the critical temperature T_c . The occurrence of a compensation point is of great technological importance, since at this point only a small driving field is required to change the sign of the resultant magnetization. This property is very useful in thermomagnetic recording (Dakhama, A. & Benayad, N., 2000).

Ferrimagnetic compounds have long been used for technological applications such as high-density magneto-optical recording, but little is known about the mechanisms responsible for this behavior. In a ferrimagnet the different temperature dependencies of the sublattice magnetizations raise the possibility of the appearance of compensation temperatures: temperatures below the critical point, where the total magnetization is zero. It has been shown experimentally that the coercive field is very strong at the compensation point favoring the creation of small, stable, magnetic domains. This temperature dependence of the coercivity near the compensation point can be applied to writing and erasing in high-density magneto-optical recording media, where the temperature changes are achieved by local heating the films by a focused laser beam.

Ferrimagnetism plays a key role in the physics behind Magneto-Optical recording and read out. The materials used for the Magneto-Optic effect are amorphous alloys of rare earth (RE) and transition metal (TM) elements. Most of these alloys are ferrimagnetic, which means the magnetization of the transition metal sublattice is antiparallel to that of the rare earth sublattice. The net magnetization for the material is thus the vector sum of the individual magnetizations of the sublattices.

For some typical materials used for Magneto-Optical recording the general shape of the curves for the magnetization of the sublattices (M_{TM} and M_{RE}) and the net-magnetization M_s as a function of temperature are depicted in figure 2.2. The coupling between the sublattices is responsible for the fact that the Curie-temperature for both is the same. At low temperatures, the magnetic moment of the RE component is bigger than that of the TM component. When the temperature increases, the magnetic moment of the RE component decreases faster than that of the TM component, which causes the net magnetic moment to decrease. At a certain temperature T_{comp} , the compensation temperature, the magnetic moments of the TM and RE component are identical but opposite, yielding a zero net magnetic moment. So, after this point there is an increase in the net magnetic moment until the magnetic moments of the sublattices start converging. In the end at the Curie temperature both magnetic moments vanish, so also the net magnetic moment. Beyond that temperature, the material is in a paramagnetic state (Bilderbeek, M., 2001).

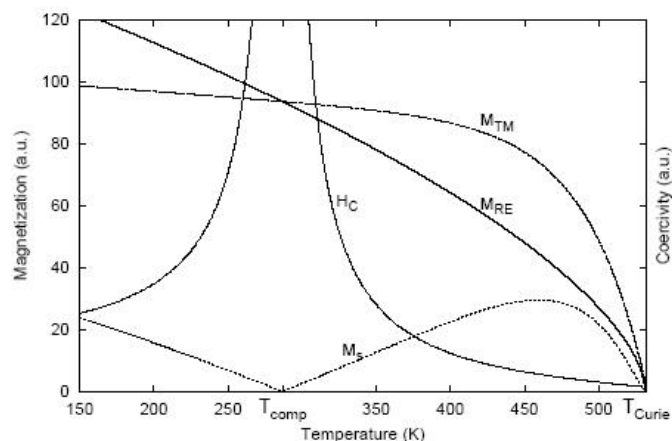


Figure 2.2 General behavior of the absolute magnetization and the coercivity (H_c) of the RE sublattice (M_{RE}) and the TM sublattice (M_{TM}) with temperature. The net magnetization of both sublattices is opposite and decreases in a different way with temperature. This means at a certain point (T_{comp}) they cancel and in the end they both vanish at the Curie temperature. The coercivity shows a great peak around (T_{comp}), where it is infinite (Bilderbeek, M., 2001).

2.3 Magneto-Optical Recording

Data recording has a long history. The biggest part of it is recording just by ink on paper or a similar recording medium. However, as we move in history to the present day, the methods of recording appear to have advanced in an exponential way. Think of the first analog recordings with the gramophone: vibrations were recorded on a roll by a scratching needle. The first magnetic recording emerged in the 1940s. This was still audio-only. The resulting tape recording techniques still prevail today, although they are getting less and less popular since there are much better alternatives nowadays. Later the technology of tape recording was extended to make video recording possible. The preliminary techniques for this were already invented in 1956, but it took until the mid-seventies until low-cost consumer products appeared on the market (Bilderbeek, M., 2001).

At the end of the 1970s computers became more and more mature, which triggered the development of digital data storage media. However, the important inventions were already done much earlier. The rotating rigid disk for digital data storage was an

innovation done in 1957 already. The flexible disk was realized in the mid-seventies indeed mainly for use on personal computers. Also for this technology we can say it is still in use today (Bilderbeek, M., 2001).

Although the disk is most common today, a long time only digital tapes were used for data storage, mainly for back up of computer files. This technology has been popular for a long time. Even today big archives are made on tape. It is recognized though that for other purposes than archiving, tape is too limited, since the information can only be accessed sequentially. Both for disk as well as for tape storage media, there has been a great development with time. Not only the media itself improved, but also the heads and the electronics, resulting in an increasing linear and track data density, higher data transfer rate and shorter access times. To give an example: the capacity of the hard-disk drives has roughly doubled every year since 1957 (Bilderbeek, M., 2001).

Since 1985 there is a new invention in the recording business: optical-beam storage technology, in short: Magneto Optical (MO) technology. It makes use of a laser beam to read out magnetically stored data via the Magneto Optical Kerr Effect. The big advantages are that it is a non-contact method (meaning less wear of components and less sensitive for dirt) and the recording density can be increased until the diffraction limit. This also enables the medium to be removable. So the removableness of the floppy is combined with the main features of the hard disk (i.e., high capacity, high data-transfer rate, rapid access) (Bilderbeek, M., 2001).

All magnetic materials have a characteristic temperature, called the Curie temperature, above which they lose magnetization due to a complete disordering of their magnetic domains. Therefore, they lose all the data they had stored before. More importantly, the material's coercivity, which is the measure of material's resistance to magnetization by the applied magnetic field, decreases as the temperature approaches the Curie point, and reaches zero when this temperature is exceeded. For the modern magnetic materials used in MO systems, this Curie temperature is on the order of 200°C .

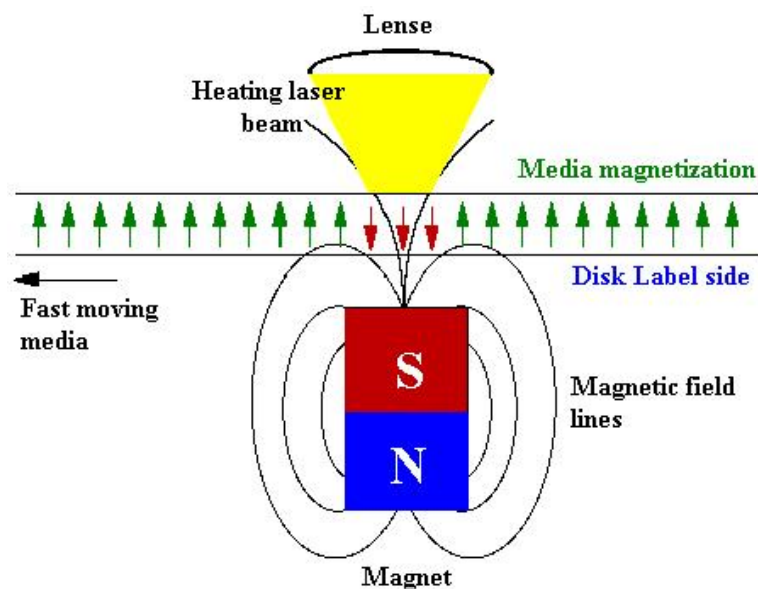


Figure 2.3 Schematically view of MO recording. The heating of the laser beam locally decreases the coercivity of the MO layer, enabling the external field to magnetize it there

It is important (since this is a multiply-erasable system) that the only change to the material when it is heated and cooled is the change in magnetization, with no damage to the material itself. This fact that the material's coercivity drops at higher temperatures allows thermally-assisted magnetic recording with relatively weak magnetic fields, which simplifies the drive's design. Even a relatively weak laser can generate high local temperatures when focused at a small spot (about 1 micron in case of MO systems). When the material is heated, and its coercivity is low, a magnetization of the media can be changed by applying a magnetic field from the magnet. When the material is cooled to room temperature, its coercivity rises back to such a high level that the magnetic data can not be easily affected by the magnetic fields we encounter in our regular daily activity. The basic schematic of this recording process is illustrated by Fig. 2.3 (Khurshudov A., 2001).

When the disk is inserted into the drive, the label side will face the magnet, and the transparent side will face the laser. The direction of magnetization in the thin magnetic films (on magnetic rigid disks, for example) can be parallel to the surface (longitudinal recording) or perpendicular to the surface (perpendicular recording). The latter has potential for higher density of magnetic recording. Most of the magnetic hard drives

nowadays utilize longitudinal recording, while the MO systems use the perpendicular direction of magnetization.

Unlike traditional magnetic recording systems, which use currents induced in the magnetic heads by the changing magnetic fluxes on the disk surface to read the data, MO systems use polarized light to read the data from the disk. The changes in light polarization occur due to the presence of a magnetic field on the surface of the disk (the Kerr effect). If a beam of polarized light is shined on the surface, the light polarization of the reflected beam will change slightly if it is reflected from a magnetized surface. If the magnetization is reversed, the change in polarization (the Kerr angle) is reversed too. The magnetized areas can not be seen in regular light, but only in polarized light. The change in direction of magnetization could be associated with numbers 0 or 1, making this technique useful for binary data storage.

2.4 Exchange Interactions

In a solid, interactions between electrons are often significant and extraordinarily complex. Fortunately Pauli's principle restricts the possible wave functions of an electron system. For most insulating solids, the problem of electron interactions can be reduced to a problem of coupled spins. The notion of energy exchange is illustrated by several examples from atomic and molecular physics. This will also serve to introduce the tools of second quantization which are essential for representing states of several electrons (Lévy, L. -P., 2000).

2.4.1 Direct Exchange Between Spins

Dipole-dipole interactions between spins, of the order

$$\mu_0 \mu_B^2 / a_0^3 \approx \alpha^2 R_y \approx 1K, \quad (2.4.1)$$

are much too weak to cause ferromagnetism. Electron magnetism comes from the Coulomb interaction between electrons which forces spins into ordered states, because of the Pauli principle. Indeed the latter requires the n -fermion wave function to be completely antisymmetric in the exchange of any two particles (including their spins). Neglecting spin-orbit interactions, the wave function is the product of spatial and spin wave functions. The symmetry of the spatial wave function is determined by the Coulomb interaction which must be minimal in the ground state. Given the global antisymmetry requirement, the spin wave function is then determined too. Exchange interactions therefore result mainly from the chemical bond. In order to understand how a certain ion gives rise to ferromagnetic exchange in an ionic solid, whilst giving antiferromagnetic exchange in a molecular solid, it must be begun by examining the chemical bonds.

The main point here is to show that the Hamiltonian for a solid, with its complex electrostatic forces, can be parametrised entirely in terms of the spins of the ions making it up. The parameters in this effective Hamiltonian involve overlaps of exact wave functions of ions in the solid and they are not easy to calculate. Experimental determination is often simpler and more accurate. The effective Hamiltonian is usually taken to be Heisenberg's (Dirac P. A. M., 1926; Heisenberg W., 1926)

$$H_{\text{eff}} = - \sum_{i,j} J_{i,j} \mathbf{S}_i \mathbf{S}_j, \quad (2.4.2)$$

where $J_{i,j}$ are the exchange constants and \mathbf{S}_i the total spin of the i th ion in the solid. Although difficult to work with, this Hamiltonian is already vastly simpler than the initial Hamiltonian which described the n electrons of each ion in a solid containing L ions all interacting together via the Coulomb interaction, and included other degrees of freedom too (Lévy, 2000).

2.4.2 *Hund Rules*

In an atom it is possible to have more than one electrons. Hund's rule are used to determine the quantum numbers that give the ground state of the multi-electron atoms

(Kittel C., 1996). Hund rules are given as:

1. The lowest energy atomic state is the one which maximizes the total value of the S . According to Pauli Exclusion Principle two electrons of the same spin can not be at the same place. Thus the electrons stay apart when they have parallel spins and the Coulomb energy is minimized.
2. The maximum value of L (consistent with rule 1) gives the lowest energy state since the electrons orbiting in the same direction can avoid each other more effectively and reduce the Coulomb energy.
3. The value of the total angular momentum J is given by $J = |L - S|$ when the shell is less than half full and by $J = L + S$ when the shell is more than half full so that spin-orbit energy is minimized.

The third rule tries to minimize the spin-orbit interaction that is due to the weak coupling of spin and orbital angular momentums. Spin-orbit coupling is a relativistic effect and proportional to Z^4 (Z is the atomic number of the atom). Hund's third rule does not always apply especially when the spin-orbit energy is less significant than other energies such as crystal field. The Hamiltonian for spin-orbit can be written as;

$$H_{so} = \lambda \mathbf{S} \cdot \mathbf{L} \quad (2.4.3)$$

When spin-orbit coupling is effective, \mathbf{L} and \mathbf{S} are not separately conserved but their total \mathbf{J} is conserved and the states of L and S split into levels of different J values ($|L - S| < J < |L + S|$).

2.4.3 Anisotropic Exchange (Magnetocrystalline) Interaction

Magnetocrystalline anisotropy is the energy cost per atom to align its magnetization from one crystallographic direction to another. It is a special case of magnetic anisotropy. The spin-orbit interaction is the primary source of the magnetocrystalline

anisotropy. The direction of a magnetization relative to body that supports it is determined mainly by two effects, shape anisotropy and magnetocrystalline anisotropy. The first arises from magnetostatic effects and the second from spin-orbit coupling between the spins and the lattice of the material. The magnetostatic effects can be worked out from micromagnetic calculations, but the magnetocrystalline anisotropy must be computed from the electronic structure of the material. This is an important quantity because it determines whether a magnetic material can be made into a good hard magnet, a good soft magnet or neither. Hard magnets are an essential component of electromagnetic motors and soft magnets are an essential component of transformers.

The magnetocrystalline energy is usually small compared to the exchange energy. But the direction of the magnetization is determined only by the anisotropy, because the exchange interaction just tries to align the magnetic moments parallel, no matter in which direction.

Single-ion anisotropy (often referred to simply as “magnetocrystalline anisotropy”) is determined by the interaction between the orbital state of a magnetic ion and the surrounding crystalline field which is very strong. The anisotropy is a product of the quenching of the orbital moment by the crystalline field. This field has the symmetry of the crystal lattice. Hence the orbital moments can be strongly coupled to the lattice. This interaction is transferred to the spin moments via the spin-orbit coupling, giving a weaker electron coupling of the spins to the crystal lattice. When an external field is applied the orbital moments may remain coupled to the lattice whilst the spins are more free to turn. The magnetic energy depends upon the orientation of the magnetization relative to the crystal axes.

2.4.3.1 *Crystal Field*

Crystal field effect is the splitting of the degenerate d-orbitals that are displayed in Figure 2.4 due to electrostatic interactions between the electrons in the d-orbitals of magnetic ion and those in the ligands (Watanabe H.,1966).

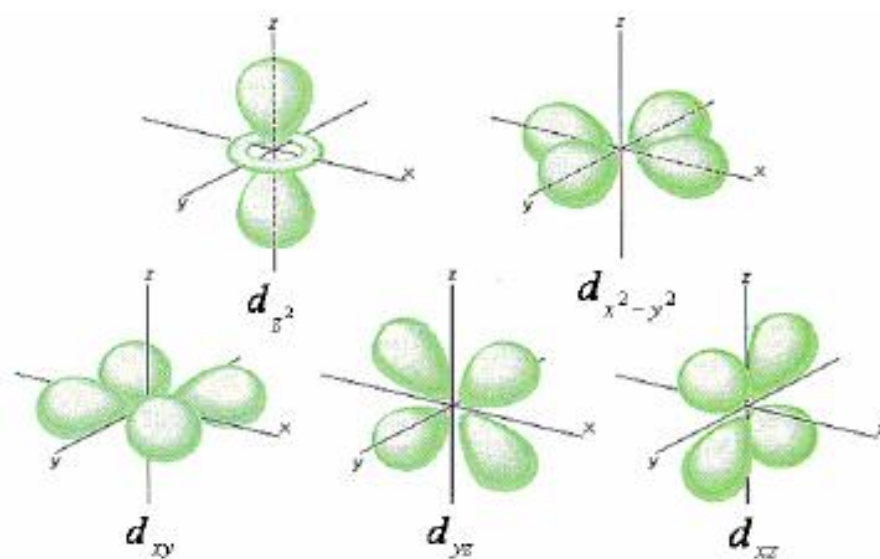


Figure 2.4 The angular distribution of d orbitals. The levels d_{z^2} and $d_{x^2-y^2}$ grouped as e_g levels. The remaining levels d_{xy} , d_{xz} and d_{yz} are grouped as t_{2g} levels (Blundell, S., 2001)

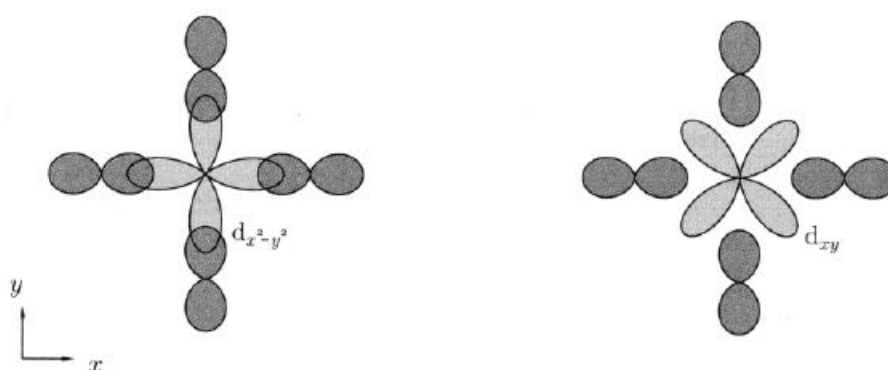


Figure 2.5 The overlap of different d orbitals with the ligands. d_{xy} orbital has lower energy compare to $d_{x^2-y^2}$ due to smaller overlap and electrostatic interaction (a) d_{γ} orbital (b) d_{ϵ} orbital (Kittel C., 1996).

In most magnetic ionic crystals or rare-earth metals, the electrons in the incompletely filled shell are in such a localized state. However, the state of the incompletely filled shell is not the same as the free-ion state, but is more or less affected by surrounding ions, notwithstanding its localized nature. Let us call influences from the surrounding ions the crystal-field effect in a broad sense. The crystal-field effect in the incompletely filled shell of iron-group metals is much larger than in the $4f$ shell of rare-earth metals. The main reason is that the $3d$ shell is outermost in the ions so that it interacts directly with the electrons of surrounding ions. In iron-group elements the crystal-field effect is larger than the LS coupling, whereas the reverse is true in rare-earth elements. Therefore, in the former case the $2L + 1$ degenerate energy levels (specified by L) split into several groups under the influence of the crystal field; the LS coupling should then be taken into account for those lowest states split off due to the crystal field. On the other hand, in the latter case, the crystal-field effect must be taken into account for the $2J + 1$ degenerate states which belong to the lowest energy split off due to the LS coupling (Yosida, K., 1998).

The simplest crystal-field effect is the electrostatic effect due to surrounding charges; It is similar to the interaction between the nuclear quadrupole moment and the electric field gradient. It is the most important crystal-field effect for electrons located at the center of the ion (like the incompletely filled $4f$ shell in rare-earth metals). In contrast, it is not presumably an important effect for the incompletely filled $3d$ shell (which is an outer orbital of the ion); these electrons interact directly with the electron on the outer closed shell of surrounding anions. Let us consider the effect of this interaction, using the molecular orbital method. First, having in mind an ionic crystal with the NaCl-type structures (like FeO), it is assumed that the magnetic ion is surrounded octahedrally by O^{2-} anions.

$$\begin{aligned}
 d\varepsilon : \varphi_{xy} &= \frac{1}{\sqrt{2}i}(\varphi_2 - \varphi_{-2}), & \varphi_{yz} &= -\frac{1}{\sqrt{2}i}(\varphi_1 + \varphi_{-1}), \\
 \varphi_{zx} &= -\frac{1}{\sqrt{2}}(\varphi_1 - \varphi_{-1}), \\
 d\gamma : \varphi_{x^2-y^2} &= \frac{1}{\sqrt{2}}(\varphi_2 + \varphi_{-2}), & \varphi_{3z^2-r^2} &= \varphi_0
 \end{aligned} \tag{2.4.4}$$

The electron-transfer Hamiltonian combines these wave functions with the p orbitals on neighboring O^{2-} ions. As a result, the $3d$ orbitals are mixed with the appropriate combinations of the p orbitals of surrounding anions. It is defined three p orbitals of O^{2-} as

$$\begin{aligned}\varphi_x &= -\frac{1}{\sqrt{2}}(\varphi_1 - \varphi_{-1}), \\ \varphi_y &= -\frac{1}{\sqrt{2}i}(\varphi_1 + \varphi_{-1}), \\ \varphi_z &= \varphi_0\end{aligned}\tag{2.4.5}$$

from symmetry, they mix with the $3d$ orbitals in (2.4.4) as depicted in Figure 2.5. As evident from the figure, the $d\varepsilon$ and $d\gamma$ orbitals mix differently with the p orbitals and consequently the $d\varepsilon$ and $d\gamma$ orbitals have different energies. Correspondingly, the p orbitals φ_x , φ_y and φ_z of the O^{2-} ion mix with surrounding d orbitals of the magnetic ions. Since the $2p$ shell is completely filled, those $p-d$ mixed orbitals are filled, with six electrons total. They are the bonding orbitals of the $p-d$ mixing, whereas the $d-p$ mixed orbitals derived from the d electrons are orthogonal to the bonding orbitals and are called the antibonding orbitals. For the antibonding orbitals, a larger mixing of the p orbitals into the d orbitals lead to a higher level. Therefore the $d\gamma$ energy becomes higher, if the energies of the $d\varepsilon$ and $d\gamma$ orbitals are completed. This tendency is the same as for the electrostatic effect, since the $d\varepsilon$ orbital has a larger amplitude in the direction avoiding the negative charge of O^{2-} , while the $d\gamma$ orbital extends along the direction toward the center of O^{2-} ion (Yosida, K., 1998).

2.4.3.2 *Single-Ion Anisotropy*

The magnetic moment of rare-earth ions is proportional to the total angular momentum J . In iron-group ions, on the other hand, the crystal-field splitting of the $2L + 1$ degenerate levels is much larger than both kT and the LS coupling, so that it have to be considered the ground state due to the crystal field. In most ionic crystals of iron-group compounds, magnetic ions are located at the center of an octahedron formed with anions. Even when ground state degeneracy is present in the cubic field,

it is usually lifted by a crystal field of lower symmetry. In most case the effect of the lower-symmetry crystal field is smaller than that of the cubic field, but is still larger than the LS coupling. In such a case one considers simply the nondegenerate ground state.

Since the crystal-field Hamiltonian is given as a real function, its eigenfunctions can be expressed also with real functions. On the other hand, the operator of the total angular momentum \mathbf{L} is pure imaginary. Since \mathbf{L} is a Hermitian operator, the diagonal matrix element must be real. From this it is seen that the expectation value of the angular momentum over a nondegenerate eigenstate must be zero: namely it is obtained for a nondegenerate ground state $|0\rangle$

$$\langle 0|\mathbf{L}|0\rangle = 0. \quad (2.4.6)$$

This means that the orbital angular momentum is quenched in a nondegenerate ground state, which is realized by the crystal-field splitting. This is called the quenching of the orbital angular momentum. The quenched orbital angular momentum is partially restored by the LS coupling.

Let E_n and $|n\rangle$ be the energy level and the corresponding eigenfunction due to the crystal-field splitting. The function $|n\rangle$ may be regarded as the eigenfunction of the Hamiltonian written with equivalent operators. In both cases one can assume that the eigenfunction including the spin is given as a product of the orbital and spin parts. At this stage the orbital state of the ion in the ground state $|0\rangle$, in which the orbital angular momentum is quenched, and the spin \mathbf{S} is completely free with $(2S + 1)$ -fold degeneracy; in this case the magnetic moment of the ion is given exclusively by the spin. The free spin couples to the lattice only when we take into account the LS coupling. Let us treat the LS coupling and Zeeman energy,

$$V = \lambda\mathbf{L} \cdot \mathbf{S} + \mu_B\mathbf{H} \cdot (2\mathbf{S} + \mathbf{L}), \quad (2.4.7)$$

as a perturbation. Since the spin wave function is independent of the orbital part, the spin \mathbf{S} is left as an operator in this perturbation calculation. Because of the quenching

of \mathbf{L} , first-order perturbation theory leads to

$$\Delta E^{(1)} = 2\mu_B \mathbf{H} \cdot \mathbf{S}. \quad (2.4.8)$$

Introducing $\Lambda_{\mu\nu}$ defined by

$$\Lambda_{\mu\nu} = \sum_n \frac{\langle 0|L_\mu|n\rangle\langle n|L_{\nu}|0\rangle}{E_n - E_0}, \quad (2.4.9)$$

we obtain the second-order energy as

$$\Delta E^{(2)} = - \sum_{\mu\nu} [\lambda^2 \Lambda_{\mu\nu} S_\mu S_\nu + 2\lambda \mu_B \Lambda_{\mu\nu} H_\mu S_\nu + \mu_B^2 \Lambda_{\mu\nu} H_{\mu\nu} H_{\nu\mu}], \quad (2.4.10)$$

where μ and ν represent x , y or z . Adding $\Delta E^{(1)}$ and $\Delta E^{(2)}$, we have

$$\begin{aligned} H_S &= \sum_{\mu\nu} [2\mu_B H_\mu (\delta_{\mu\nu} - \lambda \Lambda_{\mu\nu} S_\nu) \\ &\quad - \lambda^2 \Lambda_{\mu\nu} S_\mu S_\nu - \mu_B^2 \Lambda_{\mu\nu} H_{\mu\nu} H_{\nu\mu}] \end{aligned} \quad (2.4.11)$$

as the effective Hamiltonian for a nondegenerate ground state split of by the crystal field. The first term represents an effective Zeeman energy, which means that the g value has been replaced by the g tensor

$$g_{\mu\nu} = 2(\delta_{\mu\nu} - \lambda \Lambda_{\mu\nu}). \quad (2.4.12)$$

Here the additional tensor $-2\lambda \Lambda_{\mu\nu}$ is the induced orbital moment, which arises from the mixing with high-energy orbital states due to the LS coupling and is expressed as a change of the magnetic moment accompanied with the spin \mathbf{S} .

The second term is the spin Hamiltonian in a narrow sense or the anisotropy spin Hamiltonian, which represents the anisotropy energy for the spin direction. Let us take the principal axes of the crystal as x , y and z axes and express the components Λ as Λ_x , Λ_y and Λ_z .

Then the anisotropy spin Hamiltonian can be written as

$$\begin{aligned}
H = & -\lambda^2 \left\{ \frac{1}{3}(\Lambda_x + \Lambda_y + \Lambda_z)S(S+1) \right. \\
& + \frac{1}{3} \left[\Lambda_z - \frac{1}{2}(\Lambda_x + \Lambda_y) \right] [3S_z^2 - S(S+1)] \\
& \left. + \frac{1}{2}(\Lambda_x - \Lambda_y)(S_x^2 - S_y^2) \right\}.
\end{aligned} \tag{2.4.13}$$

The anisotropy Hamiltonian lift the $(2S+1)$ -fold degeneracy of the spin. Omitting the constant term, we obtain from (2.4.13)

$$H = DS_z^2 + E(S_x^2 - S_y^2) \tag{2.4.14}$$

For integer S the first term in this Hamiltonian splits the spin energy levels into doubly degenerate S levels $S_z = \pm S, \pm(S-1), \dots, \pm 1$ and a nondegenerate one with $S_z = 0$; for half-odd integer S it leads to doubly degenerate $S+1$ levels with $S_z = \pm S, \pm(S-1), \dots, \pm 1/2$. The second term has finite matrix elements between states with $\Delta S_z = \pm 2$. Therefore, for integer S , the doubly degenerate levels $\Delta S_z = \pm 2$, which are produced by the first term, are split by the second term; as a result the $(2S+1)$ -fold degeneracy is lifted by the anisotropy Hamiltonian. However, for half-odd integer S the integer so that there is no matrix element between these states. Consequently, the double degeneracy due to the first term remains. The case of half-odd integer S corresponds to a system with an odd number of electrons; for this case the crystal field cannot lift the degeneracy completely, leaving double degeneracy. This is called the Kramers theorem; the doubly degenerate levels remaining are called Kramers doublet.

The Kramers theorem is a general result which can be derived when the Hamiltonian for the electron system is invariant in time reversal. Under time reversal the orbital and spin orbital momenta change signs; therefore the Kramers degeneracy is lifted first by the Zeeman energy (which changes sign under time reversal).

The third term in (2.4.11) is not related to the LS coupling; it comes rather from the second-order perturbation of the Zeeman energy for the orbital angular momentum. This gives a temperature independent (anisotropic) paramagnetic susceptibility, which

is called the Van Vleck orbital paramagnetism. The Van Vleck orbital paramagnetism gives a non-negligible contribution when the energy of the excited states is not too high. In the case of transition metals, iron-group metals in particular, excited states are present continuously from the Fermi energy; therefore a large orbital paramagnetism is expected as pointed out by Kubo and Obata (Kubo, R. & Obata, Y., 1956). In vanadium metal the paramagnetic susceptibility hardly changes between the normal and superconducting states, suggesting that most of the paramagnetism in this metal originates from the orbital paramagnetism (Yosida, K., 1998).

2.5 Molecule-Based Magnets

Most research in solid state physics and much of current technology is based on the properties of simple chemical elements and compounds; for example, most magnets are made of iron, cobalt, nickel or alloys of these. An alternative strategy for making new magnetic materials is to use the flexibility of carbon chemistry which is so successful in producing the rich variety of biological systems found in nature; this approach leads to molecular magnets, that is to say magnetic materials in which the fundamental building block is the molecular unit and not the atomic unit. This idea leads to a wealth of new and highly controllable properties. (Blundell, S. J., 2007).

Molecular magnetism has been one of the active areas in molecular chemistry for the last 20 years (Kahn O., 1993). The advantages of molecule-based magnets compared to classical metal and metal oxide ones are that the magnets can be obtained through a selection of proper spin sources (e.g., transition metal ions, organic radicals) and coordinating ligands. One of the attractive targets in this field is the development of functionalized magnets, in which magnetic properties can be controlled by external stimulation (Ohkoshi S. & Hashimoto K., 2002).

To date, various molecule-based magnets have been obtained with bimetallic, metal-organic, and organic systems. For example, $Mn^{II}Cu^{II}(\text{pbaOH})(\text{H}_2\text{O})_3$ (pba = 2-hydroxy-1,3-propanediylbis(oxamato)) shows one dimensional (1-D) ferrimagnetic behavior below 4.6 K (Kahn, O., 1993). A series of $[M^{II}Cr^{III}(\text{ox})_3]^-$ (ox = oxalato,

$M^{II} = Fe^{II}, Co^{II}, Ni^{II},$ and Cu^{II}) form 2-D or 3-D network structures, showing spontaneous magnetization (Tamaki, H., et. al., 1992). In these two systems, spin sources are unpaired electrons in d orbitals of metal ions. A system having unpaired electrons in both d -orbitals and p -orbitals is also extensively studied. The prepared ionic salt $[Fe(Cp^*)_2]^{•+}[TCNE]^{•-}$ (Cp^* = pentamethylcyclopentadienide, TCNE = tetracyanoethylene) shows a ferromagnetic transition below 4.8 K (Miller, J. S. & Epstein, A.J., 1994). Moreover, $V(TCNE)_{xy}CH_2Cl_2$ obtained from the reaction of bisbenzene vanadium with TCNE in dichloromethane exhibits a high magnetic ordering temperature (T_c) of ca. 400 K (Tamaki, H., et. al., 1992).

The main targets in the field of molecule-based magnets are classified into the following two at present. One is to obtain magnets with a high T_c value. Another is to design magnets with novel functionalities. As a prototype of the system having these properties, Prussian blue analogues are attractive because various types of building blocks $[B(CN)]^{x-}$ and metal ions A, where B and A are transition metal ions having unpaired electrons, can be assembled in an alternating fashion (Ohkoshi, S. & Hashimoto, K., 2002). Recently, due to its superb magnetic characteristics, the family of Prussian blue compounds has received attention in molecule-based magnets.

2.5.1 Prussian Blue Analogues

Around 1700 Prussian Blue (PB, $Fe_4^{III}[Fe^{II}(CN)_6]_3 \cdot 14H_2O$) was accidentally discovered by Johann Jacob Diesbach, a painter from Prussian city of Berlin who actually tried to create a red coloured paint (Ludi A., 1981). Surprisingly though, the pigment thus acquired actually had a very bright blue color, which earned it the name *Prussian Blue* (PB) at the time. In terms of molecular build-up, it consists of Fe^{II} and Fe^{III} ions, which are linked through negatively charged cyano ligand molecules (CN^-), arranged in a rock-salt structure (See Fig. 2.6). Thus, both metal ions are octahedrally surrounded in this mixed-valence compound, by six carbon and six nitrogen atoms, respectively. It has turned out possible to obtain a whole range of similar materials by varying the metal ions involved, and thus a whole class of these coordinated materials exists; the so-called Prussian Blue Analogues (PBAs), named after the parent

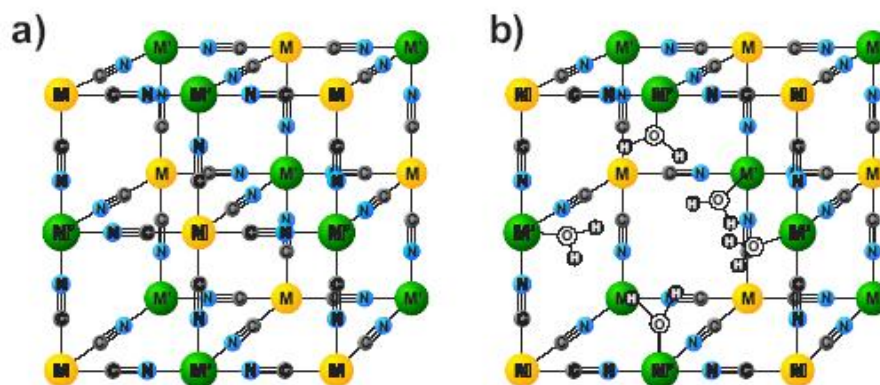


Figure 2.6 Schematic representation of the structure of Prussian Blue (Analogues). For Prussian Blue itself, $M' = Fe^{III}$ and $M = Fe^{II}$. (a) Preferred basic rock-salt structure of PBAs, where the two constituent metal ions M and M' are connected through cyano (CN) bridges. In order to acquire charge neutrality, the system incorporates $[M(CN)_6]$ defects in its structure, which are filled by H_2O molecules, as depicted on the right (b) (Lummen, T.T.A., et. al., 2008)

compound (Lummen, T.T.A., et. al., 2008).

In modern day synthesis of Prussian Blue Analogues, one typically mixes a solution of an M' salt (e.g. $FeCl_3(aq.)$) with a solution of an $M(CN)_6$ salt (e.g. $K_2Fe(CN)_6(aq.)$), where M and M' are d -block metal ions. When these building blocks meet in solution, the cubic superstructure (Fig. 2.6(a)) is formed virtually instantaneously, with the material growing in an almost “polymeric” fashion after nucleation, and the thus-formed solid Prussian Blue Analogue precipitates due to its insolubility. The preferred cubic rock-salt structure however, is often not charge neutral due to the mixed-valence nature of PBAs. In order to attain charge neutrality, the system can *choose* to incorporate either of two additional elements. Firstly, the system can leave out some $[M(CN)_6]^{3-}$ building blocks, which leaves vacancies in the structure that are subsequently filled by water molecules (Fig. 2.6(b)).

The corresponding molecular formula for Prussian Blue is $Fe_4^{III}[Fe^{II}(CN)_6]_3 \cdot zH_2O$, for example. Alternatively, the system can enclose some alkali-cations (A^+) in the structure, on the interstitial sites. In this case, the metal constituents could occur in stoichiometric amounts, which would result in the molecular formula $A_xM'[M(CN)_6] \cdot zH_2O$. Due to the very fast formation of the material, however, usually both scenarios occur

and one ends up with a material of general formula $A_xM'[M(CN)_6]_y \cdot zH_2O$ where A is alkali metal and M and M' are transition metal ions. In Prussian blue analogs the transition metals are connected by cyanide ligands (C-N) that are small and dissymmetric and create stable molecular precursors with strong metal-carbon bonds. And indeed, PBAs are notorious for the variation in their composition when only minimal changes to their synthesis conditions are made (Lummen, T.T.A., et. al., 2008).

CHAPTER THREE

MODEL AND SIMULATION METHOD

3.1 Ising Model

3.1.1 Historical Background

The Ising model is the prototype model for all magnetic phase transitions and probably the most studied model of statistical physics. The model first was proposed by Lenz and investigated by his graduate student, Ising, to study the phase transition from a paramagnet to a ferromagnet. Ising studied the simplest possible model consisting simply of a linear chain of spins, and his analysis showed that there was no phase transition to a ferromagnetic ordered state at any temperature. Ising remarks that the only contemporary citation of his paper was by Heisenberg.

Heisenberg proposed his own theory of ferromagnetism in 1928(W. Heisenberg, 1928). Thus Heisenberg used the supposed failure of the Lenz-Ising model to explain ferromagnetism as one justification for developing his own theory based on a more complicated interaction between spins. In this way the natural order of development of theories of ferromagnetism was inverted; the more sophisticated Heisenberg model was exploited first, and only later did theoreticians return to investigate the properties of the simpler Lenz-Ising model (Brush S. G., 1967).

The first exact, quantitative result for the two-dimensional Ising model was obtained by Kramers and Wannier (Kramers H. A. & Wannier G. H., 1941) who successfully located the critical temperature of the system. They did not succeed in obtaining an exact solution in closed form, but they did develop a variational method which is fairly accurate, and which has been used occasionally in later studies (Brush S. G., 1967).

They were followed by Norwegian-born chemist Lars Onsager who derived an explicit expression for the free energy in zero field and thereby established the precise

nature of the specific-heat singularity (Onsager L., 1944). He got the Nobel prize in chemistry in 1968 for his studies of nonequilibrium thermodynamics and this work proved later useful in analyzing other complex systems, such as gases sticking to solid surfaces, and hemoglobin molecules that absorb oxygen.

In order to simulate many-particle systems, appropriate models which describe the physics of these systems have to be found. The Ising model is one of the oldest and best studied models of this kind. Although it seems to be a rather simple model, it shows the main characteristics observed in a real-life many-particle system (e. g. a phase transition). Initially it was invented as a simple model of a ferromagnet, but it turned out that its applications reach into other areas of physics, chemistry, biology and even sociology. To mention just a few examples, the Ising model is used in modeling binary alloys, the adsorption of O_2 on haemoglobine, neural networks, protein folding, biological membranes, social imitation and social impact in human societies (Erkinger H., 2000).

It have been considered a number of models that can be solved analytically in statistical mechanics e.g. ideal gas, 2-level molecules, 3-level molecules, N independent harmonic oscillators. They are all non-interacting models. A major topic of interest in statistical mechanics is the understanding of phase transitions (e.g. water \rightarrow ice) which requires the study of interacting models. The two dimensional Ising model is one of the few interacting models that have been solved analytically. It also exhibits a phase transition. The analytic and numerical solutions of the Ising model are important landmarks in the field of statistical mechanics. They have also significantly influenced our understanding of phase transition in general.

In the mid-20th century it became possible to use high-speed electronic computers to set up models of magnetic materials, to study the corresponding behaviour of those models, and to compare the computational results with observations of real systems. In recent years there have been many computational studies of the behavior of magnetic materials at the critical temperature using Ising spin model. These studies often use so-called “Monte Carlo” techniques (detailed discussed in another section), which are methods relying on a stream of random numbers to drive a stochastic process, in this

case the generation of a succession of many states of the spin model.

3.1.2 Theoretical Background

Ising model has been used to model phase transitions in solid state physics, with a particular emphasis on ferromagnetism and antiferromagnetism. Metals like iron, nickel, cobalt and some of the rare earths (gadolinium, dysprosium) exhibit a unique magnetic behavior which is called ferromagnetism because iron is the most common and most dramatic example. Ferromagnetic materials exhibit a long-range ordering phenomenon at the atomic level which causes the unpaired electron spins to line up parallel with each other in a region called a domain.

The long range order which creates magnetic domains in ferromagnetic materials arises from a quantum mechanical interaction at the atomic level. This interaction is remarkable in that it locks the magnetic moments of neighboring atoms into a rigid parallel order over a large number of atoms in spite of the thermal agitation which tends to randomize any atomic-level order. Sizes of domains range from a 0.1 mm to a few mm. When an external magnetic field is applied, the domains already aligned in the direction of this grow at the expense of their neighbors.

Another physical case where the application of the Ising model enjoys considerable success is the description of antiferromagnetism. This is a type of magnetism where adjacent ions spontaneously align themselves at relatively low temperatures into opposite, or antiparallel, arrangements throughout the material so that it exhibits almost no gross external magnetism. In antiferromagnetic materials, which include certain metals and alloys in addition to some ionic solids, the magnetism from magnetic atoms or ions oriented in one direction is canceled out by the set of magnetic atoms or ions that are aligned in the reverse direction. This spontaneous antiparallel coupling of atomic magnets is disrupted by heating and disappears entirely above a certain temperature, called the Néel temperature, characteristic of each antiferromagnetic material. Antiferromagnetic solids exhibit special behavior in an applied magnetic field depending upon the temperature. At very low temperatures, the solid exhibits no response to

the external field, because the antiparallel ordering of atomic magnets is rigidly maintained. At higher temperatures, some atoms break free of the orderly arrangement and align with the external field. This alignment and the weak magnetism it produces in the solid reach their peak at the Néel temperature. Above this temperature, thermal agitation progressively prevents alignment of the atoms with the magnetic field, so that the weak magnetism produced in the solid by the alignment of its atoms continuously decreases as temperature is increased (Hjorth-Jensen, M., 2007).

The Ising model provides a simple way of describing how a magnetic material responds to thermal energy and an external magnetic field. In this model, each domain has a corresponding spin of north or south. The spins can be thought of as the poles of a bar magnet. The direction of the spins influences the total potential energy of the system.



Figure 3.1 Spin interactions with its nearest neighbors in one dimensional Ising model.

Ising introduced a model consisting of a lattice of “spin” variables: S_i , which can be only take the values $+1$ for an ‘up’ (\uparrow) spin and -1 for an ‘down’ (\downarrow) spin. Every spin interacts with its nearest neighbors (2 in 1D as illustrated in fig. 3.1) as well as with an external magnetic field h .

The macroscopic properties of a system are determined by the nature of the accessible microstates. Hence, it is necessary to know the dependence of the energy on the configuration of spins. In mathematical physics, the Hamiltonian is the total energy of a system, and it governs the dynamics. For the Ising model, the Hamiltonian is defined by

$$H(\{S_i\}) = -J \sum_{\langle ij \rangle} S_i S_j - h \sum_i S_i \quad (3.1.1)$$

where h is proportional to a uniform external magnetic field. The first sum $\langle ij \rangle$ in

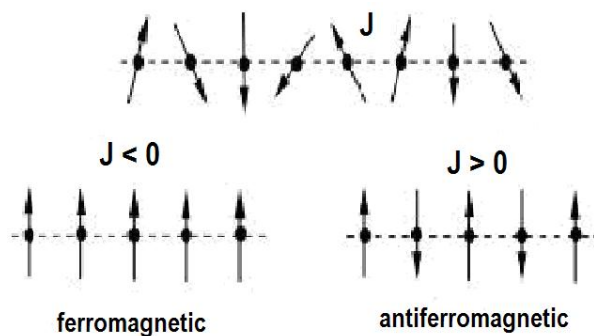


Figure 3.2 Spin chain: Coupling J between spins of arbitrary orientation. $J < 0$: ferromagnetic alignment preferred; $J > 0$: antiferromagnetic alignment preferred

(3.1.1) is over all nearest neighbor pairs ($j = i = \pm 1$ in 1D). The exchange constant J is a constant specifying the strength of interactions (fig. 3.2). The second sum in (3.1.1) represents the energy of interaction of the magnetic moments associated with the spins with an external magnetic field.

If $J > 0$, then the states $\uparrow\uparrow$ and $\downarrow\downarrow$ are energetically favored in comparison to the states $\uparrow\downarrow$ and $\downarrow\uparrow$. Hence for $J > 0$, it is expected that the state of lowest total energy is ferromagnetic, i.e., the spins all point in the same direction. If $J < 0$, the states $\uparrow\downarrow$ and $\downarrow\uparrow$ are favored and the state of lowest energy is expected to be antiferromagnetic, i.e., alternate spins are aligned. If the spins are subjected to an external magnetic field directed upward, the spins \uparrow and \downarrow possess an additional internal energy given by $-h$ and $+h$ respectively.

An important virtue of the Ising model is its simplicity. Some of its simplifying features are that the kinetic energy of the atoms associated with the lattice sites has been neglected, only nearest neighbor contributions to the interaction energy have been included, and the spins are allowed to have only two discrete values. In spite of the simplicity of the model, it exhibits very interesting behavior (Gould, H. & Tobochnik, J., 1996).

It is easy to solve the Ising model in the absence of external magnetic field in one dimensional case exactly. The Hamiltonian of a linear chain of N spins with nearest

neighbor interactions is given by

$$H_{1d} = -J \sum_{\langle nm \rangle} S_i S_{i+1} \quad (3.1.2)$$

It is used periodic boundary conditions, that means that the spins will be arranged on a ring as given in figure (3.3). Thus, the first spin and the N -th spins are nearest neighbor and the system is periodic.

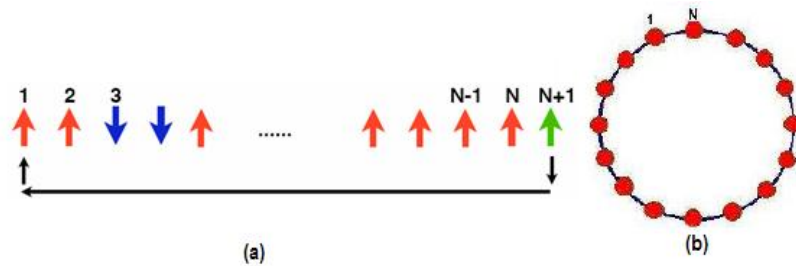


Figure 3.3 (a) In one dimensional Ising Model all spins interact with two spins and $S_{N+1} = S_1$ with periodic boundary conditions. (b) The N -th spin interacts with the first spin so that the chain forms a ring. As a result, all the spins have the same number of neighbors and the chain does not have a surface.

The energy of the one-dimensional Ising Model is with periodic boundary conditions is given by

$$H = -J(S_1 S_2 + S_2 S_3 + S_3 S_4 + \dots + S_{N-1} S_N + S_N S_1). \quad (3.1.3)$$

The partition function for this model become

$$Z = (2 \cosh \beta J)^N \cdot [1 + (\tanh \beta J)^N]. \quad (3.1.4)$$

Consider the two dimensional Ising model defined over a square lattice of N spins under periodic boundary conditions as seen fig. (3.4).

In this model each spin has four nearest neighbors. Onsager's solution in the absence of magnetic field ($h=0$) in the thermodynamic limit $k_B T_c / J$ becomes $2 / \ln(1 + \sqrt{2}) \approx 2.269$.

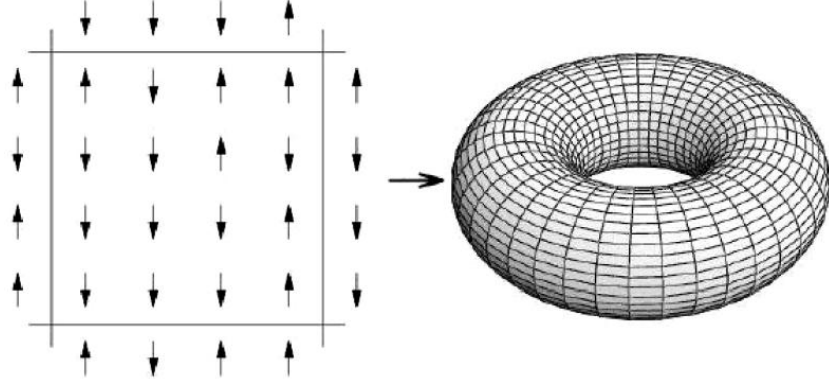


Figure 3.4 (a) One of the possible 2^N configurations of Ising spin system for $N = 16$ in square lattice. (b) Periodic boundary condition (imagine the top wrapping around to attach to the bottom and the left wrapping around to attach to the right) in two dimensional Ising model.

3.1.3 Statistical Mechanics of Ising Model

Although the Ising model is too simple, it already contains much of the physics of the ferromagnetic phase transition. In order to explore the properties of this model, it is needed to calculate some physical quantities of interest, including the mean energy $\langle E \rangle$, the mean magnetization $\langle M \rangle$, the heat capacity C , and the magnetic susceptibility χ .

In order to calculate expectation values such as the mean energy $\langle E \rangle$ or magnetization $\langle M \rangle$ in statistical physics the thermal average of a quantity A at a finite temperature T is given by a sum over all states:

$$\langle A \rangle = \frac{1}{Z} \sum_i A_i \exp(-\beta E_i), \quad (3.1.5)$$

with $\beta = 1/kT$ being the inverse temperature, k the Boltzmann constant, A_i is the value of the quantity A in the configuration i . E_i is the energy of that configuration. Z is the partition function

$$Z = \sum_{i=1} \exp(-\beta E_i) \quad (3.1.6)$$

normalizes the probabilities $p_i = \exp(-\beta E_i)/Z$. The mean energy is thermal equilibrium is

$$\langle E \rangle = \frac{1}{Z} \sum_i E e^{-\beta E_i} = -\frac{\partial}{\partial \beta} \ln Z. \quad (3.1.7)$$

One way to measure the heat capacity differentiate $\langle E \rangle$ with respect to the temperature T :

$$C = \frac{\partial \langle E \rangle}{\partial T}. \quad (3.1.8)$$

Another way is to use the statistical fluctuations for the total energy in the canonical ensemble:

$$C = \frac{1}{kT^2} (\langle E^2 \rangle - \langle E \rangle^2). \quad (3.1.9)$$

To obtain the system's mean magnetization $\langle M \rangle$, it is differentiated the Gibb's free energy F with respect to h :

$$\langle M \rangle = -\frac{\partial f}{\partial h} = \frac{1}{\beta} \frac{\partial \ln Z}{\partial h} = \langle \sum_i s_i \rangle. \quad (3.1.10)$$

The magnetic susceptibility χ is an example of a “response function”, since it measures the ability of a spin to “respond” o flip with a change in the external magnetic field. The zero isothermal magnetic susceptibility is defined by the thermodynamic derivative

$$\chi = \lim_{h \rightarrow 0} \frac{\partial \langle M \rangle}{\partial h}. \quad (3.1.11)$$

The zero field susceptibility can be related to the magnetization fluctuations in the system:

$$\chi = \frac{1}{kT} (\langle M^2 \rangle - \langle M \rangle^2), \quad (3.1.12)$$

where $\langle M^2 \rangle$ and $\langle M \rangle^2$ are zero field values. (Feiguin, A.E., 2012)

The Ising model exhibits a phase transition, except for the one-dimensional case. In zero external magnetic field there are two phases, separated by the transition temperature T_c (or critical temperature). For temperatures larger than T_c , the system is in a paramagnetic phase, whereas temperatures $T < T_c$ lead to a spontaneous magnetization that makes the system evolve from a disordered phase ($T \gg T_c$) to an ordered phase ($T \ll T_c$). The latter point, and the model's simplicity as well as the fact that it is exactly solvable in one dimension, and particularly in two dimensions, makes the Ising model a standard toy model in statistical physics.

These phase transitions are of general interest due to the universality of the critical behavior of different systems. Conventionally one divides phase transitions into those of first-order and those of higher than first-order, also called continuous phase transitions (Werde, F., 2007). First-order phase transitions involve a latent heat, which means the system absorbs or releases a fixed amount of energy. In the Ehrenfest classification of phase transitions, results from a discontinuity in the first derivative of the Gibbs free energy with respect to a thermodynamic variable. Continuous phase transitions involve no latent heat, but they exhibit discontinuities in higher than first-order derivatives of the Gibbs free energy. They therefore correspond to divergent susceptibilities which in turn are related to effective long-range interactions between the system's constituents (Werde, F., 2007).

A way to characterize phase transition is through studying the “critical behavior” of the system. First, it has to be defined a quantity called “order parameter” which vanishes above the critical temperature, and is finite below it. It is clearly seen that the magnetization satisfies this criterion, and is a suitable candidate. The critical behavior of the system is determined by the functional form of the order parameter near the phase transition. In this region, physical quantities show a power law behavior

$$m(T) \sim (T - T_c)^\beta, \quad (3.1.13)$$

where β is the “critical exponent”. Although M vanishes with T , thermodynamic derivatives such as the heat capacity and susceptibility diverge at T_c :

$$\chi \sim |T - T_c|^{-\gamma}, \quad (3.1.14)$$

and

$$C \sim |T - T_c|^{-\alpha}. \quad (3.1.15)$$

It has been assumed that the exponent is the same on both sides of the transition.

Another measure of the magnetic fluctuations is the linear dimension $\xi(T)$ of a typical magnetic domain. It is expected that this “correlation length” to be the order of the lattice spacing for $T \gg T_c$. Since the alignment of the spins will become more

correlated as T approaches T_c from above, ξ will increase. It can be characterized the divergent behavior of $\xi(T)$ near T_c by a critical exponent η

$$\xi(T) \sim |T - T_c|^{-\eta}. \quad (3.1.16)$$

As mentioned in previous section, the Ising model has a phase transition at finite T if $d > 1$. In one-dimensional ($d = 1$) the transition is at zero temperature. Therefore it can be said that one-dimensional is the lower critical dimension of the Ising model.

In the low-temperature phase, the symmetry is broken, the spins are ordered, the order parameter is $m \neq 0$, whereas in the high-temperature phase the symmetry is not broken, m vanishes, the spins are disordered. Hence Ising model is a prototype of all “order-disorder” transitions. These systems have the same critical behavior (depends on d), for given d they all belong to the same universality class.

3.2 Monte Carlo Simulation Method

3.2.1 History of Monte Carlo Method

The idea of Monte Carlo calculation is a lot older than the computer. The name *Monte Carlo* is relatively recent -it was coined by Nicolas Metropolis in 1949- but under the older name of *statistical sampling* the method has a history stretching back well into the last century, when numerical calculations were performed by hand using pencil and paper and perhaps a slide-rule (Newman M. E. J & Barkema G.T., 1999, p23).

Historically, the Monte Carlo method was considered to be a technique, using random numbers, to find a solution of a model under study. To solve numerical problems, random sampling had been used much earlier in isolated and undeveloped instances. An example is the experiment performed in the middle of the nineteenth century, consisting of throwing a needle randomly on a board notched with parallel lines and inferring the numerical value of π from the number times the needle intersects a line.

This experiment is known as “Buffon’s needle”. A number of investigator made use of this method over the years to calculate approximate values for π . The most famous of these is Mario Lazzarini, who in 1901 announced that he had calculated a value of 3.1415929 for π from an experiment in which a 2.5 cm needle was dropped 3408 times onto a sheet of paper ruled with lines 3 cm apart.

Possibly the first systematic application of statistical sampling techniques in science and engineering was by Enrico Fermi in the early 1930’s to predict the results of experiments related to the properties of the neutron which had recently been discovered by James Chadwick in 1932 (Jäckel, P. & Platen, E., 2002).

Shortly after World War II, Los Alamos was a hotbed of applied mathematics and theoretical physics. Much of the work was motivated by the intense focus on developing nuclear weapons. One particularly difficult problem was to estimate the behavior of large (e.g., 10^{23}) collections of atomic particles. The physical laws governing their behavior-thermodynamics, statistical physics, and quantum mechanics-were inherently probabilistic and so complicated that traditional methods were not sufficient for the sort of detailed analysis needed. In this setting a new idea took hold; instead of searching for closed form, analytic solutions, one could simulate the behavior of the system in order to estimate the desired solution. Producing simulations was a challenge. Before the late 1940s no device existed that could quickly and accurately carry out large-scale random simulations. By the end of World War II, things were different. Researchers at Los Alamos had access to such a device, the ENIAC (Electronic Numerical Integrator and Computer) at the University of Pennsylvania. It was huge (24 meters long, 18000 vacuum tubes), and could run at a (then) phenomenal rate of 5000 operations per second.

The spirit of this method was consistent with Stanislaw Ulam’s interest in random processes-from the simple to the sublime. He relaxed playing solitaire; he was stimulated by playing poker; he would cite the times he drove into a filled parking lot at the same moment someone was accommodatingly leaving. More seriously, he created the concept of “lucky numbers,” whose distribution was much like that of prime numbers; he was intrigued by the theory of branching processes and contributed much to

its development, including its application during the war to neutron multiplication in fission devices. For a long time his collection of research interests included pattern development in two-dimensional games played according to very simple rules. Such work has lately emerged as a cottage industry known as cellular automata (Metropolis N., 1987).

In 1947, von Neumann and others were working on methods to estimate neutron diffusion and multiplication rates in fission devices (i.e., nuclear bombs). Following Ulam's suggestion, von Neumann proposed a simple plan: create a relatively large number of "virtual" neutrons and use the computer to randomly simulate their evolution through the fissionable material. When finished, count the number of neutrons remaining to estimate the desired rates. In modern terms, the scale was extremely modest: a simulation of just 100 neutrons with 100 collisions each required about five hours of computing time on the ENIAC. Nonetheless, the utility of this approach was immediately apparent. From this point forward, randomized simulations—soon to be called Monte Carlo methods—were an important technique in physics (Richey M., 2010).

Their coworker Nicholas Metropolis dubbed the numerical technique "the Monte Carlo method" partly inspired by Ulam's anecdotes of his gambling uncle who just had to go to "Monte Carlo". A team headed by Metropolis carried out the first actual Monte Carlo calculations on the ENIAC computer in 1948. In 1949, Metropolis and Ulam published a paper on Monte Carlo methods, which sparked a lot of work on the methods in the 50's. Also in 1949 the first conference on Monte Carlo methods was held in Los Alamos, attracting more than a hundred participants.

The calculations received a further boost in 1948 with the arrival at Los Alamos of a new computer, humorously called the MANIAC. (Apparently the name was suggested by Enrico Fermi, who was tiring of computers with contrived acronyms for names—he claimed that it stood for "Metropolis and Neumann Invent Awful Contraption".) MANIAC was a significant technical improvement over the ENIAC. It was faster and contained a larger memory (40 kilobits, or 5 kilobytes in modern terms). A still more sophisticated computer, MANIAC 2, was built at Los Alamos two years later, and

both machines remained in service until the late fifties, producing a stream of results, many of which have proved to be seminal contributions to the field of Monte Carlo simulation (Newman M. E. J & Barkema G.T., 1999).

In 1953 of the paper by Nick Metropolis, Arianna and Marshall Rosenbluth, Edward and Mici Teller, in which they describe for the first time the Monte Carlo technique that has come to be known as Metropolis algorithm. This algorithm was cited in Computing in Science and Engineering as being among the top 10 algorithms having the “greatest influence on the development and practice of science and engineering in the 20th century.”

3.2.2 *Random Sequences*

Computing is completely deterministic by nature, and reproducing or simulating naturally random processes is a particularly delicate matter. For carrying out a Monte Carlo simulation, it is required that a sequence of numbers which are random, independent, real and uniformly distributed in the range zero to one. Strictly, it can be called a sequence of numbers random, if and only if it is generated by a random physical process like radioactive decay, thermal noise in electronic devices, cosmic ray arrival times, tossing of a coin etc.

A sequence of numbers are defined r_1, r_2, \dots, r_n as *random* if there are no correlations among the numbers in the sequence. A random sequence can have a distribution, i.e. the probability of a number to appear in the sequence would correspond to some distribution. If the distribution is uniform, all numbers are equally probable to appear. Mathematically, the likelihood of a number to occur is described by a distribution function $P(r)$. This means that the probability of finding r_i in the interval $[r, r + dr]$ is given by $P(r)dr$.

The usual random number generators provided by compilers or libraries generate a uniform distribution between 0 and 1, that means $P(r) = 1$. Ideally this numbers have equal probability, and it is independent of the previous one. The computer, the

sequences are “pseudo-random because knowing a number r_m and the preceding r_i , it can be predicted the next one r_{m+1} . This is evident in the correlations (Feiguin, A.E., 2012).

3.2.3 *Pseudo-Random Numbers*

Since a computer is a deterministic machine, truly random numbers do not exist on a computer. One uses therefore pseudo-random numbers. Pseudo-random numbers are produced in the computer deterministically by a simple algorithm, and are therefore not truly random, but any sequence of pseudo-random numbers is supposed to appear random to someone who does not know the algorithm. More quantitatively one performs for each proposed pseudo-random number generator a series of tests T_1, T_2, \dots, T_n . If the outcome of one test differs significantly from what one would expect from a truly random sequence, the pseudo-random number generator is classified as “bad. Note that if a pseudo-random number generator has passed n tests, we can not conclude that it will also pass test T_{n+1} . In this context also the term “quasi-random numbers appears. Quasi-random numbers are not random at all, but produced by a numerical algorithm and designed to be distributed as uniformly as possible, in order to reduce the errors in Monte Carlo integration.

A good random number generator should satisfy the following criteria:

- *Good distribution.* The points should be distributed according to what one would expect from a truly random distribution. Furthermore a pseudo-random number generator should not introduce artificial correlations between successively generated points.
- *Long period.* Both pseudo-random and quasi-random generators always have a period, after which they begin to generate the same sequence of numbers over again. To avoid undesired correlations one should in any practical calculation not come anywhere near exhausting the period.
- *Repeatability.* For testing and development, it may be necessary to repeat a cal-

ulation with exactly the same random numbers as in the previous run. Furthermore the generator should allow the possibility to repeat a part of a job without doing the whole thing. This requires to be able to store the state of a generator.

- *Long disjoint subsequences.* For large problems it is extremely convenient to be able to perform independent subsimulations whose results can later be combined assuming statistical independence.
- *Portability.* This means not only that the code should be portable (i.e. in a high-level language like Fortran or C), but that it should generate exactly the same sequence of numbers on different machines.
- *Efficiency.* The generation of the pseudo-random numbers should not be too time-consuming. Almost all generators can be implemented in a reasonably efficient way (Weinzierl S., 2000).

3.2.4 *Importance Sampling*

There are several well-established numerical integration methods based on sample points, which are equally spaced, e.g. the midpoint or trapezoidal rules, as well as some more evolved adaptive methods. These methods work fine in lower dimensions. However, if the space of integration is of higher dimension, they are practically not applicable anymore, since the number of sample points grows exponentially with the number of dimension. That is, numerical quadrature rules are inefficient for multidimensional integrals. Monte Carlo integration offers a tool for numerical evaluation of integrals in high dimensions. Furthermore Monte Carlo integration works for smooth integrands as well as for integrands with discontinuities. This allows an easy application to problems with complicated integration boundaries.

In numerical integration, it is needed M different sums, but in Monte Carlo integration only one is enough! This leads us to understand why Monte Carlo integration is so important in many dimensions. In one dimensional there really is no major difference, and indeed using methods like Simpson's the numerical integration can easily be made quite accurate and efficient. But with increasing numbers of dimensions M ,

doing the M sums becomes increasingly cumbersome, and eventually using the Monte Carlo approach which only needs one sum will clearly be simpler. Analogue simulation is going to be extremely difficult and most often impossible. It is need to resort to techniques that reduce the variance without in any way changing the averages of the desired quantities. These are called variance reduction techniques and one of them is called importance sampling.

The expectation values of thermodynamic observable are calculated in statistical mechanics. For a spin system, the expectation value is defined as

$$\langle A \rangle = \frac{\sum_s A e^{-\beta H}}{\sum_s e^{-\beta H}} \quad (3.2.1)$$

For example in an Ising system, the sum is over 2^N configurations. This number is extremely large for all but very small systems. Therefore one must find a method which estimates thermodynamic properties by sampling a small subset of representative configurations. One possible strategy would be to scan randomly the whole configuration space (scan randomly over all spin configurations). The expectation value of A would then be obtained as a sum over the scanned configurations, weighted by the appropriate Boltzmann factors. However, this random sampling has a very serious drawback. Because of the Boltzmann factor which brings a negligible weight to most of the configurations, very few configurations will contribute to the expectation value of A and a very unreliable estimate will result. This problem occurs because only an extremely restricted part of the configuration space is occupied with a considerable probability in the thermodynamic limit. Therefore it makes sense to restrict the sampling only to these states. This is the importance sampling (Vilfan I., ICTP).

In classical statistical mechanics, to evaluate the ensemble average of a well-behaved phase space function $A(x)$ given by

$$\langle A \rangle = \frac{\int dx \rho(x) A(x)}{\int dx \rho(x)} \quad (3.2.2)$$

where x is a point in phase space of dimension D and $\rho(x)$ is an unnormalized probability distribution of the statistical ensemble.

In importance sampling, the multidimensional integration over the ensemble average is numerically evaluated by generating a sequence of n phase space points $x^{(i)}$, ($i = 1, \dots, n$) by a stochastic process such that the probability distribution of the points being generated in this process is proportional to the probability distribution $\rho(x)$ of the statistical ensemble. Importance sampling thus ensures that the regions of phase space that make the most important contributions to the integral will be sampled most frequently. This method evaluates averages of the form of Eq. (3.2.2) as

$$\langle A \rangle \approx \frac{1}{n} \sum_{i=1}^n A(x^{(i)}) \equiv \bar{A}_n, \quad (3.2.3)$$

where the summation is taken over a sequence of random states $x^{(i)}$ generated from the target distribution. An ingenious method has been devised by Metropolis et al. (Metropolis N. et al., 1953) to generate such a sequence of random points $x^{(i)}$ in a way that \bar{A}_n converges to the ensemble average $\langle A \rangle$ after a large number of trials n . The method is based on constructing a Markov chain (Tongsik L., 2010).

3.2.5 Markov Chain

A Markov chain is a sequence of randomly occurring trials in phase space in which each trial depends only on the microscopic state that immediately proceeds it and not on the previous history of the states. It can be shown that a unique equilibrium distribution exists after a finite number of trials if every state of the system is accessible from any other state. In this case, such a Markov chain is referred to as *ergodic*. A process or algorithm is said to be ergodic, or to satisfy ergodicity, if any state can be obtained from any other state, provided a sufficiently long simulation time to sample all possible states of a system (Tongsik L., 2010).

An ergodic Markov chain is characterized by an irreducible matrix $P(B|A)$ of the stochastic transitions that link two states A and B , under which the distribution $\rho(A)$ is stationary, i.e. $\rho(A)$ satisfies the eigenvalue equation for *balance*:

$$\rho(B) = \sum_A P(B|A)\rho(A) \quad (3.2.4)$$

with eigenvalue unity, where the summation is taken over all states A , and

$$\sum_B P(B|A) = 1 \quad (3.2.5)$$

The condition Eq. (3.2.4) is conventionally replaced by the stronger requirement of microscopic reversibility or *detailed balance*:

$$P(B|A)\rho(A) = P(A|B)\rho(B), \quad (3.2.6)$$

which is a sufficient but not necessary condition for ergodicity. In Eq. (3.2.6) $\rho(A)$ and $\rho(B)$ are probabilities of occupation at equilibrium. Working with classical systems, the equilibrium distribution used is the Boltzmann distribution, which in a specific state i is given by

$$p_i = \frac{1}{Z} e^{-\beta E_i}, \quad (3.2.7)$$

where $\beta = 1/kT$ with k the Boltzmann constant ($1.38 \times 10^{-23} JK^{-1}$) and T the temperature, E_i is the internal energy for the state i and Z is the partition function ($Z = \sum_i e^{-\beta E_i}$). Thus, to satisfy detailed balance with a system following the Boltzmann distribution, Eq. (3.2.6) becomes

$$\frac{P(A|B)}{P(B|A)} = e^{-\beta(\Delta E)}, \quad (3.2.8)$$

where $\Delta E \equiv E_B - E_A$. The stochastic transition probability $P(B|A)$ can be written as the product of the trial probability $T(A \rightarrow B)$ from state A to state B and an acceptance probability $acc(A \rightarrow B)$ for such a trial:

$$P(B|A) = T(A \rightarrow B)acc(A \rightarrow B), \quad (3.2.9)$$

where the stochastic matrix $T(A \rightarrow B)$ is also called the underlying transition matrix of the Markov chain. The selection probability is the probability that the algorithm generates a specific state B from state A and the acceptance ratio is the probability for the system to change from state A to this state B .

3.2.6 Metropolis Algorithm

The condition of detailed balance does not uniquely determine what transition probabilities should be used. As such, this gives some flexibility to develop an efficient algorithm that applies to the problem at hand, so long as the ergodicity and detailed balance conditions are satisfied. For example, any implementation of $P(A|B)$ and $P(B|A)$ that satisfies Eq. (3.2.8) will give a correct result. However, most choices are simply not efficient and will not be useful.

As mentioned previous section the Metropolis-Hastings algorithm (Metropolis N. et al.,1953), named after Nicholas Metropolis and W. Keith Hastings, is a particular choice of the transition probabilities so as to very efficient. The original algorithm was developed in 1953 by N. Metropolis using the Boltzmann distribution and was extended to the general case in 1970 by W. K. Hastings. It is the most commonly used Markov Chain Monte Carlo method due to its simplicity and efficiency.

The Metropolis algorithm has single-spin-flip dynamics, as it only considers a single spin at a time. The derivation of the Metropolis algorithm follows from a few simple steps (Newman M. E. J & Barkema G.T., 1999). From state A , there are N possible states that can be reached after one flip to create different states. The probability to create a specific state B from A is thus $T(A \rightarrow B) = 1/N$ as they are all equally favored; the probability of creating state A from B is also the same. The condition of detailed balance, which mentioned above, can then be stated as

$$\frac{P(A|B)}{P(B|A)} = \frac{T(A \rightarrow B)acc(A \rightarrow B)}{T(B \rightarrow A)acc(B \rightarrow A)} = \frac{acc(A \rightarrow B)}{acc(B \rightarrow A)} = e^{-\beta(\Delta E)}. \quad (3.2.10)$$

The choice of acceptance ratio can be made in almost any fashion, so long as this equation is obeyed; however, a low acceptance ratio would lead to many wasted calculations, and as such a large acceptance ratios is therefore generally more efficient. For this purpose, the larger of two acceptance ratios is usually taken to be unity while the other one is adjusted accordingly.

With this single-spin-flip algorithm, there are three situations: the energy of new state can be either smaller or larger than the one of the current state or remain the same. If $\Delta E > 0$, $e^{-\beta\Delta E}$ will be smaller than unity, as $\beta > 0$. This means that $P(B|A) > P(A|B)$, so $P(B|A)$ is set to 1 and $P(A|B) = e^{-\beta\Delta E}$. If, however, $\Delta E < 0$, the exponential will be greater than unity and a similar logic is applied: $P(A|B)$ is set to 1 and $P(B|A) = e^{-\beta\Delta E}$. Having $\Delta E = 0$ has $P(A|B) = P(B|A) = 1$, such that the spin is flipped with no change in energy.

What this means is that when the spin flip reduces the energy ($\Delta E < 0$), the probability of accepting the new configuration is 1. On the other hand, when the spin flip increases the energy, the new configuration is accepted with a probability given by the weight $\omega = e^{-\beta\Delta E}$. To implement this, a random number r is chosen such that $0 \leq r < 1$. If $r < \omega$, the spin is flipped. This is the Metropolis algorithm, which has seen remarkable success. Other implementations of the acceptance ratio can be used if they prove to be more applicable to the problem at hand, but the Metropolis algorithm has shown itself to generally be very efficient. Ergodicity is assured by being able to flip one spin at a time, indefinitely, to go from any state to another (Le Blanc M., 2010).

The flowchart of Monte Carlo simulation with Metropolis Algorithm is shown in Fig. 3.5. As a summary to the usage of the Metropolis algorithm in Monte Carlo simulations, the following steps are done for one application of the algorithm:

1. Establish an initial state with energy E_i by positioning yourself at a random position in the lattice
2. Change the initial configuration by flipping e.g., one spin only. Compute the energy of this trial state E_f .
3. Calculate $\Delta E = E_f - E_i$. The number of values ΔE is limited to five for the Ising model in two dimensions
4. $\Delta E \leq 0$ we accept the new configuration, meaning that the energy is lowered and we are hopefully moving towards the energy minimum at a given temperature.

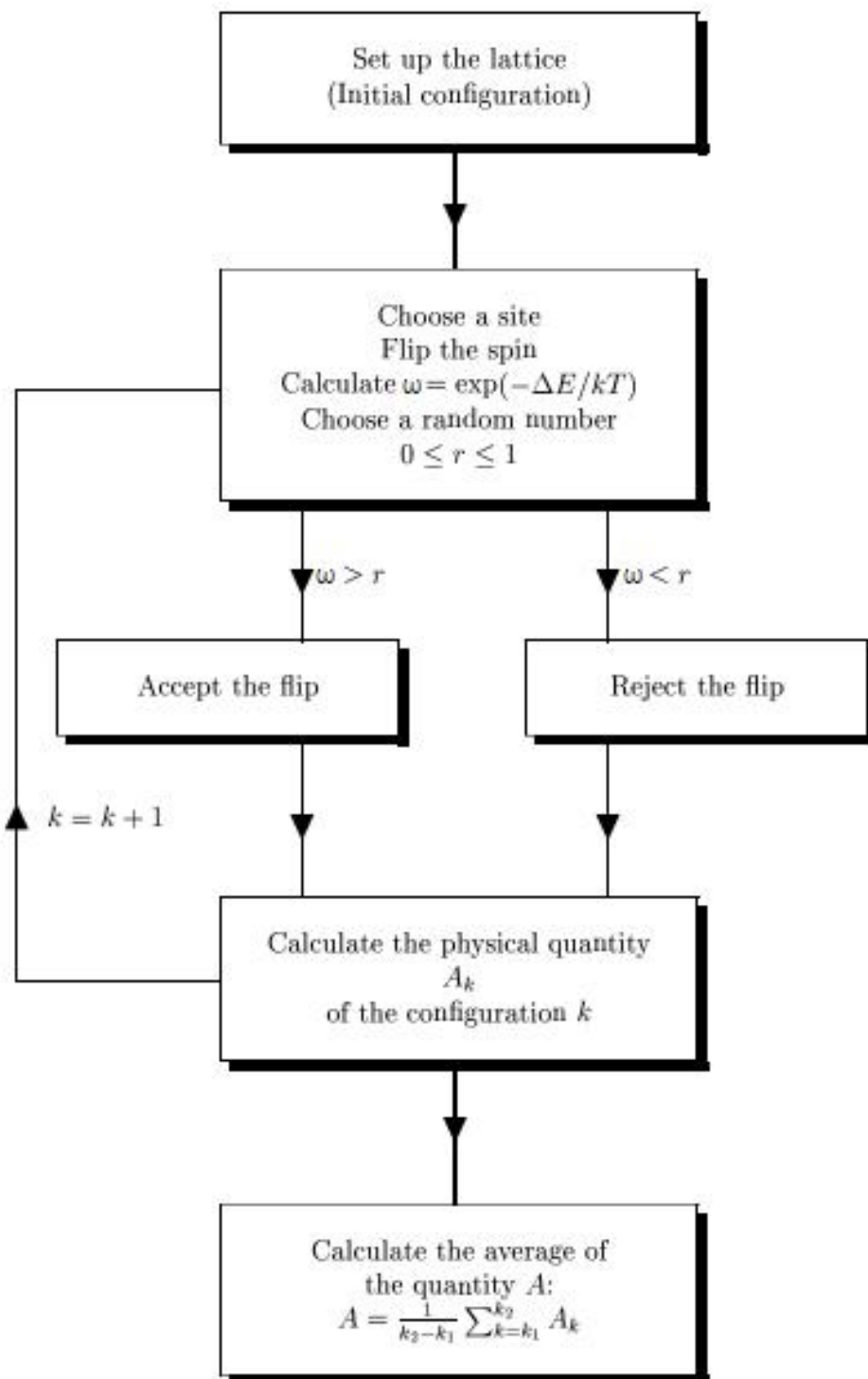


Figure 3.5 The flowchart of Monte Carlo simulation with Metropolis Algorithm.

Go to step 7.

5. If $\Delta E > 0$, calculate $\omega = e^{-\beta\Delta E}$.
6. Compare ω with a random number r . If $r \leq \omega$, then accept the new configuration, else we keep the old configuration.
7. The next step is to update various expectations values.
8. The steps (2)-(7) are then repeated in order to obtain a sufficiently good representation of states.
9. Each time you sweep through the lattice, i.e., when you have summed over all spins, constitutes what is called a Monte Carlo cycle. You could think of one such cycle as a measurement. At the end, you should divide the various expectation values with the total number of cycles. You can choose whether you wish to divide by the number of spins or not. If you divide with the number of spins as well, your result for e.g., the energy is now the energy per spin.

The crucial step is the calculation of the energy difference and the change in magnetization. This part needs to be coded in an as efficient as possible way since the change in energy is computed many times. In the calculation of the energy difference from one spin configuration to the other, it can be limited the change to the flipping of one spin only. For the Ising model in two dimensions it means that there will only be a limited set of values for ΔE . Actually, there are only five possible values. To see this, select first a random spin position x,y and assume that this spin and its nearest neighbors are all pointing up. The energy for this configuration is $E = 4J$, yielding $\Delta E = 8J$.

$$\begin{array}{ccccccc}
 & & & \uparrow & & & \uparrow \\
 E = -4J & & \uparrow & \uparrow & \uparrow & \Rightarrow & E = 4J & & \uparrow & \downarrow & \uparrow \\
 & & & \uparrow & & & & & \uparrow & & \uparrow
 \end{array}$$

The four other possibilities are as follows

$$E = -2J \quad \begin{array}{c} \uparrow \\ \downarrow \uparrow \uparrow \\ \uparrow \end{array} \quad \Rightarrow \quad E = 2J \quad \begin{array}{c} \uparrow \\ \downarrow \downarrow \uparrow \\ \uparrow \end{array}$$

with $\Delta E = 4J$,

$$E = 0 \quad \begin{array}{c} \uparrow \\ \downarrow \uparrow \uparrow \\ \downarrow \end{array} \quad \Rightarrow \quad E = 0 \quad \begin{array}{c} \uparrow \\ \downarrow \downarrow \uparrow \\ \downarrow \end{array}$$

with $\Delta E = 0$,

$$E = 2J \quad \begin{array}{c} \downarrow \\ \downarrow \uparrow \uparrow \\ \downarrow \end{array} \quad \Rightarrow \quad E = -2J \quad \begin{array}{c} \downarrow \\ \downarrow \downarrow \uparrow \\ \downarrow \end{array}$$

with $\Delta E = -4J$ and finally

$$E = 4J \quad \begin{array}{c} \downarrow \\ \downarrow \uparrow \downarrow \\ \downarrow \end{array} \quad \Rightarrow \quad E = -4J \quad \begin{array}{c} \downarrow \\ \downarrow \downarrow \downarrow \\ \downarrow \end{array}$$

with $\Delta E = -8J$. This means in turn that it could be constructed an array which contains all values of $e^{\beta\Delta E}$ before doing the Metropolis sampling. Else, it would have to be evaluated the exponential at each Monte Carlo sampling. For the two-dimensional Ising model there are only five possible values. It is rather easy to convince oneself that for the one-dimensional Ising model only three possible values exist (Jensen M.H, 2007).

CHAPTER FOUR
DEPENDENCE ON DILUTION OF CRITICAL
AND COMPENSATION TEMPERATURES OF A TWO DIMENSIONAL
MIXED SPIN-1/2 AND SPIN-1 SYSTEM

4.1 Introduction

Recently, ferrimagnetic (i.e., mixed spin) systems consist of two sublattices have compensation temperature T_{comp} have been attached to attention due to technological applications such as magneto-optical materials. This kind of materials can be applied to writing and erasing in high-density magneto-optical recording media since they have compensation temperature T_{comp} . Therefore, theoretical studies for mixed spin systems may be give useful results to examine properties of the ferrimagnetic materials.

Compensation point in ferrimagnetic materials are observed below the Néel temperature (Néel, 1948) which is known as critical temperature T_c . Sublattices in ferrimagnetic materials have inequivalent moments with interacting antiferromagnetically. At low temperatures, these inequivalent moments are antiparallel but do not cancel (Néel, 1948; Buendia & Novotny, 1997). However, sublattices compensate each other completely at $T = T_{comp}$ below critical temperature T_c owing to the different temperature dependencies of the sublattice magnetization. Hence compensation point occur in ferrimagnetic system. At $T = T_{comp}$, the total magnetization of the system vanishes. At the compensation point of ferrimagnetic material, only a small driving field is required to reverse the sign of magnetization of locally heating magnetic domain by a focused laser beam. Hence writing and erasing processes can be achieved at this point.

To develop high-density magneto-optical recording materials, many complex two- and three-dimensional ferrimagnetic materials have been experimentally synthesized such as organometallic ferrimagnets (Tamaki et al., 1992), networks of the mixed-metal material (Drillon et al., 1983; Decurtins et al., 1994) and ferrimagnetic amorphous oxides containing Fe^{3+} ions (Srinivasan et al., 1991).

The conditions for the appearance of a compensation point as well as the composition dependencies of the transition and the compensation temperatures have been extensively investigated by a variety of techniques, for example, Cluster Variational Method (Balcerzak et al., 2002), Effective-Field Theory (Kaneyoshi, 1987, 1988, 1989, 1990; Siqueira & Fitipaldi, 1986; Li & Kaneyoshi, 1988; Benayad et al., 1989; Benyoussef et al., 1994), renormalization group theory (Schofield & Bowers, 1980; Quadros & Salinas, 1994), high temperature series expansions (Hunter et al., 1983; Yousif & Bowers, 1984), mean field theory (Kaneyoshi & Chen, 1991), Bethe-Pierls method (Iwashita & Uryu, 1984). Critical temperatures and exponents of mixed spin-(1/2,1) system with crystal field i.e., single ion anisotropy interaction are studied by finite-size scaling theory with Monte Carlo simulation (Zhang & Yang, 1983). Compensation temperature for two dimensional square lattice under crystal and external fields has been obtained considering next nearest interactions (Buendia & Novotny, 1997; Buendia et al., 1998).

On the other hand, recently, dilution effect on the compensation temperature and magnetic properties of mixed spin systems have been studied and interesting phenomena have been found out. For example, some investigations have been made for mixed spin-1/2 and spin-1 diluted honeycomb lattice by using effective field theory with correlations (Bobák & Jascur, 1995; Xin et al., 1997). In these studies, it has been shown mixed spin system in which two sublattices were independently diluted with different number of non-magnetic atoms has two compensation points which was not predicted in Néel theory when crystal field interaction is neglected. Tricritical point, reentrant phenomena and two compensation points have been found out by using effective field theory in diluted square lattice with crystal field (Xin et al., 1998a). Similarly, in the study of diluted honeycomb lattice, tricritical point, reentrant phenomena and two compensation points have been carried out for negative crystal field (Xin et al., 1997b). Other magnetic and thermal properties of diluted mixed honeycomb and square lattice have been discussed in ref. (Xin et al., 1998b). Dependence of magnetic properties of mixed honeycomb lattice on dilution has been investigated by effective-field theory (Xin et al., 1998c). Similar discussion are made using diluted honeycomb lattice in which two sublattices diluted with equal number of non-magnetic atoms (Benyoussef et al., 1994, Kaneyoshi, 1995). In a recent study, numerical and analytical results is

given for the magnetic ordering in a bond-diluted spin-1/2 and spin-1 Ising system on a honeycomb lattice with transverse field (Shi-Lei, 2002).

As it can be seen from pervious theoretical studies that to dilute the ferrimagnetic lattice with vacancies such as non magnetic atoms, non-occupied sites play important role on the compensation and critical temperature as well as in others magnetic properties of the system. Therefore, to understand the effects of the dilution on the systems is important. Because, non magnetic atoms (or non-occupied sites) can be exist in lattice formation of the materials which are experimentally synthesized.

As mentioned above discussion, it can be clearly concluded that dilution effect on the system is depend on interactions considered Hamiltonian and type of lattice. Therefore, we study behavior of the compensation, critical temperatures and other magnetic and thermal properties of the site-diluted square lattice with Monte Carlo simulation methods.

4.2 Model and Simulation Technique

In this study, we consider randomly diluted ferrimagnetic square lattice which consist of two interpenetrating sublattices which can take the values $\sigma = \pm 1/2$ and $S = \pm 1, 0$. Both of two sublattices are randomly diluted with equal number of non magnetic atom. We underline that in order to observe compensation point next-nearest-neighbor interactions should be taken into account as discussed in ref. (Buendia & Novotny, 1997; Buendia & Liendo, 1997; Landau D.P, Mon K. K & Schuttler H. B., 1994).

In this case, the Hamiltonian is given by

$$H = -J_1 \sum_{\langle nm \rangle} \sigma_i S_j - J_4 \sum_{\langle nmm \rangle} \sigma_i \sigma_k + D \sum_j S_j^2 \quad (4.2.1)$$

where the first sum is over the nearest-neighbor and the second one is over the next-nearest-neighbor spins. J_1 and J_4 parameters define an exchange interaction between

the neighbor spins and D is the crystal field. Note that there is no exchange interaction between the nearest-neighbor and the next-nearest-neighbor sites if there is a non magnetic atom exists in the neighbor site. Similarly, the last term of the Hamiltonian vanishes in case of there is a non magnetic atom instead of a spin variable in the S sublattice. Here, the J_1 , J_4 and D are all in energy units.

We employed standard importance sampling methods (Binder, K., 1979) to simulate the system described by the Hamiltonian (4.2.1) on a $L \times L$ square lattice with periodic boundary conditions. The initial configurations were taken as saturated i.e. both the S and σ sublattices are fully aligned. Equal number of site dilutions per sublattice were distributed randomly after setting the lattice up with spin variables. Configurations were generated by selecting the sites in sequence through the lattice and making single-spin-flip attempts, which were accepted or rejected according to the Metropolis algorithm. Data were generated with 25000 Monte Carlo steps per site after discarding the first 2500 steps over 100 realization for $L = 16, 32$ and 64 with different numbers of non-magnetic atoms.

In order to study the effects of the random site dilution on compensation and critical temperatures, we computed some basic magnetic and thermodynamic quantities like the sublattice magnetization M_A and M_B , the total magnetization M , the magnetic susceptibility χ and the specific heat C for different densities of diluted sites. These quantities are calculated as

$$M_A = \frac{2}{L^2} \left\langle \sum_j S_j \right\rangle \quad (4.2.2)$$

$$M_B = \frac{2}{L^2} \left\langle \sum_i \sigma_i \right\rangle \quad (4.2.3)$$

$$M = \frac{1}{2} (M_A + M_B) \quad (4.2.4)$$

$$\chi = \frac{1}{k_B T} (\langle M^2 \rangle - \langle M \rangle^2) \quad (4.2.5)$$

$$C = \frac{1}{k_B T^2} (\langle E^2 \rangle - \langle E \rangle^2) \quad (4.2.6)$$

where T denotes temperature, E is the internal energy of the system, and k_B is Boltz-

mann constant (here $k_B = 1$).

To determine the compensation temperature T_{comp} from the computed magnetization data, we have found the intersection point of the absolute values of the sublattice magnetization. So, at the compensation point we must have

$$|M_A(T_{comp})| = |M_B(T_{comp})| \quad (4.2.7)$$

$$sign(M_A(T_{comp})) = -sign(M_B(T_{comp})) \quad (4.2.8)$$

with $T_{comp} < T_c$, where T_c is the critical temperature. Compensation temperature appears at temperatures $T < T_c$ where total magnetization is zero, whereas, at the same temperature sublattice magnetization is different from zero.

4.3 Results and Discussion

In order to see the effect of the non-magnetic atoms on the magnetic and thermal behaviors of a two dimensional mixed spin system defined with Eq.(4.2.1), choosing $J_1 = -2$, $J_4 = 8$ and $D = 2.6$ we give the results of 64×64 square lattice for $N = 0, 64, 256, 512$ in Figs. 4.1-6. Here we must state that the nearest-neighbor interaction J_1 in Eq.(4.2.1) does not play a role on the compensation temperature, whereas observation of the compensation temperature depends on the parameters J_4 and D . This point has been discussed in refs. (Buendia & Novotny, 1997; Buendia et. al., 1998). Therefore, in this study, we have particularly focused on the effect of the different dilution rates with non-magnetic atoms N for arbitrary fixed J_1 , J_4 and D . On the other hand, to analyze the effect of the non-magnetic atoms on the critical and compensation temperatures, for fixed $J_1 = -2$, $J_4 = 8$ and two different crystal field values $D = 1.6$ and $D = 2.6$ we give the results of different lattice sizes ($L = 16, 32, 64$) for different densities of diluted site in Figs. 4.7 and 4.8.

Monte Carlo simulation results for spin-1/2 and spin-1 mixed ferrimagnetic square lattice which is described by Eq. (4.2.1) are as follow: Firstly, in order to see temperature dependencies of sublattice magnetization M_A , M_B and susceptibility χ of non

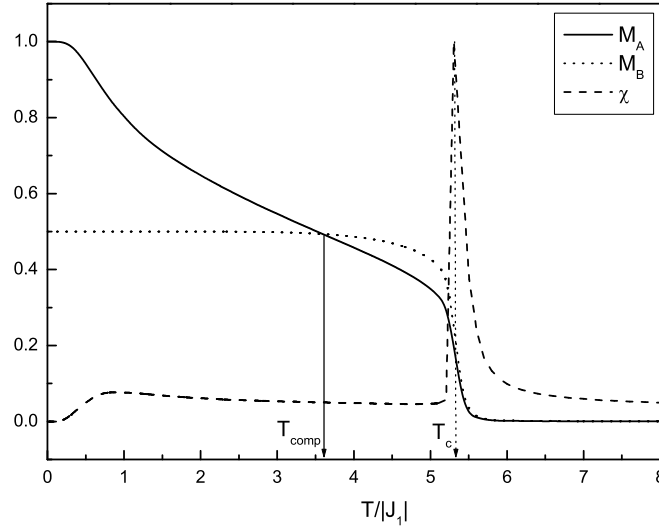


Figure 4.1 The temperature dependencies of sublattice magnetization M_A , M_B and susceptibility χ of non diluted square lattice for $J_1 = -2$, $J_4 = 8$ and $D = 2.6$.

diluted square lattice, these physical quantities are plotted for $J_1 = -2$, $J_4 = 8$ and $D = 2.6$ in Fig. (4.1). As expected that the system has a compensation point near $T/|J_1| = 3.6$ and a critical point near $T/|J_1| = 5.3$ for chosen parameters as seen from Fig. (4.1). The results of M_A , M_B and χ for these parameters are in an excellent agreement with the results of ref. (Buendia & Novotny, 1997).

As stated in previous section , we carried out that diluting the lattice with non magnetic atoms plays significant role, particularly, on compensation and critical temperature as well as other thermal and magnetic properties such as sublattice magnetization, specific heat and susceptibility.

Using Eq. (4.2.4), total magnetization versus reduced temperature is plotted for several numbers of nonmagnetic atoms N ($N = 0, 64, 256, 512$) with $D = 2.6$ and $J_1 = -2$, $J_4 = 8$ in Fig. (4.2). In this figure, there are two temperatures of total magnetization curve which is zero for different numbers of non-magnetic atoms. First temperature value at which total magnetization M is zero corresponds to compensation temperature point and, on the other hand, second temperature value at which $M = 0$ corresponds to critical temperature point. One can see some quantitative differences in the total

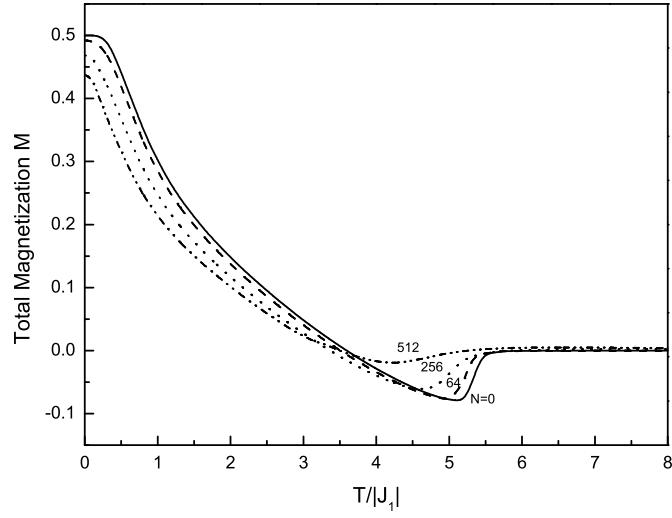


Figure 4.2 Total magnetization M versus reduced temperature $T/|J_1|$ for different N with $J_1 = -2$, $J_4 = 8$ and $D = 2.6$.

magnetization curves for different number of non-magnetic atoms, but it is hard to comment on this naive picture about dependence on dilution of the critical and compensation temperatures. However, it might be also predicted that the compensation and critical points appear near $T/|J_1| = 3.6$ and $T/|J_1| = 5.3$ for different numbers non-magnetic atoms.

For different N ($N = 0, 64, 256, 512$) and fixed $J_1 = -2$, $J_4 = 8$, $D = 2.6$ values, behavior of the compensation and critical temperatures of spin-1 and spin-1/2 sublattice magnetization M_A and M_B given Eqs. (4.2.2) and (4.2.3) are separately demonstrated in Figs. (4.3) and (4.4), respectively. As seen from these figures, sublattice magnetization is different from zero at compensation temperature values while as seen in Fig. 4.2, the total magnetization value is zero at the compensation point for all values of N . These two figures inform us about behavior of the compensation points for different N values. Indeed, it is possible to obtain the compensation points for different N values if M_A is mapped onto M_B in the same figure as well as in Fig. 4.1. The first crosses in the sublattice magnetization curves of M_A and M_B correspond to the compensation points. One can easily predict from these figures that the compensation temperatures decrease as the number of non-magnetic atoms N increases. The dilution dependence of compensation temperature which we have obtained from Figs. 4.3 and 4.4 is given

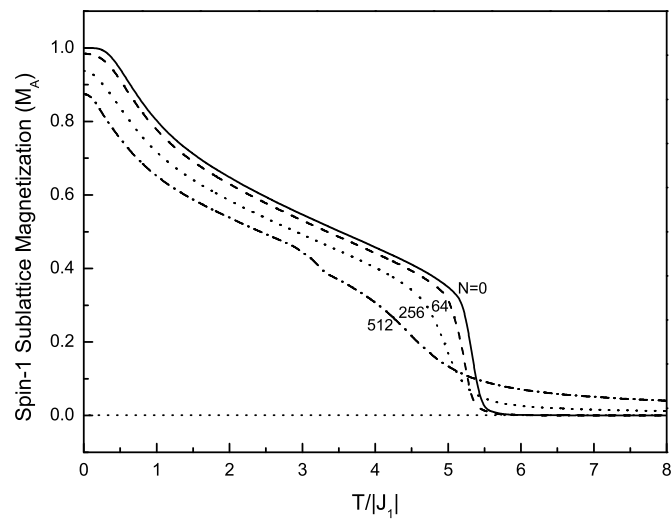


Figure 4.3 Spin-1 sublattice magnetization M_A versus reduced temperature $T/|J_1|$ for different N with $J_1 = -2$, $J_4 = 8$ and $D = 2.6$.

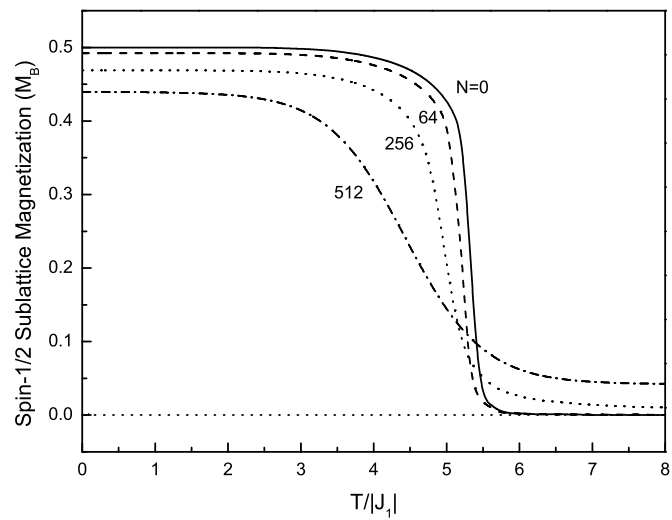


Figure 4.4 Spin-1/2 sublattice magnetization M_B versus reduced temperature $T/|J_1|$ for different N with $J_1 = -2$, $J_4 = 8$ and $D = 2.6$.

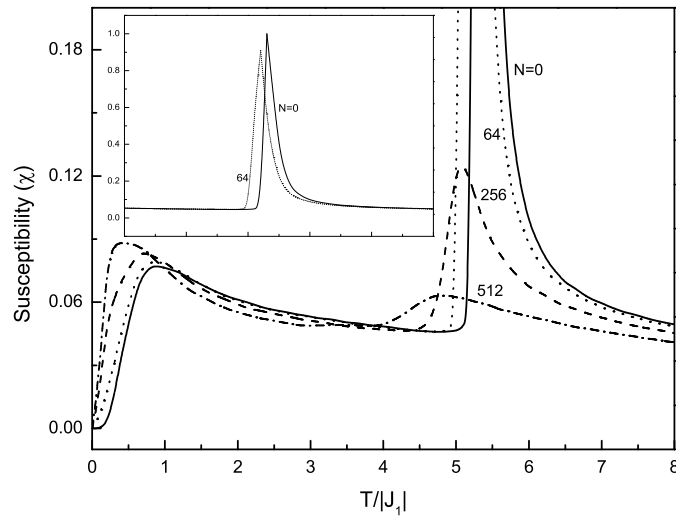


Figure 4.5 Magnetic susceptibility χ versus reduced temperature $T/|J_1|$ for different N with $J_1 = -2$, $J_4 = 8$ and $D = 2.6$. In the inset, susceptibility curves for $N = 0, 64$ are given.

above. However, it is still hard to comment on these figures about the dependence on dilution of the critical temperature points.

Magnetic susceptibility defined Eq. (4.2.5) versus reduced temperature has been plotted in Fig. (4.5) for several numbers of non-magnetic atoms N for the same values of parameters. As it can be seen from Fig. (4.5) that there are two relatively sharp peaks and humps in magnetic susceptibility curves. Each curve in the second peaks and humps indicate the phase transition from ferrimagnetic to paramagnetic at critical temperature, however, the curves in the first hump originate from D and they do not indicate a compensation temperature or a phase transition in the model. The effect of numbers of nonmagnetic atoms N on the two humps can be clearly seen in this figure. In fact, in the second hump, the maximum points of the susceptibility curves become smaller and slide to left with increasing N values, which means critical temperature decreases with increasing N , while in the first hump, the maximum points of the susceptibility curves getting increased and slide to the left with increasing N values as also seen from inset figure in Fig. (4.5). The reason for increment in the maxima of the susceptibility curves in the first hump probably arises from that the increasing N

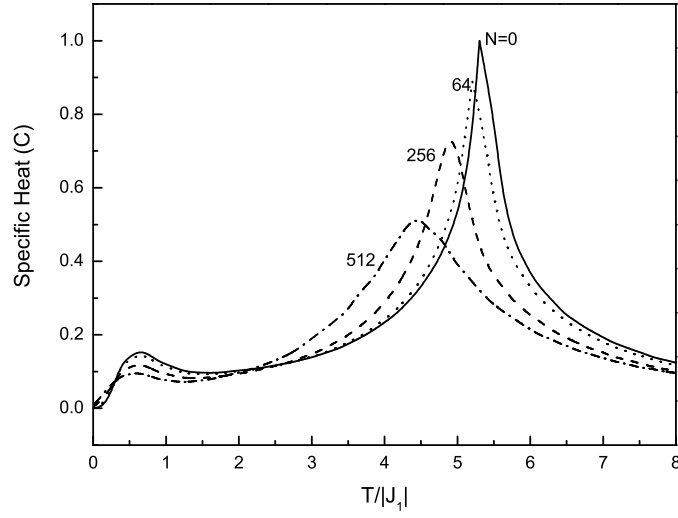


Figure 4.6 Temperature dependence of the specific heat C for different N values with $J_1 = -2$, $J_4 = 8$ and $D = 2.6$.

values may strengthen the effects of D . The existence of the non-magnetic atoms on the lattice also affects the shapes of these humps in the susceptibility curves.

Similarly, temperature dependence of the specific heat given Eq. (4.2.6) is plotted in Fig. (4.6) for different N values and fixed $J_1 = -2$, $J_4 = 8$, $D = 2.6$. There are also two relatively sharp humps and peaks in specific heat. The first hump which behaves ambiguously probably may also originate from D as well as first humps in magnetic susceptibility. The second humps and peaks indicate the phase transition. As seen from Fig. (4.6), maxima of the specific heat curves becomes smaller and slide to left with increasing N values. It means critical temperature decreases with increasing N .

In order to understand effect of non magnetic atoms (i.e., dilution) on the compensation temperature T_{comp} and critical temperature T_c , using fixed $J_1 = -2$, $J_4 = 8$ and for two different crystal field values $D = 1.6$ and $D = 2.6$ with different lattice sizes, temperature versus different N values are plotted in Fig. (4.7) and Fig. (4.8). As it can be seen from Fig. (4.7), non-magnetic atoms play an important role on the critical temperature of the system. Indeed, critical temperature of diluted system linearly decreases for fixed J and D with increasing density of diluted site in the lattice. Similarly, the crystal field also affects the critical temperature of the system. It can be seen from Fig. 4.7 that the critical temperature of the system decreases systematically

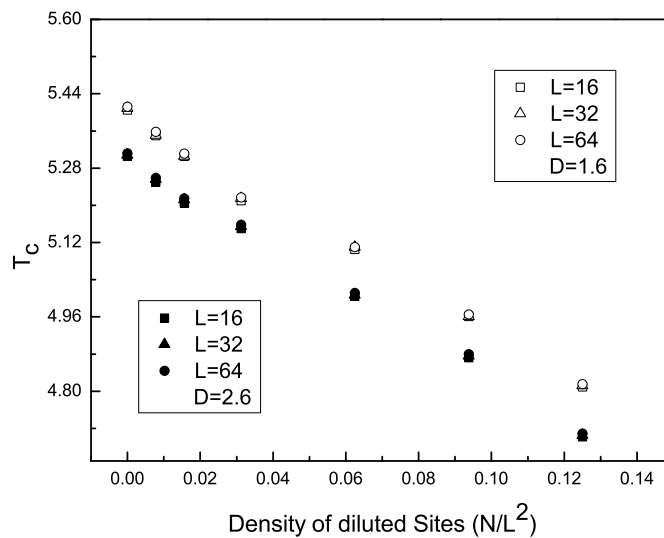


Figure 4.7 Dependence on the density of diluted sites of the critical temperature for fixed $J_1 = -2$, $J_4 = 8$ and two different crystal field values $D = 1.6$ and $D = 2.6$.

when the crystal field value is increased. On the other hand, we can say that the critical temperature of the diluted mixed system does not affected from the lattice size.

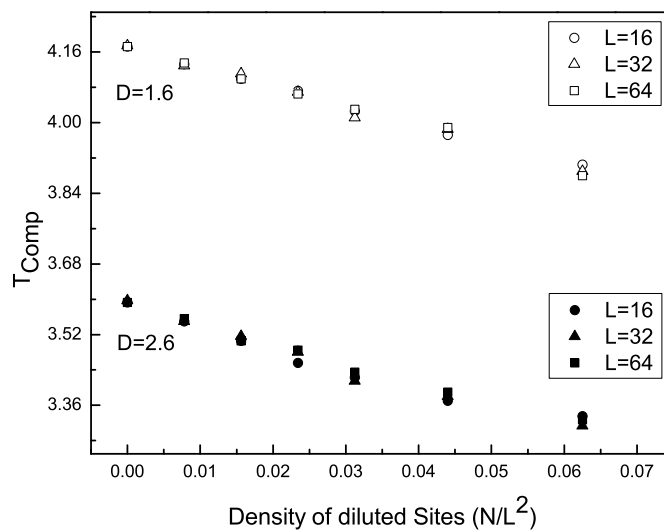


Figure 4.8 Dependence on the density of diluted sites of the compensation temperature for fixed $J_1 = -2$, $J_4 = 8$ and two different crystal field values $D = 1.6$ and $D = 2.6$.

Fig. 4.8 shows the dependence on density of diluted sites of the compensation temperature for same values values in fig. (4.7) with different lattice sizes. Similarly, non-magnetic atoms and the crystal field play a significant role on the compensation temperature of the system as well as the critical temperature. As it can be seen from Fig. 4.8, the compensation temperature of diluted system linearly decreases for fixed J and D with increasing density of diluted sites in the lattice, and on the other hand, compensation temperature of the system decreases systematically when the crystal field value is increased. Finally, we can say that compensation temperature of the diluted mixed system does not affected from lattice size as well as the critical temperature.

CHAPTER FIVE

COMPENSATION TEMPERATURE OF 3D MIXED FERRO-FERRIMAGNETIC TERNARY ALLOY

5.1 Introduction

During the past several decades there has been intensive interest in the experimental and theoretical research of the ferrimagnetic compounds because of their potential device applications in technologically important materials such as high-density magneto-optical recording (Tanaka et al., 1987; Alex et al., 1990). In contrast to ferromagnets and antiferromagnets, there is in ferrimagnetic materials two inequivalent moments, interacting antiferromagnetically. These materials have a special temperature point at which the resultant magnetization vanishes below the transition temperature T_c (Néel, 1948), because of the different dependence of the sublattice magnetization on temperature. This point can appear at a temperature below the critical one, where the sublattice magnetization cancel exactly each other, so it is called compensation point.

The occurrence of a compensation point is of highly technological importance, because to change the sign of resultant magnetization require only a small driving field at this point. It has been shown experimentally that the coersive field is very strong at the compensation point favoring the creation of small, stable, magnetic domains (Hansen, 1987; Hernando & Kulik, 1994; Multigner et al., 1996). In magneto-optical recording devices the coercivity is changed by local heating of the media with a focused beam. Temperature dependence of the coercivity near the compensation point can be applied to writing and erasing in high-density magneto-optical recording media. Direct overwrite capability has been indicated in magneto-optic thin films with compensation temperatures higher than room temperatures (Mansuripur, 1987).

In the past two decades there has been a growing interest in the preparation and study of the magnetic properties of molecular-based magnets is to obtain novel molecular magnetic materials with high transition temperature (Ferlay et al., 1995;

Buschmann et al., 1997; Day & Underhill, 1999; Holmes & Giolami, 1999). The

superiorities of these type of magnets can be obtained through a choice of proper spin sources (e.g, transition metal ions, organic radicals) and coordinating ligands when they compared to classical-metal and metal-oxides ones. In consequence of the multi-compensation behavior appearing in the mixed ternary molecular magnets gave a new impetus to this area research. Notably, the multi-metal prussian blue analogs are a special class of among molecular-based magnets. These materials may display one or even two compensation temperatures such as $(X_p^{II}Mn_{1-p}^{II})_{1.5}[Cr^{III}(CN)_6].nH_2O$ ($X^{II} = Ni^{II}, Fe^{II}$) (Ohkoshi et al., 1997a) or $(Ni_p^{II}Mn_q^{II}Fe_r^{II})_{1.5}[Cr^{III}(CN)_6].nH_2O$ (Ohkoshi et al., 1999), respectively and some of these compounds with high critical temperatures T_c (Mallah et al., 1993; Entley & Girolami, 1994, 1995; Ferlay et al., 1995; Sato et al., 1996).

Furthermore Prussian blue analogs are available for the molecular design of magnetic properties because various types of metal ions can be conveniently incorporated as spin centers (Güdel et al., 1973; Klenze et al., 1980; Gadet et al., 1992; Mallah et al., 1993; Entley & Girolami, 1995; Ferlay et al., 1995; Sato et al., 1996). Thus the magnetic properties like transition temperature, coercive field, etc. of these multi-metal Prussian blue analogs can be tuned during the synthesis process by changing the composition of different transition metal ions.

Up to the present, many striking properties have been discovered in these materials, for example, occurrence of one (Ohkoshi et al., 1997a) or even two (Ohkoshi et al., 1999) compensation points, magnetic pole inversion (Ohkoshi et al., 1997a, Ohkoshi & Hashimoto, 1999a), the photoinduced magnetization effect (Sato et al., 1996; Pejakovic et al., 2001). The reason of such an unusual behavior in the Prussian blue analogs is that these compounds can incorporate both ferromagnetic ($J > 0$) and antiferromagnetic ($J < 0$) superexchange interactions between the neighboring metal ions through the cyanide bridging ligands. Therefore, these magnets are called mixed ferro-ferrimagnets.

In general, the theoretical investigations of magnetic properties of the multi-metal Prussian blue analogs are difficult because of their structural complexity. Up to now analytical descriptions of their properties have been performed in the mean-field ap-

proximation (MFA) (Ohkoshi & Hashimoto, 1999b; Bobak & Dely, 2004), the effective field theory (Bobak et al., 2002), variational method in pair approximation (Tucker et al., 1998), and Monte Carlo simulation method (Carling et al., 2001; Buendia & Villarroel, 2007; Dely et al., 2009).

Prussian blue analogs have been studied extensively in last decade in search of three-dimensional molecular magnetic materials with high transition temperature (Gadet et al., 1992; Ferlay et al., 1995; Entley & Girolami, 1995). Their common cubic structure allows an easy modification of their spin structures and consequently their magnetic properties, which are difficult to observe in conventional metal oxide magnets, due to various types of magnetic interactions involved. The interaction between the neighboring spins is strongly influenced by the existence of cyanide (CN) bridging ligands which are the main element responsible for the above mentioned magnetic properties.

Recent researches introduce a simple ternary ferro-ferrimagnetic alloy model of the type AB_pC_{1-p} consisting of different Ising spins which includes both ferromagnetic $J_{AB} > 0$ and antiferromagnetic $J_{AC} < 0$ interactions. Magnetic properties of this model have been performed by changing the proportion of magnetic ions p and interaction ratio $R = |J_{AC}|/J_{AB}$. There are a few studies in mixed ferro-ferrimagnetic ternary alloy Ising model by using Monte Carlo (MC) simulation method. One of these works was presented by Buendía and Villarroel (Buendía & Villarroel, 2007) in square lattice. They studied the behavior of compensation temperature of ternary compound in this work. Taking this into account, in this study we carried out the MC simulation method in three-dimensional(3D) lattice for the studies of magnetic properties of the AB_pC_{1-p} ternary alloy corresponding to the Prussian blue analog of the type $(Ni_p^{II}Mn_{1-p}^{II})_{1.5}[Cr^{III}(CN)_6].nH_2O$ (Ohkoshi et al., 1997a) by using the same hamiltonian in (Buendía & Villarroel, 2007).

To simulate the structure of this model, we consider that A and X (X=B or C) magnetic ions are alternately connected and have different spins $S^A = 3/2$, $S^B = 1$, and $S^C = 5/2$, respectively. The p parameter can control the type of magnetic ordering and denotes the proportion of magnetic ions B and C which are randomly distributed

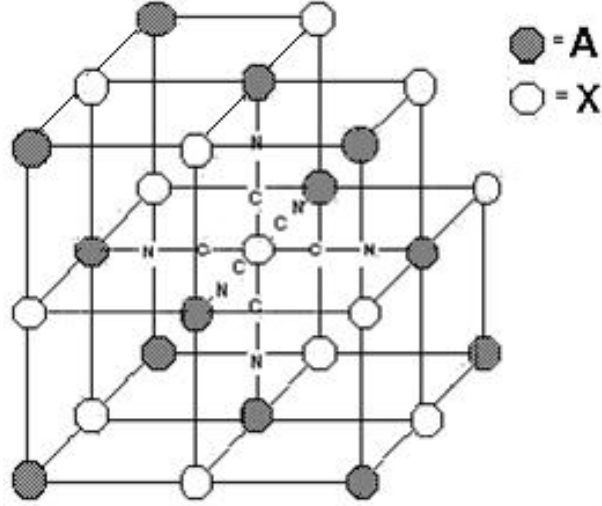


Figure 5.1 The crystallographic structure of prussian blue analog with two interpenetrating cubic lattices.

over the lattice.

The purpose of this work is to clarify the effects of the concentration p and the interaction ratio R on the magnetic properties of the three-dimensional ferro-ferrimagnetic ternary alloy model corresponding to the prussian blue analog with MC simulation method.

5.2 Model and Its Monte Carlo Simulation

We consider a mixed ferro-ferrimagnetic ternary alloy model of the type AB_pC_{1-p} consisting of three kinds of magnetic ions A, B, and C with different Ising spins $S_i^A = 3/2$, $S_j^B = 1$, and $S_j^C = 5/2$, respectively. To be consistent with a structure of the Prussian blue analog (Ohkoshi et al., 1997a), we assume that the S_i^A and either S_j^B or S_j^C spins, which are randomly distributed in the three dimensional lattice, are linked in an alternating fashion and include both ferromagnetic $J_{AB} > 0$ and antiferromagnetic $J_{AC} < 0$ interactions.

To simulate this model, we performed Metropolis Monte Carlo simulation algorithm (Binder, K., 1979) to the on a $L \times L \times L$ three dimensional lattice with periodic

boundary conditions. Configurations were generated by making single-spin-flip attempts, which were accepted or rejected according to the Metropolis algorithm. We choose $L = 20$ for the simulations. Data were generated by using 50000 Monte Carlo steps per site after discarding 10000 steps.

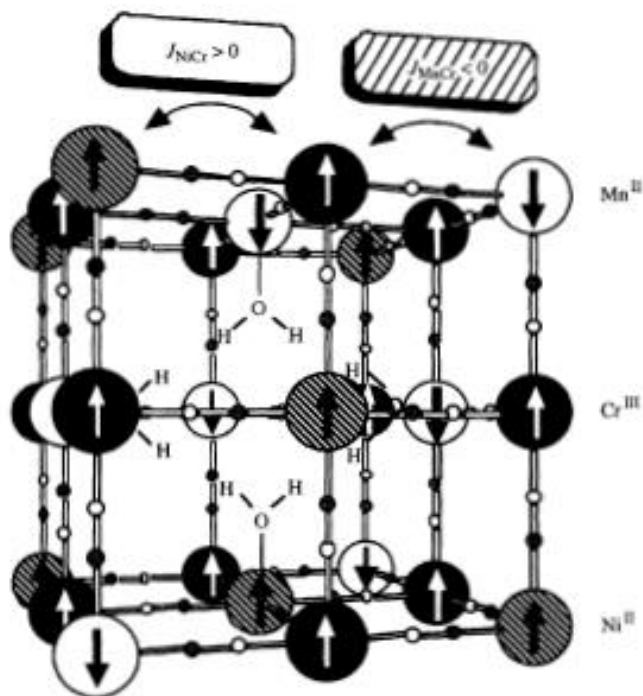


Figure 5.2 Schematic illustration of a ternary metal Prussian blue analogue containing both ferromagnetic and antiferromagnetic interactions. Cr^{III} and either Ni^{II} or Mn^{II} , which are randomly incorporated in the lattice, are linked in an alternating fashion (Hashimoto K. & Ohkoshi S., 1999).

3D mixed Ising AB_pC_{1-p} model includes two interpenetrating cubic sublattices, each one of $L^3/2$ sites as in Fig. 6.1. The A ($S_A = \pm 3/2, \pm 1/2$) ions of one sublattice are alternately connected with B ($S_B = \pm 1, 0$) or C ($S_C = \pm 5/2, \pm 3/2, \pm 1/2$) ions randomly located on the other sublattice with concentration p or $1 - p$, respectively. We choose these spin values corresponding to the Prussian blue analog of the type $(Ni_p^{II}Mn_{1-p}^{II})_{1.5}[Cr^{III}(CN)_6].nH_2O$ (see fig. 5.2). Both localization of spin ions and different interaction parameter in lattice of this compound can be seen in experimental work in Ohkoshi et al. (Ohkoshi et al., 1997a).

The hamiltonian of the model is the following:

$$H = - \sum_{\langle nn \rangle} S_i^A [J_{AB} S_j^B \varepsilon_j + J_{AC} S_j^C (1 - \varepsilon_j)] - J_{AA} \sum_{\langle nnn \rangle} S_i^A S_k^A \quad (5.2.1)$$

where ε_j takes the value of unity if there is a spin X(B or C) at the site j, if not is zero. The first sum in Eq. (5.2.1) is over the nearest-neighbor(nn) and the second one is over the next-nearest-neighbor(nnn) spins. The nearest neighbor interactions are chosen as $J_{AB}(J_{NiCr}) > 0$ and $J_{AC}(J_{MnCr}) < 0$ corresponding to Prussian blue analog.

The sublattice average magnetizations per site are calculated,

$$M_A = \frac{2}{L^3} \left\langle \sum_i S_i^A \right\rangle, \quad M_B = \frac{2}{L^3} \left\langle \sum_{j=1}^{N_B} S_j^B \right\rangle, \quad M_C = \frac{2}{L^3} \left\langle \sum_{j=1}^{N_C} S_j^C \right\rangle \quad (5.2.2)$$

where N_B denotes the number of B ions $N_B = pL^3/2$, whilst N_C represents the number of C ions $N_C = (1 - p)L^3/2$ on the same cubic lattice.

5.3 Results and Discussion

The simulation results of the ternary alloy model AB_pC_{1-p} have been given and also the dependence of the critical and compensation temperatures on the concentration and other interaction parameters in the Hamiltonian have been discussed in this section. It is also noted that the critical temperature of the system for different interaction ratios and concentrations have been obtained by using the method of the finite-size scaling (Binder, K., 1979).

We show the critical temperature of the 3D mixed ternary model with $J_{AA} = 0$ as a function of R for various values of p in Fig. 5.4. When $p = 1$ and $p = 0$, the model reduces to the ferromagnetic mixed spin-3/2 and spin-1 and ferrimagnetic mixed spin-3/2 and spin-5/2 Ising system, respectively. It is easy to see from Fig. 5.4 that there is a special value of the exchange interaction ratio R_c . When $R = R_c = 0.513$, the critical temperature has a fixed value of $T_c = 5.47$. Namely, T_c does not depend on concentration p at this special value. In other words, the critical temperature of the

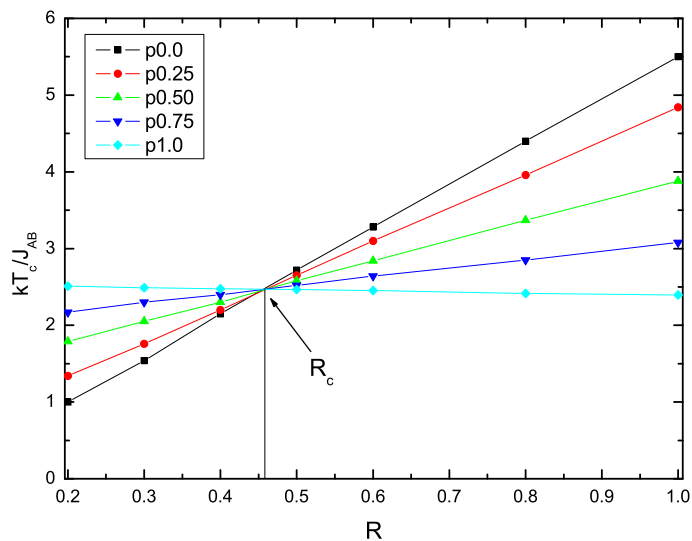


Figure 5.3 Dependence of the critical temperature on interaction ratio R for different values of p in two-dimensional lattice, for $J_{AA} = 0.0$.

mixed spin-3/2 and spin-1 Ising system is equal to that of the mixed spin-3/2 and spin-5/2 Ising one for R_c value. Thus, neither the spin-1 ions nor spin-5/2 ions substitution to system change the critical temperature in this special case.

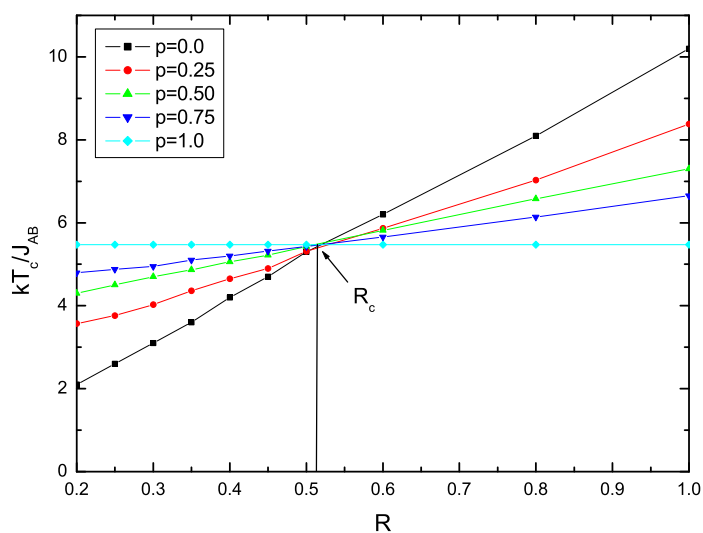


Figure 5.4 Dependence of the critical temperature on interaction ratio R for different values of p in three-dimensional lattice, for $J_{AA} = 0.0$.

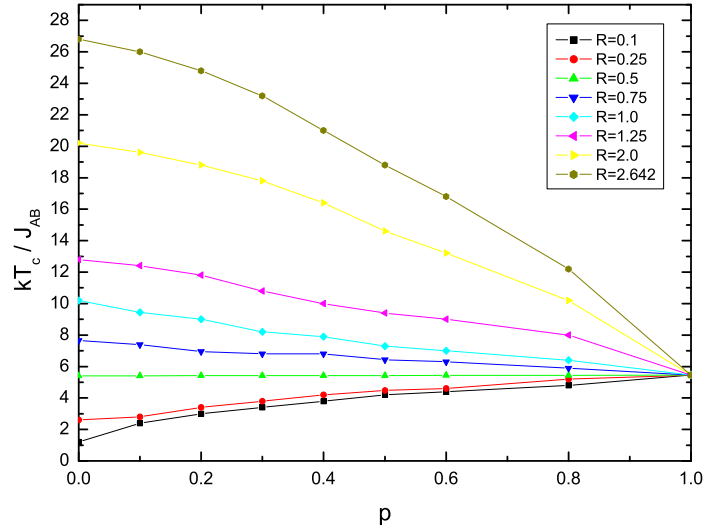


Figure 5.5 Dependence of the critical temperature on the concentration p in three-dimensional lattice when the ratio R is changed, for $J_{AA} = 0.0$.

This result may be compared with the counterparts in the literature. First one Bobák et al. studied in (Bobak et al., 2003) for the ternary alloy composed of spins $S^A = 3/2$, $S^B = 1$ and $S^C = 5/2$. They have obtained $R_c = 0.4781$ value by using mean field approximation and the second one is presented by Buendía and Villarroel (Buendía & Villarroel, 2007) in square lattice by using MC simulation method ($R_c = 0.49$). The value of $R_c = 0.513$ obtained in this work is very close to above mentioned values. If we compare Fig. 5.4 with two dimensional work (see fig. 5.3) in Buendía & Villarroel (Buendía & Villarroel, 2007) the results obtained this work is more similar to the previous work in the literature as an example Bobák et al. (Bobak et al., 2003).

The dependence of critical temperature of the system on the interaction ratio R for different values of p is very different above and below of R_c . Indeed, when $R < R_c$, the critical temperature of the mixed spin-3/2 and spin-5/2 system is smaller than mixed spin-3/2 and spin-1 system. On the contrary, when $R > R_c$, the critical temperature of the mixed spin-3/2 and spin-5/2 system has the highest value and also we can say that T_c of the system depends linearly on R parameter, as seen Fig. 5.4.

In Fig. 5.5 we indicate the critical temperature of the system as a function of p for

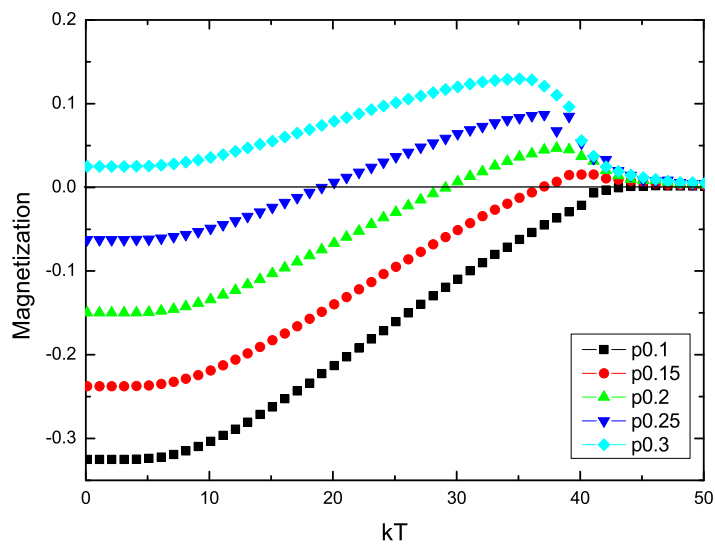


Figure 5.6 The temperature dependence of the total magnetization for different values on concentration p for ($J_{AA} = 7.5, R = 1.0$) to observe compensation temperature in 2D model.

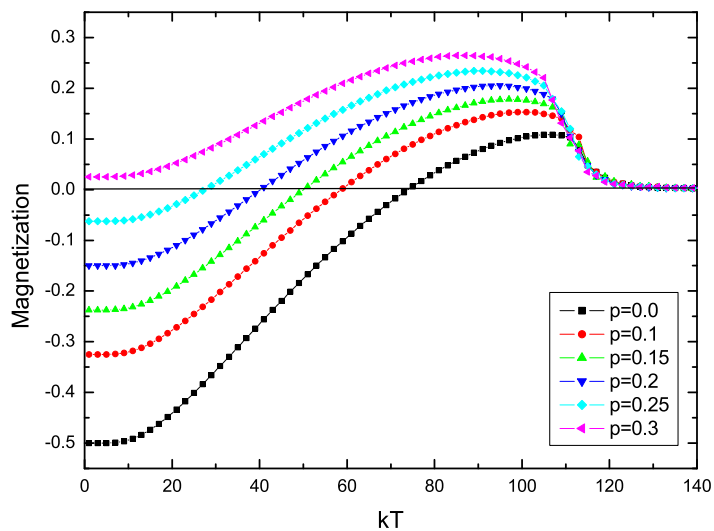


Figure 5.7 The temperature dependence of the total magnetization for different values on concentration p for ($J_{AA} = 7.5, R = 1.0$) to observe compensation temperature in 3D model.

several values of R for $J_{AA} = 0$. The lines in Fig. 5.5 represent a part of the second-order transition separating the paramagnetic and ferrimagnetic phases. This figure clearly shows that the critical temperature of the three dimensional AB_pC_{1-p} system is changed by the p concentration when interaction ratio R has fixed values. It is seen from Fig. 5.5 that the critical temperature of the system increases with increasing of p when $R < R_c$. On the contrary, when $R > R_c$ the critical temperature of the system decreases with increasing of p for fixed values of R . However, when the value of R is equal to R_c the critical temperature of the system denoted by triangle-line in fig. 5.5 is independent of the concentration p . The straight line in this figure shows R_c value obtained this work as $R_c = 0.513$ and critical temperature of the three dimensional ternary model is consistent with previous result of Bobák et al. (Bobák et al., 2003).

In present study, it is observed that the system has one compensation point when there is no next-nearest neighbor interaction between A ions ($J_{AA} = 0$), however, it has one or multi compensation points when A ions have next-nearest neighbor interaction each other in lattice ($J_{AA} \neq 0$) and other conditions are satisfied. The value of J_{AA} used in this study is chosen based on previous MC study of Buendía & Villarroel (Buendía & Villarroel, 2007). It is clearly seen that compensation behavior is strongly affected by the concentration and interaction parameters but there is no compensation point for all R and p values. The dependence of compensation behavior on concentration and interaction parameters has been discussed below.

When the system has been simulated in intervals $0.0 \leq p \leq 1.0$ and $0.1 \leq R \leq 2.642$, there exists compensation behavior in the range $0.0 \leq p \leq 0.4$ for some value of R . Namely, there is no compensation point when $p > 0.4$ and the maximum compensation points are observed at $p = 0.3$. For this value of p when $R > R_c$, there is one compensation temperature in all R interaction ratio values. Also, when $R = 2.642$ (the interaction ratio which is special value in Prussian blue analog in ref Ohkoshi et al., 1997c), the system has compensation points for $p \leq 0.4$.

It is shown in Fig. 5.7 that the temperature dependencies of the total magnetization of the system for several values of p , when the fixed value of $R = 1.0$. According to this figure, in the interval of $0.0 \leq p < 0.3$ there exists compensation behavior. How-

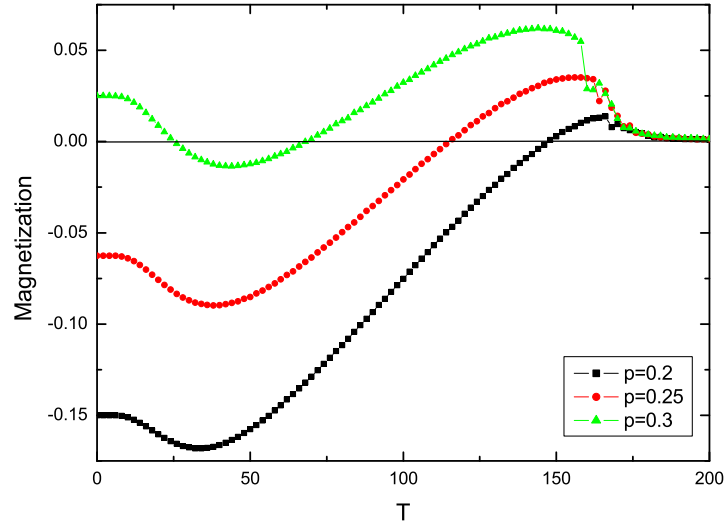


Figure 5.8 The total magnetization as a function of temperature when special value of $R = 2.642$ and $J_{AA} = 7.5$ for different values of p .

ever, there is no compensation temperature in two-dimensional (2D) work (Buendía & Villarroel, 2007) for $p = 0$ and $p = 0.1$ (see fig. 5.6). We can say that mixed spin-3/2 and spin-5/2 system shows compensation behavior in three-dimensional model as seen Fig. 6.7. In addition, when our result compared to 2D work, it is seen that both critical and compensation temperatures are higher than in their results. It is also noteworthy that, although the compensation temperature depends considerably on concentration p , the critical temperature is independent from it. For $p = 0.0$ and $R = 1.0$, while critical and compensation temperatures are approximately 50 when $J_{AA} = 0.0$, it is seen from fig. 5.7 that they are higher than 50 when $J_{AA} \neq 0$. This result shows that T_{crit} and T_{comp} temperatures are influenced by the existence of next nearest neighbor interaction J_{AA} for chosen parameters $p = 0$ and $R = 1.0$.

In Fig. 5.8 we plot total magnetization as a function of temperature for the fixed value of $J_{AA} = 7.5$ and $R = 2.642$. When the total magnetization varies with temperature in interval of $0.0 \leq p \leq 0.5$, it is seen that there exists a compensation behavior only for $0.2 \leq p \leq 0.3$. While the system has one compensation point for $0.2 \leq p < 0.3$, there are two compensation points at $p = 0.3$. This result shows that the system has multi-compensation behavior with suitable R , p and J_{AA} parameters.

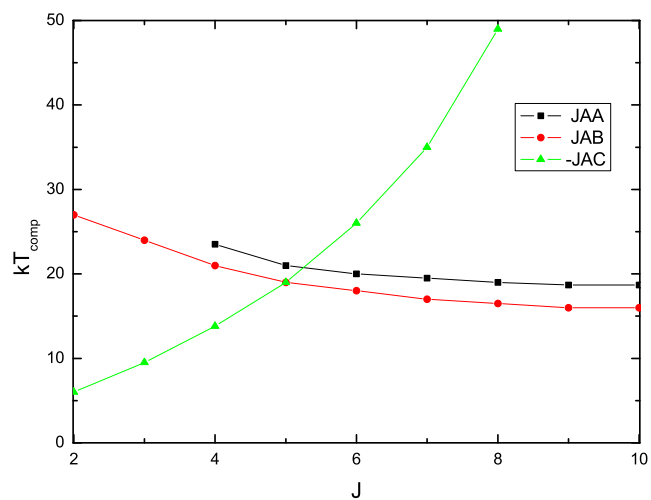


Figure 5.9 Dependence of the compensation temperature T_{comp} on the different interaction parameters in Hamiltonian in 2D model.

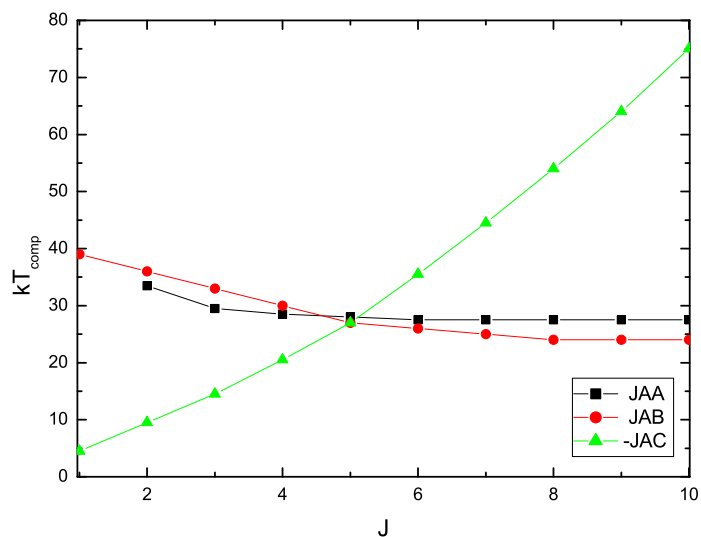


Figure 5.10 Dependence of the compensation temperature T_{comp} on the different interaction parameters in Hamiltonian in 3D model.

The last figure shows dependence of T_{comp} on different interaction parameter in Hamiltonian for a fixed value of concentration parameter ($p = 0.25$). It is seen from Fig. 5.10 that, while T_{comp} depends strongly on $J_{AC}(J_{MnCr})$ parameter, it depends scarcely on $J_{AA}(J_{CrCr})$ and $J_{AB}(J_{NiCr})$ parameters. T_{comp} decreases slowly with increase of J_{AA} and J_{AB} parameters. Contrarily, T_{comp} quickly increases with increase of $-J_{AC}$ parameter. These results indicate that compensation behavior has a strong dependence on the parameter J_{AC} whereas its dependence on J_{AA} and J_{AB} is relatively weak. When this figure compared with in square lattice work in (Buendía & Villarroel, 2007), it is seen that the results of 2D and 3D lattice different from each other. 3D lattice has more extensive interval compensation behavior than 2D lattice (see fig. 5.9).

CHAPTER SIX

THE EFFECTS OF SINGLE-ION ANISOTROPY ON MAGNETIC PROPERTIES OF THE PRUSSIAN BLUE ANALOG

6.1 Introduction

Prussian blue analogs which type of the AB_pC_{1-p} model are new molecular-based magnetic materials (for more details see ref. (Miller, J. S. & Drillon, M., 2005). They have been received considerable attention recently since they have potential application in technology such as magnetic recording media or quantum computing devices (Leuenberger & Loss, 2001). Prussian blue analogs, for instance, $(Fe_p^{II}Mn_{1-p}^{II})_{1.5}[Cr^{III}(CN)_6].nH_2O$ (Ohkoshi et al., 1997a) which is ternary alloy consisting of three different Ising spins $S_A = 3/2$, $S_B = 2$ and $S_C = 5/2$. This ternary alloy has $L \times L \times L$ lattice that consists of two interpenetrating face-centered cubic (fcc) sublattices, each one comprising $L^3/2$ sites. In this lattice formation, the Cr ions of one sublattice are alternately connected with the Fe or Mn ions randomly located on the other sublattice with the concentration p or $1 - p$, respectively. Hence it includes both ferromagnetic ($J_{FeCr} > 0$) and antiferromagnetic ($J_{MnCr} < 0$) super-exchange interactions between the neighboring metal ions through the cyanide bridging ligands due to their fcc structure.

Magnetic Prussian blue analogs show unusual remarkable properties such as the magnetic pole inversion (Ohkoshi et al., 1997a; Ohkoshi & Hashimoto, 1999), photoinduced magnetization (Sato et al., 1996; Pejakovic et al., 2001), inverted magnetic hysteresis loop (Ohkoshi et al., 2001) and the multi-compensation points (Ohkoshi et al., 1997b; Ohkoshi et al., 1999b). It is known that the magnetic properties such as compensation temperature point and critical temperature point of the considered Prussian blue analogs can be tuned during a synthesis process by changing the mixing ratio (i.e. concentration) p of the different incorporated metal ions. Up to now, in order to understand unusual magnetic and thermal behavior of the ternary alloys which contain three various kinds of magnetic ions with different Ising spins, many models which correspond to ternary alloys have been investigated by the use of a mean-field (MFT) (Ohkoshi & Hashimoto, 1999; Bobák & Dely, 2004; Dely & Bobák, 2006, 2007) or

an effective-field theory (EFT) (Bobak et al., 2002), Monte Carlo (MC) simulations (Buendia & Villarroel, 2007; Dely et al., 2009; Dely et al., 2010; Žukovič & Bobák, 2010; Kış Çam & Aydın, 2010) and exact recursion relations on the Bethe lattice (Deviren et al., 2009, Albayrak, 2011).

Although many theoretical studies have been devoted on the Prussian blue analogs, but effect of the single-ion anisotropy on the magnetic properties of these compounds has not been studied extensively. Therefore, in this study, we will investigate the effects of single-ion anisotropy on magnetic properties of the ternary alloy model AB_pC_{1-p} which type of the Prussian blue analog $(Fe_p^{II}Mn_{1-p}^{II})_{1.5}[Cr^{III}(CN)_6].nH_2O$ consisting of three different Ising spins $S_A = 3/2$, $S_B = 2$, $S_C = 5/2$ with help of Monte Carlo simulation method. We will also discuss the concentration parameter p , interaction parameter $R = |J_{AC}|/J_{AB}$ and temperature dependence of the three dimensional ternary alloy model.

6.2 Model and Simulation Method

The Hamiltonian for the three dimensional ferro-ferrimagnetic AB_pC_{1-p} ternary alloy model which correspond to the Prussian blue analog of the type $(Fe_p^{II}Mn_{1-p}^{II})_{1.5}[Cr^{III}(CN)_6].nH_2O$ can be given as

$$\begin{aligned}
 H = & - \sum_{\langle i,j \rangle} S_i^A [J_{AB} S_j^B \epsilon_j + J_{AC} S_j^C (1 - \epsilon_j)] \\
 & - D \left[\sum_{i=1}^{N_A} (S_i^A)^2 + \sum_{j=1}^{N_B} (S_j^B)^2 \epsilon_j + \sum_{j=1}^{N_C} (S_j^C)^2 (1 - \epsilon_j) \right] \\
 & - h \left[\sum_{i=1}^{N_A} S_i^A + \sum_{j=1}^{N_B} (S_j^B) \epsilon_j + \sum_{j=1}^{N_C} (S_j^C) (1 - \epsilon_j) \right]
 \end{aligned} \tag{6.2.1}$$

where $S^A = \pm 3/2, \pm 1/2$, $S^B = \pm 2, \pm 1, 0$ and $S^C = \pm 5/2, \pm 3/2, \pm 1/2$ are spin operators which respectively correspond A, B and C in the ternary alloy model in the form AB_pC_{1-p} . Also ϵ_j is a random variable which takes the value of unity if there is a spin S^B or S^C at the site j , otherwise is zero. In this Hamiltonian, J_{AB} and J_{AC} are the nearest

Monte Carlo steps per site after discarding 10000 steps. The magnetization per site for this model was computed using these relations

$$M_A = \frac{2}{L^3} \left\langle \sum_i S_i^A \right\rangle \quad (6.2.2)$$

$$M_B = \frac{2}{L^3} \left\langle \sum_{j=1}^{N_B} S_j^B \right\rangle \quad (6.2.3)$$

$$M_C = -\frac{2}{L^3} \left\langle \sum_{j=1}^{N_C} S_j^C \right\rangle \quad (6.2.4)$$

where N_B denotes the number of B ions $N_B = pL^3/2$, whilst N_C represents the number of C ions $N_C = (1-p)L^3/2$ on the same cubic lattice.

6.3 Monte Carlo Simulation Results

In this section we have given the numerical results obtained using by Monte Carlo simulation and we have discussed effects of the single-ion anisotropy on the magnetic properties of the three dimensional ferro-ferrimagnetic AB_pC_{1-p} ternary alloy. Numerical results and related discussions are presented follows.

In Fig. (6.2), the interaction ratio R dependence of critical temperature T_c and single-ion anisotropy D dependence of the critical ratio value R_c of the three dimensional ternary alloy model given by Hamiltonian (6.2.1) are presented. We have plotted the critical temperature versus interaction ratio R for different values of the concentration p and $D = 0$ in Fig. 6.2(a). As it can be seen from this figure, the critical temperature of the model linearly change dependent upon interaction ratio R and slope of the linear curves decrease for increasing value of the p . Furthermore, all linear curves cross each others at the critical R_c point. Linear curves present critical temperature of the model for the parameters p , R and D . At critical R_c all critical temperature values are equal for the different p values at fixed D value.

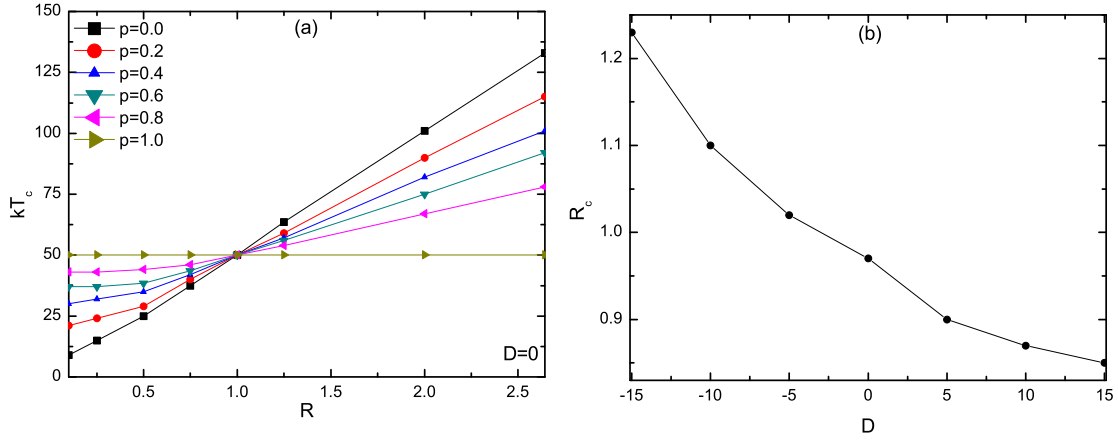


Figure 6.2 (a) Critical temperatures T_c vs interaction ratio R for $D = 0$ and several values of p concentration. (b) Critical interaction ratio R_c vs single ion anisotropy D .

We say that with variations of p from 0 to 1, the system is turned into from the ferrimagnetic mixed spin-3/2 and spin-5/2 binary system to the ferromagnetic mixed spin-3/2 and spin-2 binary system. The straight line with $p = 1$ corresponds to the critical temperatures of the mixed spin systems with $S^A = 3/2$, $S^B = 2$ which is not affected by changing of the ratio R . Throughout this line the critical temperature value of the mixed spin-3/2 and spin-2 Ising system is equal to the mixed spin-3/2 and spin-5/2 system at R_c . The critical value of interaction ratio obtained in this work is $R_c = 0.98$ for $D = 0$ which is close to another results obtained using by Monte Carlo simulation ($R_c = 0.83$) in ref (Dely et al., 2010) and a MFT work ($R_c = 0.8281$) in Ref (Dely & Bobák, 2007). To demonstrate and unify the dependence of the critical ratio R_c on the single-ion anisotropy D , we plotted interaction ratio R_c versus single-ion anisotropy D in Fig. 6.2(b) (Also, in Fig. 6.3, it is detailed shown that the critical temperature T_c and critical ratio value R_c dependence on single-ion anisotropy D). As it can be seen from this figure there is no symmetry in the R_c dependent upon D , moreover, the value of the critical interaction ratio R_c for the model unexpectedly decreases for increasing negative and positive D values as to nearly exponential form. The interesting behavior in Fig. 6.2(b) may probably emerge from trend of the contribution of the single-ion anisotropy into the critical temperature of the model for all different p values. We can conclude that the critical temperature of the model is mainly determined by interaction between spins, however when the single-ion anisotropy is added

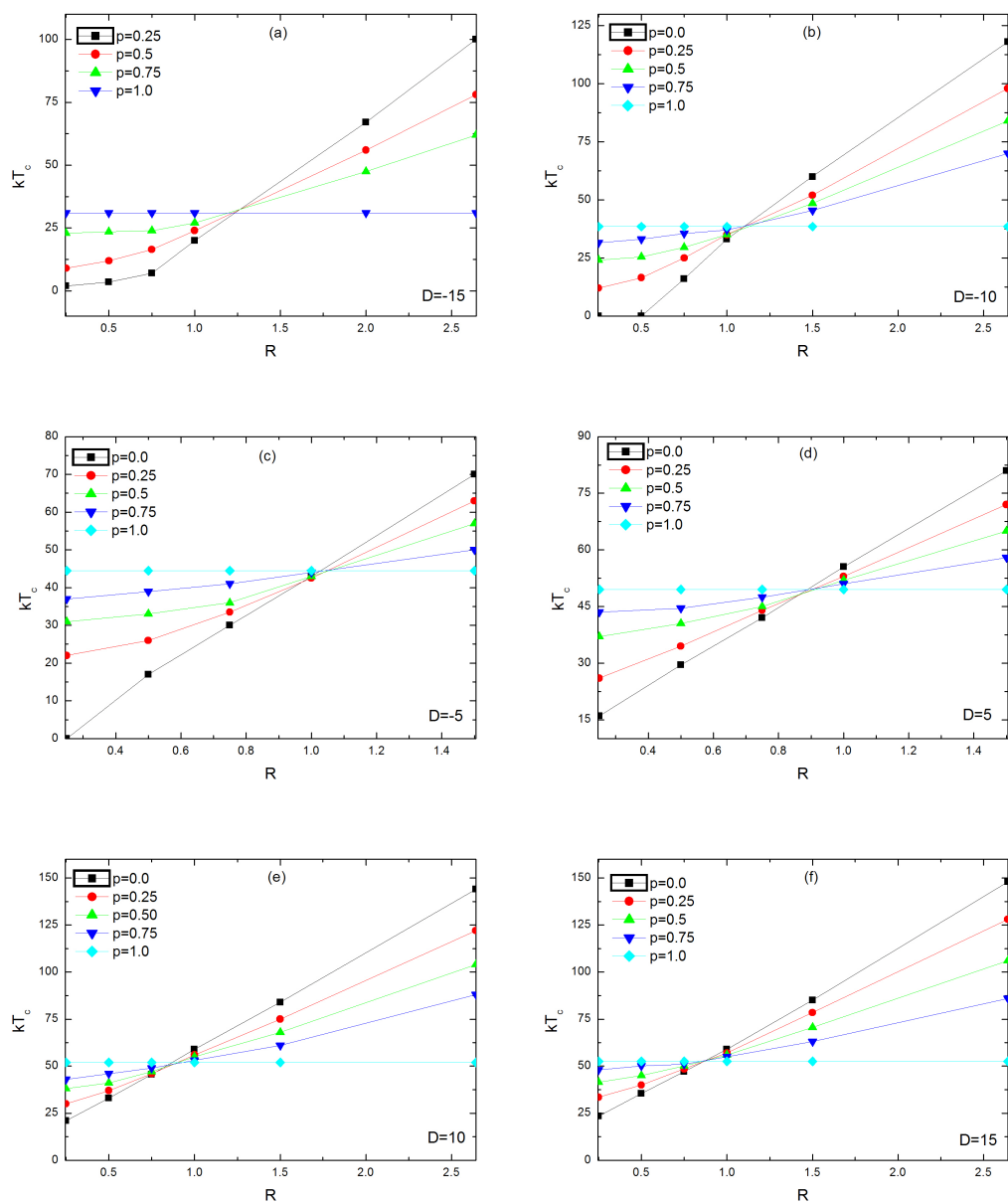


Figure 6.3 Single-ion anisotropy D dependence on the critical ratio value R_c of the three dimensional ternary alloy model.

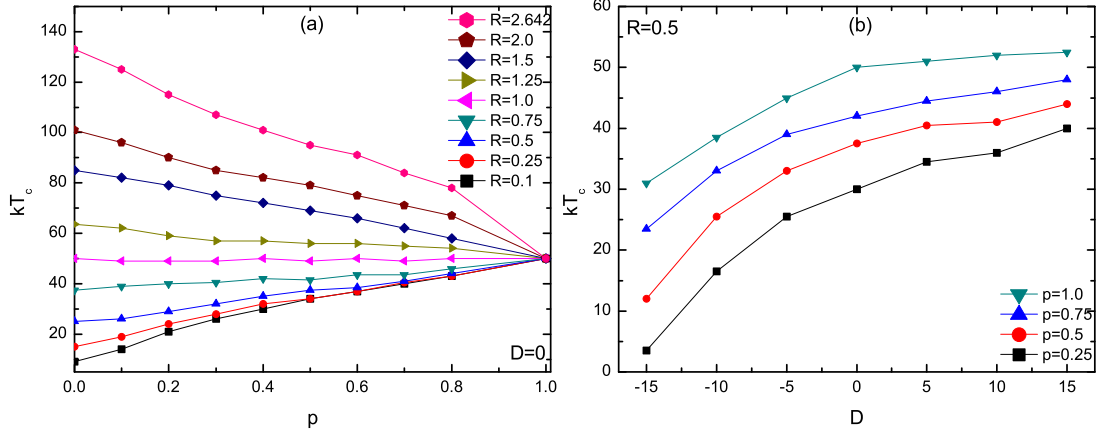


Figure 6.4 (a) Critical temperatures T_c vs concentration p for $D = 0$ and different values of interaction ratio $R = |J_{AC}|/|J_{AB}|$. (b) Critical temperatures T_c vs single ion anisotropy D for different p values.

into Hamiltonian, critical temperature curves being shift up or down for any p value. Therefore, the intersection point of curves for all p values slides to left or slides right systematically. Therefore, when D is decreased, interaction ratio R_c increases, even this increasing continues for decreasing D in negative region.

The concentration ratio p and single-ion anisotropy D dependence of critical temperature T_c of the three dimensional ternary alloy model given by Hamiltonian (6.2.1) are presented Figs. 6.4(a) and (b), respectively. As it can be seen from Fig. 6.4(a) that all critical temperature curves come together at $p = 1$ as linearly increasing for $R < R_c$ and as linearly decreasing for $R > R_c$. This figure shows that for the critical temperature values are independent from interaction value R at $p = 1$ in the case $D = 0$. Indeed, we know that the interaction ratio R determines the interaction type in the model Hamiltonian (6.2.1). Therefore, we can conclude from this figure that the system behaves as ferrimagnetic for $R < R_c$ and ferromagnetic for $R > R_c$. On the other hand, as it can be seen from Fig. (6.4b) the critical temperature of the system goes to a saturation value for different p when D value is increased from negative to positive values. The other important result is that the critical temperature curves being systematically shift dependent upon the concentration. These results are compatible with results in Fig. (6.2). When $p = 1$, the type of AB_pC_{1-p} ternary alloy

model reduces spin-3/2 and spin-2 mixed spin system. This binary system has been investigated in previous works (Bobák & Dely, 2007; Deviren et al., 2010; Espriella & Buendía, 2011) in which variation of critical temperature with single ion anisotropy is consistent with present work.

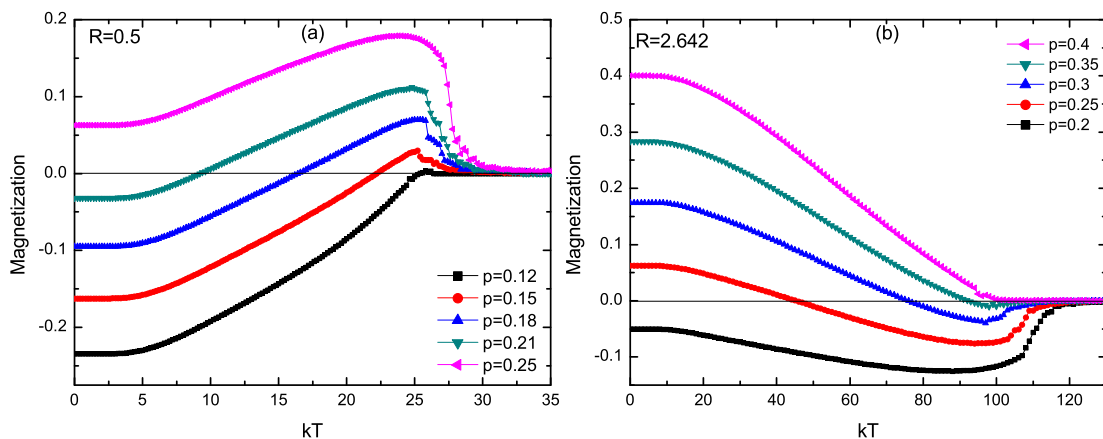


Figure 6.5 Total magnetization vs. temperature for several values of concentration p in absence of single ion anisotropy for (a) $R = 0.5$ and (b) $R = 2.642$.

In order to demonstrate the temperature dependence of the total magnetization M and to show critical points of the three dimensional ternary alloy model, magnetization profiles are given in Fig. (6.5) for various of p and fixed R values. As it can be seen that the critical and compensation temperature of the model appear depending on rate of concentration p and interaction ratio R . For example, for $R = 0.5$ in Fig. (6.5a) the compensation temperature points appear in the interval of $0.12 \leq p \leq 0.22$ at low temperature values. However, for $R = 2.642$ in Fig. (6.5b) only one compensation temperature point appear in the interval of $0.2 < p \leq 0.35$. Furthermore, Fig. (6.5a) shows that value of the compensation temperature decreases for increasing p , however, value of the critical temperature increases for the same p values in the case $|J_{AC}| < J_{AB}$. On the other hand, Fig. (6.5b) also shows that value of the compensation temperature increases for increasing p , however, value of the critical temperature decreases for the same p values unlike Fig. (6.5a) in the case $|J_{AC}| > J_{AB}$. As a result, we can conclude that total magnetization profile and the compensation and critical temperature points in this profile change dependent upon concentration p and interaction ratio R .

The behavior of total and sublattices magnetization is shown as a function of temperature at $R = 1.0$ and $p = 0.215$ fixed values in fig. 6.6(a). As seen from this figure, it can be observed that the magnitude of total magnetization is very small. When sublattices and total magnetization were plotted together, total magnetization curve is seen as on zero line. That is, this figure shows that, magnitude of spin-C ($5/2$) sublattice magnetization is approximately equal to other two magnitudes of sublattices spin-A ($3/2$) and spin-B (2) addition. So total magnetization curve was plotted on another graphic in fig. 6.6(b) in interval $0.212 \leq p \leq 0.225$. It can be seen from this figure, this system has multi-compensation phenomena when $p = 0.215$ and $R = 1.0$. For the small interval of $0.212 \leq p \leq 0.222$, the system has two compensation points. The same data were reported in (Dely, J., et. al. 2009). When this p region were plotted, with increasing of p value, the first compensation point decreases but the second compensation point increases with increasing of p value.

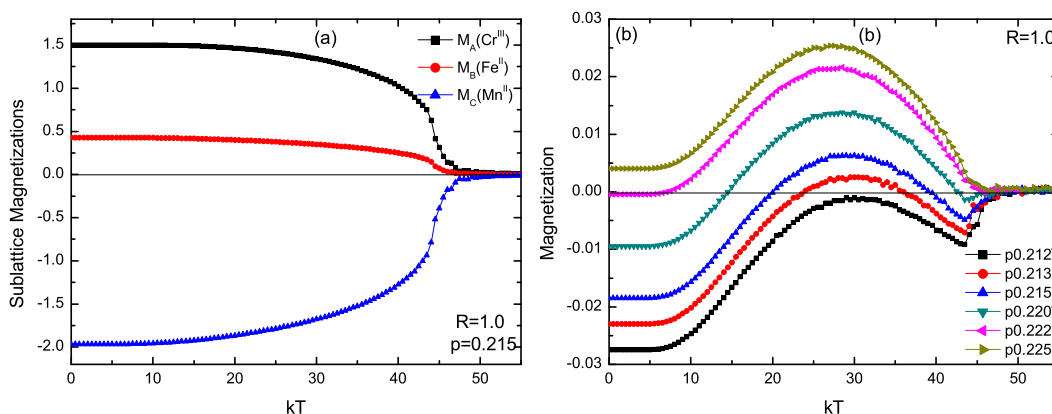


Figure 6.6 (a) Sublattice magnetizations vs. temperature for fixed $R = 1.0$ and $p = 0.215$ values. (b) Total magnetization vs. temperature at various value of concentration p .

We know that the Prussian blue analog $(\text{Fe}_p^{\text{II}}\text{Mn}_{1-p}^{\text{II}})_{1.5}[\text{Cr}^{\text{III}}(\text{CN})_6].n\text{H}_2\text{O}$ is a complex material. The concentration ratio p determines magnetic properties of this complex material. In the limit of $p = 0$, ternary alloy model $\text{AB}_p\text{C}_{1-p}$ reduces to relatively more simple AC model, however, in the limit of $p = 1$, it reduces to other simple AB model. It means that in the limit of $p = 0$, Fe atoms do not appear in the complex material, hence Prussian blue analog reduces to binary system $\text{Mn}_{1.5}^{\text{II}}[\text{Cr}^{\text{III}}(\text{CN})_6].n\text{H}_2\text{O}$. However, in the limit of $p = 1$, Mn atoms disappear in host material, hence it reduces

to another binary system $\text{Fe}^{\text{II}}_{1.5}[\text{Cr}^{\text{III}}(\text{CN})_6]_n\text{H}_2\text{O}$. It is expected that both binary systems shows different magnetic behavior. In order to see the behavior of total magnetization M of ternary alloy model in the limit values of concentration p dependent upon single-ion anisotropy, we have plotted the magnetization in the limit $p = 0$ and $p = 1$ in Fig. (6.7) for various single-ion anisotropy values D .

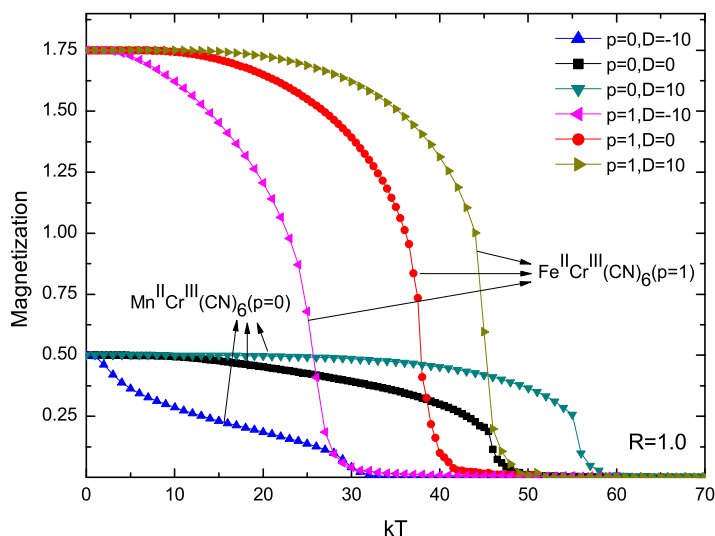


Figure 6.7 Magnetization vs. temperature for $\text{Mn}^{\text{II}}\text{Cr}^{\text{III}}(\text{CN})_6$ and $\text{Fe}^{\text{II}}\text{Cr}^{\text{III}}(\text{CN})_6$ for $R = 1.0$ and several values of anisotropy D .

As it can be seen from Fig. (6.7) that the $\text{AB}_p\text{C}_{1-p}$ model of the Prussian blue analog shows completely different magnetic behavior in the limit $p = 0$ and $p = 1$. First of all, critical temperature values and magnitude of the magnetization of both two systems are different for the same value of the anisotropy at fixed value of R . This figure clearly show that the critical temperature of each binary system increases for increasing single-ion anisotropy values. These results are compatible with the results in Fig. (6.4b).

It is known that the compensation temperature points of the ternary alloy model appear depending on p and R values. However we show in Figs. (6.5a) and (6.5b) that system may not has a compensation point for all combination of p and R . Since in this study we focus effects of the single-ion anisotropy on the system, we have discussed in the Fig. (6.8) the behavior of the compensation temperature depending on D for

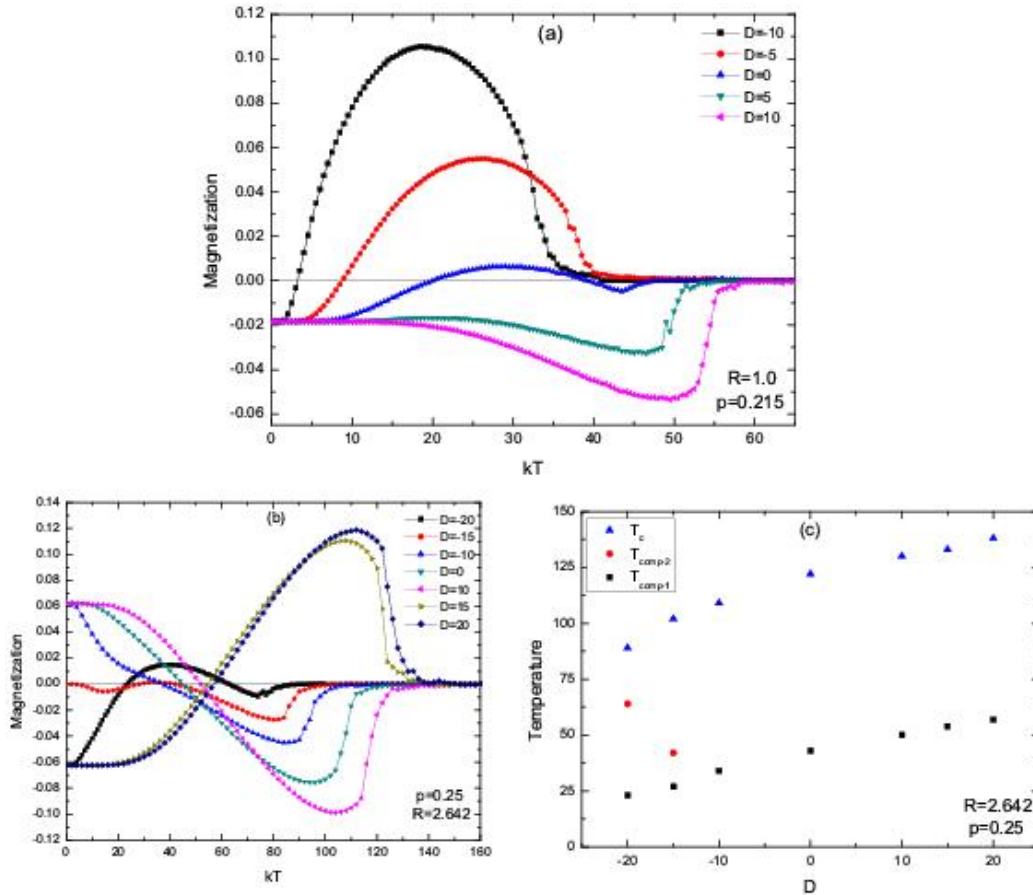


Figure 6.8 (a) Total magnetization vs. temperature for fixed $R = 1.0$, $p = 0.215$ and different D values. (b) Total magnetization vs. temperature for fixed $R = 2.642$, $p = 0.25$ and different D values. (c) Dependence of compensation and critical temperatures on single ion anisotropy for fixed $R = 2.642$, $p = 0.25$ values.

various values of R and p .

Therefore, in order to demonstrate the single-ion anisotropy dependence of the compensation temperature of the model, we have plotted total magnetization versus temperature for different p , R and D values in Figs. (6.8a) and (6.8b). As it can be seen from these figures that while p and R are responsible from appearing of different magnetization profile as in Figs. (6.8a) and (6.8b), then the single-ion anisotropy is responsible to determine values of the the compensation temperature points. Indeed, single-ion anisotropy in the Hamiltonian (6.2.1) affects the position of the compensation point as well as in the case of the critical temperature. In fact, one can see from Fig. (6.8c) that the compensation temperature increases for example at fixed $p = 0.25$ and $R = 2.642$ when the value of the D is increased. Similar behavior can be observed

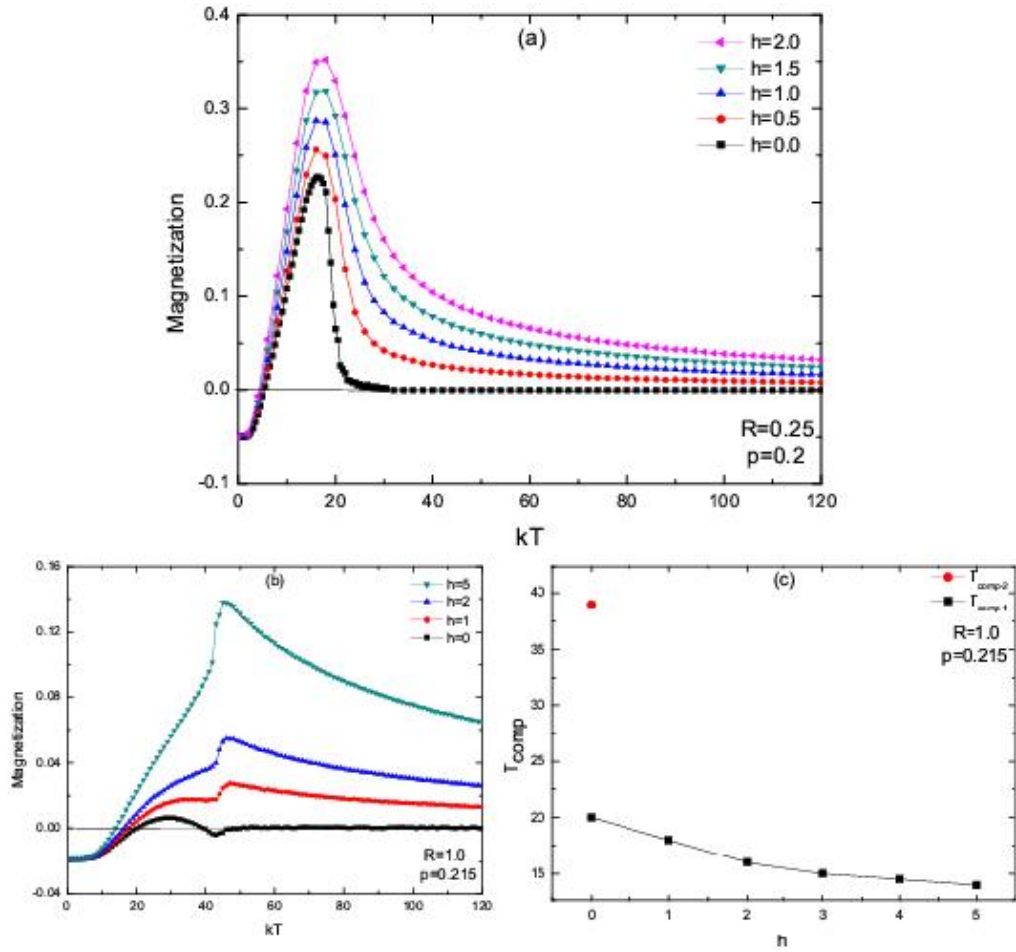


Figure 6.9 (a) Effects of magnetic field on compensation and critical temperatures for $R = 0.25$ and $p = 0.2$ values. (b) Effects of magnetic field on compensation and critical temperatures for $R = 1.0$ and $p = 0.215$ values. (c) Compensation point versus magnetic field for $R = 1.0$ and $p = 0.215$ values.

in the critical temperature for the same values of the parameter p and R . In Fig. (6.8c), behavior of the compensation (and the critical) temperature depending on single-ion anisotropy are consistent with the results in Figs. (6.2b), (6.4a) and (6.7). Figure (6.8) also shows that system has two compensation points for the some negative D values at fixed $p = 0.25$ and $R = 2.642$. In addition we note that the magnetic pole inversion can be observed in this Prussian blue analog as seen in Fig.(6.5b) dependent upon some parameter values. For example this inversion appears for $p = 0.25$ and $R = 2.642$ values when around $D > 13.2$.

Finally we have also considered external magnetic field on the critical behavior of the three dimensional ternary model in Fig. (6.9) for arbitrary fixed values of p and

R in the case of $D = 0$. As expected that the values of the critical temperature for $p = 0.2$ and $R = 0.25$ in Fig. (6.9a) and for $p = 0.215$ and $R = 1.0$ in Fig. (6.9b) increase for increasing values of the external field. Besides, critical temperature point disappear in the temperature axis for large value of the magnetic field as in Fig. (6.9b). Similar behavior has been found in ref. (Yusuf et al., 2009). However, unlike critical temperature, values of the the compensation temperature points decrease for increasing magnetic fields in both figure for different values of the parameters. Furthermore, multi-compensation point does not appear when the magnetic field is applied. This behavior is presented in Fig.(6.9c) for $p = 0.215$ and $R = 1.0$.

CHAPTER EIGHT

CONCLUSION

In this thesis enclosure, three different ferrimagnetic mixed Ising model is investigated by using Monte Carlo simulation method. These different three model are presented in fifth, sixth and seventh chapter. In first study, it is studied the compensation and critical temperatures of the mixed spin-1 and spin-1/2 randomly diluted two dimensional ferrimagnetic lattice with Monte Carlo simulation technique. It is investigated that the effect of the non magnetic atoms on the thermal and magnetic behavior of the mixed spin system. It is found that the change of the thermal and magnetic behaviors are clearly depend on the number of non magnetic atoms in the lattice as seen drawn figures. Especially, one can see that both of the compensation and the critical temperatures linearly decrease with increasing number of non magnetic atoms. Significant results in this study are assumed to be meaningful from technological point of view. Finally we state that the nearest neighbor interaction J_1 does not play a role on the compensation and the critical temperatures as known from previous theoretical studies. However, unlike the nearest neighbor interaction, we see in simulations that crystal field D and the next nearest neighbor interactions J_4 play an effective role on them. The results of this study show that dilution plays a significant role on the critical and compensation points of a two dimensional mixed spin-1/2 and spin-1 system. On the other hand, these numerical results indicate that the compensation temperature of the real ferrimagnetic spin systems can be changed by diluting the lattice with non-magnetic atoms, in order to obtain desired compensation temperature.

In second study, it is investigated that the compensation temperature of the mixed ferro-ferrimagnetic AB_pC_{1-p} ternary alloy composed of three different Ising spins $S^A = 3/2$, $S^B = 1$ and $S^C = 5/2$ in the presence of next nearest neighbor interaction J_{AA} between A ions by using Monte Carlo simulation method in cubic lattice. The spin values in this lattice corresponds to the Prussian blue analog of the type $(Ni_p^{II}Mn_{1-p}^{II})_{1.5}[Cr^{III}(CN)_6].nH_2O$. It have been observed that the behavior of the critical temperature and the existence of compensation points strongly depend on interaction and concentration parameters. Particularly, it have been found that the critical temperature of the model is independent on concentration of different types of spins at

a critical R_c value and the model has one or two compensation temperature points in a certain range of values of the concentration of the different spins. It is concluded that magnetic properties of the system AB_pC_{1-p} can be controlled by changing the relative concentration of the different species of ions. As a result, we would like to stress that these theoretical results can be very useful for designing molecular magnets in experimental studies since the existence of compensation in the ternary alloy AB_pC_{1-p} that can be setup by adjusting the proportion of compounds.

In third study, by employing Monte Carlo simulation method to three dimensional ferro-ferrimagnetic AB_pC_{1-p} ternary alloy model we have investigated magnetic properties and effects of the single-ion anisotropy on the magnetic properties of the Prussian blue analog $(Fe_p^{II}Mn_{1-p}^{II})_{1.5}[Cr^{III}(CN)_6].nH_2O$ consisting of three different Ising spins $S_A = 3/2$, $S_B = 2$ and $S_C = 5/2$. We have found that the critical temperature T_c of the model linearly changes dependent upon interaction ratio R for any concentration p value, and critical interaction ratio R_c decreases for increasing D values. On the other hand, we have shown that the critical and compensation temperature of the model smoothly increase for increasing D values. In addition, we have demonstrated that magnetic pole inversion can appear and compensation temperature T_{comp} decrease for increasing external magnetic dependent upon some values of the Hamiltonian parameters. As a result, we have concluded that single-ion anisotropy may play important role as a control parameter like mixing ratio p to arrange the critical and compensation temperature points of the Prussian blue analog $(Fe_p^{II}Mn_{1-p}^{II})_{1.5}[Cr^{III}(CN)_6].nH_2O$.

REFERENCES

- Albayrak, E. (2011). The mixed-spin ternary alloy in the form of AB_pC_{1-p} on the Bethe lattice. *J. Magn. Magn. Mater.*, 323, 992.
- Alex, M., Shono, K., Kuroda, S., Koshino, N. & Ogawa, S. (1990). Ce-substituted Garnet Media for Magneto-optic Recording. *J. Appl. Phys.*, 67, 4432-4434.
- Balcerzak, T., Gzik-Szumiata, M., Bobak, A., Jascur, M. & Horvath, D. (2002). Theoretical Studies of the Ising Bilayer System Consisting of Spin-1/2 and Spin-1 Atoms. *Czech. J. Phys.*, 52, 113-118.
- Benayad, N., Klümper, A., Zittartz, J. & Benyoussef, A. (1989). Two-dimensional Mixed Spin Ising Models with Bond-dilution and Random $\pm J$ interactions. *Z. Phys. B*, 77(2), 339-341.
- Benyoussef, A., El Kenz, A. & Kaneyoshi, T. (1994). Diluted Mixed Spin-1 and Spin-1/2 Honeycomb Lattice. *J. Magn. Magn. Mater.*, 131(1-2), 173-178.
- Benyoussef, A., El Kenz, A. & Kaneyoshi, T. (1994). Tricritical Behavior in Diluted Mixed Spin-1 and Spin-1/2 on Square Lattice. *J. Magn. Magn. Mater.*, 131(1-2), 179-182.
- Bilderbeek, M. (2001). *A study of the physical properties of high density Magneto-Optical media Why does MAMMOS ("Magnetically Amplified Magneto-Optical System") work?*, Master's Thesis, University of Nijmegen, Netherlands.
- Binder, K.(Ed.) (1979). *Monte Carlo Methods in Statistical Physics*, Berlin:Springer.
- Blundell, S. (2001). *Magnetism in Condensed Matter*. Oxford University Press.
- Blundell, S. J. (2007). Molecular Magnets. *Contemporary Physics*, 48, 275-290.
- Bobák, A., Abubrig O. F., ve Horváth, D. (2002). Magnetic properties of a mixed ferro-ferrimagnetic ternary alloy. *Physica A*, 312(1-2),187-207.
- Bobák, A., Abubrig, F. O. ve Balcerzak, T. (2003). Multicritical points in the mixed ferromagnetic-ferrimagnetic ternary alloy with a single-ion anisotropy. *Physical Review B*, 68(22), 224405(1-9).

- Bobák, A. & Dely, J., (2007). Phase Transitions and Multicritical Points in the Mixed Spin-3/2 and Spin-2 Ising System with a single-ion Anisotropy. *J. Magn. Magn. Mater.*, 310, 1419-1421.
- Bobák, A. & Jascur, M. (1995). Ferrimagnetism in Diluted Mixed Ising Spin Systems. *Phys. Rev B*, 51, 11533-11537.
- Bobák, A., Dely J. (2004). The effect of a single-ion anisotropy on the phase diagram of a mixed ferro-ferrimagnetic ternary alloy. *Physica A*, 341, 281-298.
- Brush, S. G. (1967). History of Lenz-Ising Model. *Revs. Mod. Phys.*, 39 (4), 883-893.
- Buendia, G. M. & Machado, E. (2000). Magnetic Behavior of a mixed Ising Ferrimagnetic Model in an Oscillating Magnetic Field. *Phys. Rev. B*, 61, 14686.
- Buenda, G. M. & Villarroel, J. E. (2007). Compensation temperatures of mixed ferro-ferrimagnetic ternary alloys. *J. Magn. and Magn. Mater.*, 310(2), e495-e497.
- Buendia G. M. & Novotny M. A. (1997). Numerical Study of a Mixed Ising Ferrimagnetic System. *J. Phys. Condens. Matter*, 9, 5951.
- Buendia, G. M., Machado, E. & Novotny, M. A. (1998). Compensation Temperature of a Mixed Ising Ferrimagnetic Model in the Presence of External Magnetic Fields. *MRS Proceedings*, 517, 361-366.
- Buendía, G. M. & Liendo, J. A. (1997). Monte Carlo Simulation of a Mixed Spin-2 and Spin-1/2 Ising Ferrimagnetic System. *J. Phys.: Condens. Matter*, 9, 5439-5448.
- Buschmann, W.E., Paulson, S. C., Wynn, C. M., Girtu, M. A., Epstein, A. J., White, H. S. & Miller, J. S. (1997). Magnetic Field Induced Reversed(Negative) Magnetization for Electrochemically Deposited $T_c = 260\text{K}$ Oxidized Films of Chromium Cyanide Magnets. *Adv. Mater.*, 9(8), 645-647.
- Carling, S.G., ve Day, P., (2001). A Monte Carlo study of honeycomb lattice ferrimagnets. *Polyhedron*, 20, 1525.
- Dakhama, A. & Benayad, N. (2000). On the Existence of Compensation Temperature in 2d Mixed-spin Ising Ferrimagnets: an Exactly Solvable Model. *J. Magn. Magn. Mater.*, 213, 117-125.

- Day, P. & Underhill, A.E., (1999). Molecular-based Magnets: Setting the Scene. *Philos. Trans. Soc. Lond. A*, 357, 2851-2853.
- Dely, J. ve Bobk, A. (2007). Magnetic properties of the ternary alloy with a structure of Prussian blue analogs. *Physica B*, 388(1-2), 49-58.
- Decurtins, S., Schmalle, H.W., Oswald, H. R., Linden, A., Ensling, J., Gütlich, P. & Hauser, A. (1994). A Polymeric Two-Dimensional Mixed-Metal Network. Crystal Structure and Magnetic Properties of $\{[P(Ph)_4][MnCr(ox)_3]\}$. *Inorg. Chim. Acta*, 216(1-2), 65-73.
- Dely, J. & Bobk, A. (2007). Magnetic properties of the ternary alloy with a structure of Prussian blue analogs. *Physica B*, 388(1-2), 49-58.
- Dely, J., Bobák, A, Zukovic, M., (2009). Compensation temperatures and magnetic susceptibility of a mixed ferro-ferrimagnetic ternary alloy. *Phys. Lett. A*, 373, 3197.
- Dely, J., Bobk, A., Zukovic, M., (2010). Critical temperaure of a mixed ferro-ferrimagnetic ternary alloy. *Journal of Physics : Conference Series*, 200, 022005.
- Dely, J. ve Bobak, A., (2006). Phase diagrams of the ternary alloy with a single-ion anisotropy in the mean-field approximation. *J. Magn. Magn. Mater.*, 305, 464.
- Deviren, B., Canko, O., Keskin, M., (2009). Magnetic properties of the mixed ferri-magnetic ternary system with a single-ion anisotropy on the Bethe lattice. *J. Magn. Magn. Mater.*, 321, 1231.
- Deviren, B., Kantar, E. & Keskin, M. (2010). Magnetic Properties of a Mixed Spin-3/2 and Spin-2 Ising Ferrimagnetic System within the Effective-Field Theory. *Journal of the Korean Physical Society*, 56(6), 1738-1747.
- Drillon, M., Coronado, E., Beltran, D. & Georges, R. (1983). Classical Treatment of a Heisenberg Linear Chain with Spin Alternation: Application to the MnNi(EDTA)-6H₂O Complex. *J. Chem. Phys.*, 79, 449-453.
- Entley, W. R. & Girolami, G. S. (1994). New Three-dimensional Ferrimagnetic Materials: $K_2Mn[Mn(CN)_6]$, $Mn_3[Mn(CN)_6]_2 \cdot 12H_2O$ and $CsMn[Mn(CN)_6] \cdot 1/2H_2O$. *Inorg. Chem.*, 33, 5165-5166.

- Entley, W. R. & Girolami, G.S., (1995). High-Temperature Molecular Magnets Based on Cyanovadate Building Blocks: Spontaneous Magnetization at 230 K. *Science*, 268, 397.
- Erkinger, H. M. (2000). A new cluster algorithm for the Ising model, Diploma Thesis, Graz University of Technology.
- Espriella, N. D. & Buendía, G. M. (2011). Magnetic Behavior of a Mixed Ising 3/2 and 5/2 Spin Model. *J. Phys:Condens. Matter.*, 23, 176003(1-7).
- Etzkorn, S. J. (2003). *Magnetic Relaxation in Organic-Based Magnets*. PhD thesis, The Ohio State University.
- Feiguin, A.E. (2012). *Modern Computational Methods in Solids*, <http://physics.uwyo.edu/~adrian/phys5870>, pg.76.
- Ferlay, S., Mallah, T., Ouahès, R., Veillet, P. & Verdaguer, M. (1995). A room-temperature organometallic magnet based on Prussian blue. *Nature*, 378, 701.
- Gadet, V., Mallah, T., Castro, I., Verdaguer, M. & Veillet, P. (1992). High- T_c Molecular-based Magnets: a Ferromagnetic Bimetallic Chromium(III)-Nickel(II) Cyanide with $T_c = 90\text{K}$. *J. Am. Chem. Soc.*, 114(23), 9213-9214.
- Gould, H. & Tobochnik, J. (1996). *An Introduction to Computer Simulation Methods*. Addison Wesley Publishing Company, pg.551.
- Güdel, H. U., Stucki, H. & Ludi, A. (1973). The Crystal Structure of Manganese(II) Hexacyanochromate(III), $\text{Mn}_3[\text{Cr}(\text{CN})_6]_2 \cdot x\text{H}_2\text{O}$. *Inorg. Chim. Acta*, 7, 121-124.
- Hansen, P. (1987). Thermomagnetic Switching in Amorphous Rare-Earth Transition Metal Alloys. *J. Appl. Phys.*, 62, 216.
- Heisenberg, W. (1928). Zur Theorie des Ferromagnetismus. *Z. Physik*, 49, 619.
- Hernando, A. & Kulik, T. (1994). Exchange Interactions Through Amorphous Paramagnetic Layers in Ferromagnetic Nanocrystals. *Phys. Rev. B*, 49, 7064-7067.
- Hjorth-Jensen, M. (2007). *Computational Physics*. University of Oslo.

- Holmes, S. M. & Girolami, G. S. (1999). Sol-Gel Synthesis of $KV^{II}[Cr^{III}(CN)_6] \cdot 2H_2O$: A Crystalline Molecule-based Magnet with a Magnetic Ordering Temperature Above 100 °C. *J. Am. Chem. Soc.*, *121*, 5593.
- Ising, E. (1925). Report on the Theory of Ferromagnetism. *Z. Physik*, *31*, 253.
- Iwashita, T. & Uryû, N. (1984). The Curie Temperature of the Two-Dimensional Quadratic Ising Ferromagnet with Mixed Spins of $S = 1/2$ and $S = 1$. *J. Phys. Soc. Jpn.*, *53* 721-728.
- Jäckel, P. & Platen, E. (2002). *EQF13/26:Monte Carlo Simulation*, www.jaeckel.org.
- Kac, M & Ward, J. C. (1952). A Combinatorial Solution of the Two-Dimensional Ising Model. *Phys. Rev.*, *88*, 1332-1337.
- Kahn, O. (1993). *Molecular Magnetism*, VCH, New York.
- Kahn O. (1987). Magnetism of the Heteropolymetallic Systems. *Struct Bonding*, *68*, 89.
- Kahn M. L., Sutter J. P., Golhen S., Guionneau P., Ouahab L., Kahn O. & Chasseau D. (2000). Systemic Investigation of the Nature of the Coupling between a Ln(III) Ion (Ln=Ce(III) to Dy(III)) and Its Aminoxly Radical Ligands. *J. Am. Chem. Soc.*, *122*, 3413.
- Kaneyoshi, T. (1987). Curie Temperatures and Tricritical Points in Mixed Ising Ferromagnetic Systems. *J. Phys. Soc. Jpn.*, *56*, 2675-2680.
- Kaneyoshi, T. (1988). Phase Transition of the Mixed Spin System with a Random Crystal Field. *Physica A*, *153*, 556-566.
- Kaneyoshi, T. (1989). A Compensation Temperature Induced by a Crystal-Field Interaction in a Ferrimagnetic Mixed Ising System. *Solid State Commun.*, *70*, 975-977.
- Kaneyoshi, T. (1990). Magnetic Properties of a Mixed Spin Ising Model with Random Nearest-Neighbor Interactions. *J. Magn. Magn. Mater.*, *92*, 59-67.
- Kaneyoshi, T. & Chen, J. C. (1991). Mean-Field Analysis of a Ferrimagnetic Mixed Spin System. *J. Magn. Magn. Mater.*, *98*, 201-204.

- Kaneyoshi, T. (1995). Phase Diagrams and Tricritical Behavior of a Diluted Mixed Spin Ising Model in a Random Field. *J. Magn. Magn. Mater.*, 151, 45-53.
- Kırs-Çam, E. ve Aydın, E., (2010). Compensation temperature of 3d mixed ferroferrimagnetic ternary alloy. *J. Magn. Magn. Mater.*, 322, 1706.
- Kittel, C. (1996). *Introduction to Solid State Physics*. John Wiley and Sons, Inc., 7th edition ed.
- Khurshudov, A. (2001). *Essential Guide to Computer Data Storage: From Floppy to DVD*. United States of America: Prentice Hall, Inc.
- Klenze, R., Kanellakopoulos, B., Trageser, G. & Eysel, H. H. (1980). Manganese Hexacyanomanganate: Magnetic Interactions via Cyanide in a Mixed Valence Prussian Blue Type Compound. *J. Chem. Phys.*, 72(11), 5819-5828.
- Kramers H. A. & Wannier, G.H. (1941). Statistics of the Two-Dimensional Ferromagnet Part I. *Phys. Rev.*, 60, 252-262.
- Kubo, R. & Obata, Y. (1956). Note on the Paramagnetic Susceptibility and the Gyromagnetic Ratio in Metals. *J. Phys. Soc. Jpn*, 11, 547-550.
- Landau, D. P., Mon, K. K. & Schuttler, H. B. (1994). (Eds.) *Computer Simulations in Condensed Matter Physics VII*. Berlin: Springer, pg.223.
- Le Blanc M., (2010). *MC simulations of inter and intra grain spin structure of Ising and Heisenberg Models*. MSc Thesis, Memorial University of Newfoundland.
- Lee, T. (2010). *Monte Carlo simulations of Structural Phase transitions in Metal and Alloys*, PhD Thesis, Brown University, Rhode Island.
- Leuenberger, M. & Loss, D. (2001). Quantum Computing in Molecular Magnets. *Nature* (London), 410, 789-793.
- Lévy, L. -P. (2000). *Magnetism and Superconductivity*. Berlin: Springer.
- Li, Z. Y. & Kaneyoshi, T. (1988). Magnetic Properties of Amorphous Mixed Alloys with Low Dimensionalities. *Phys. Rev. B*, 37, 7785-7792.
- Ludi, A. (1981). Prussian blue, an inorganic evergreen. *J. Chem. Educ.*, 58(12), 1013.

- Lummen, T. T. A, Gengler, R. Y. N, Rudolf P. & Lucitani F. (2008). Bulk vs. Surface Switching in the Mn-Fe Prussian Blue Analogue. *Journal of Physical Chemistry*, *112*, 14158-14168.
- Mallah, T., Thiébaud, S., Verdaguer, M., Veillet, P., (1993). High-Tc Molecular-based Magnets: Ferrimagnetic Mixed-Valance Chromium(III)-Chromium(II) Cyanides with Tc at 240 and 190 Kelvin. *Science*, *262*, 1554.
- Mansuripur, M. (1987). Magnetization Reversal Coersivity and the Process of Thermomagnetic Recording in Thin Films of Amorphous Rare Earth-Transition Metal Alloys. *J. Appl. Phys.*, *61*, 1580-1588.
- Metropolis, N., & Ulam, S. (1949). The Monte Carlo Method. *Journal of the American Statistical Association*, *44*, 335-341.
- Metropolis, N. (1987). The Beginning of the Monte Carlo Method, *Los Alamos Science Special Issue*.
- Metropolis, N., Rosenbluth, A.W., Rosenbluth, Teller, M. N. & Teller, M. (1953). Equation of State Calculations by Fast Computing Machines, *Journal of Chemical Physics*, *21*, 1087-1091.
- Meyer, P. J. G. (2000). *Computational Studies of Pure and Diluted Spin Models*. MSc Thesis, University of Derby.
- Miller J. S., Epstein A.J. & Reiff, W. M. (1988). Molecular/Organic Ferromagnets. *Science*, *240*, 40.
- Miller J. S. & Epstein A.J. (2000). Molecule-Based Magnets-An Overview, *Mrs Bulletin*, November.
- Miller, J. S., Drillon, M.(2005). *Magnetism: Molecules to Materials V ed*. Weinheim: WILEY-VCH., chapter 9, pp 283-346.
- Miller, J. S. & Epstein, A.J. (1994). *Angew. Chem. Int. Ed. Engl.*, *33*, 385.
- Mon K. K & Schuttler H. B. (1994). *Computer Simulations in Condensed Matter Physics*. Berlin: Springer, p.223.

- Multigner, M., Läkamp, S., Pourroy, G., Hernando, A. & Valenzuela, R. (1996). Co-doped Ferrite Single Domains and the Effect of Metallic Nanoinclusions. *Appl. Phys. Lett.*, *69*, 2761-2763.
- Néel L. (1948). Magnetic Properties of Ferrites: Ferrimagnetism and Antiferromagnetism. *Ann. Phys. Paris*, *3*, 137.
- Nelson, K. J. (2007). *Nonaqueous synthesis of Prussian Blue Structured Materials*, PhD thesis, University of Utah.
- Newman, M. E. J. & Barkema, G. T. (1999). *Monte Carlo Methods in Statistical Physics*. Oxford: Clarendon Press.
- Ohkoshi, S., Iyoda, T., Fujishima, A. & Hashimoto, K. (1997). Magnetic properties of mixed ferro-ferrimagnets composed of Prussian blue analogs. *Physical Review B*, *56*(18), 11642-11652.
- Ohkoshi, S., Yorozu, S., Sato, O., Iyoda, T., Fujishima, A., Hashimoto, K., (1997). Photoinduced magnetic pole inversion in a Ferro-ferrimagnet: $(Fe^{II}_{0.40}Mn^{II}_{0.60})_{1.5}Cr^{III}(CN)_6$. *Appl. Phys. Lett.*, *70*, 1040.
- Ohkoshi, S. & Hashimoto, K. (1999). Theoretical treatment of the mixed ferro-ferrimagnets composed of ternary-metal Prussian blue analogs in a paramagnetic region. *Physical Review B*, *60*(18) 12820-12825.
- Ohkoshi, S. & Hashimoto, K., (1999). Design of a Novel Magnet Exhibiting Photoinduced Magnetic Pole Inversion Based on Molecular Field Theory. *J. Am. Chem. Soc.*, *121*, 10591.
- Ohkoshi, S., Abe, Y., Fujishima, A. ve Hashimoto, K. (1999). Design and Preparation of a Novel Magnet Exhibiting Two Compensation Temperatures Based on Molecular Field Theory. *Physical Review Letters*, *82*(6), 1285-1288.
- Ohkoshi, S., Hozumi, T. & Hashimoto, K. (2001). Design and preparation of a bulk magnet exhibiting an inverted hysteresis loop. *Physical Review B*, *64*(13), 132404(1-4).
- Onsager, L. (1944). Crystal Statistics. I. A Two-Dimensional Model with an Order-Disorder Transition, *Phys. Rev.*, *65*, 117-149.

- Pejakovic, D. A., Manson, J. L., Miller, J. S., Eipstein, A. J., (2001). Manipulating Magnets With Light: Photoinduced Magnetism of Prussian Blue Analogs. *Current Appl. Phys.*, 1, 15.
- Quadros, S. G. A. & Salinas, S. R. (1994). Renormalization-group Calculations for a Mixed-Spin Ising Model. *Physica A*, 206, 479-496.
- Richey, M. (2010). The evolution of Markov chain Monte carlo methods, *The American Mathematical Monthly*, vol.117, No.5 ,pp.383-413
- Sato, O., Iyoda, T., Fujishima, A. & Hashimoto, K. (1996). Electrochemically Tunable Magnetic Phase Transition in a High- T_c Chromium Cyanide Thin Film. *Science*, 271, 49-51.
- Sato, O. , Iyoda, T., Fujishima, A. & Hashimoto, K., (1996). Photoinduced Magnetization of a Cobalt-Iron Cyanide. *Science*, 272, 704.
- Schofield, S. L. & Bowers, R. G. (1980). Renormalisation Group Calculations on a Mixed-Spin System in Two Dimensions. *J. Phys. A: Math. Gen.*, 13, 3697-3706.
- Shi-Lei, Y. (2002). Magnetic Ordering of the Band-Diluted Two Dimensional Mixed Spin Ising Model. *Chin. Phys.*, 11, 1066-1072.
- Shum W. W. (2008). *Magnetic Interactions in Novel Molecule-Based Materials*. PhD thesis, University of Utah.
- Siqueira, A.F. & Fittipaldi, I. P. (1986). Thermodynamical Properties of a Mixed Ising Ferromagnet System. *J. Magn. Magn. Mater.*, 54, 678-680.
- Tanaka, F., Tanaka, S. & Imamura, N. (1987). Magneto-Optical Recording Characteristic of TbFeCo Media by Magnetic Field Modulation Method. *Jpn. J. Appl. Phys.*, 26(1), 231-235.
- Tamaki H., Zhong Z. J., Matsumoto N., Kida S., Koikawa M., Achiwa N., Hashimoto Y. & Okawa H. (1992). Design of Metal-Complex Magnets. Syntheses and Magnetic Properties of Mixed-Metal Assemblies $\{NBu_4[MCr(ox)_3]\}_x$ (NBu_4^+ = Tetra(n-butyl) Ammonium Ion; ox^{2-} = OxalatoIon; Mn^{2+} , Fe^{2+} , Co^{2+} , Ni^{2+} , Cu^{2+} , Zn^{2+}). *J. Am. Chem. Soc.*, 114, 6974-6679.

- Tucker, J. W., Balcerzak, T., Gzik, M. & Sukiennicki, A. (1998). Phase Diagram of a Spin-1 Magnetic Bilayer by Cluster Variational Theory: Exact Results for a BEG Model on a Bethe Lattice with Five Fold Coordination. *J. Magn. Magn. Mater.*, 187, 381-392.
- Vilfan, I., *Lecture Notes on Statistical Mechanics*, The Abdus Salam ICTP, Trieste.
- Yosida, K. (1998). *Theory of Magnetism*, Springer.
- Yousif, B. Y. & Bowers, R. G. (1984). High-Temperature Series Expansion Studies of Mixed Spin-1/2-Spin-S Ising Models. *J. Phys. A: Math. Gen.*, 17, 3389-3394.
- Yusuf, S.M., Kumar, A., Yakhmi, J. V., (2009). Temperature -and magnetic-field - controlled magnetic pole reversal in a molecular magnetic compound. *Appl. Phys. Lett.*, 95, 182506.
- Watanabe, H. (1966). *Operator methods in ligand field theory*. Prentice-Hall.
- Weinzierl, S. (2000). *Introduction to Monte Carlo Methods*. arXiv:hep-ph/0006269v1.
- Werde, F. (2007). *Simulation of models on CUDA*, pg. 11.
- Xin, Z. H., Wei, G. Z. & Liu, T. S. (1997). Properties of Diluted Mixing Ising Spin Ferrimagnetic System. *Phys. Stat. Sol.(b)*, 199(1), 205-212.
- Xin, Z. H., Wei, G. Z. & Liu, T. S. (1997). Magnetic Properties of Ground State in Diluted Mixed-Spin Ising Ferrimagnetic Systems. *J. Magn. Magn. Mater.*, 176(2-3), 206-212.
- Xin, Z. H., Wei, G. Z. & Liu, T. S. (1998). Phase Diagrams of Diluted Mixed Spin Ising Model on Square Lattice. *Phys. Stat. Sol.(b)*, 210(1), 229-235.
- Xin, Z. H., Wei, G. Z. & Liu, T.S. (1998). Thermodynamics of Diluted Mixed Spin Ising Systems. *Phys. Stat. Sol.(b)*, 209, 145-151.
- Xin, Z. H., Wei, G. Z. & Liu, T. S. (1998). Phase diagram of the diluted mixed-spin Ising model on a honeycomb lattice. *Physica A*, 248, 442-453.

Zhang, G. M. & Yang, C. Z. (1993). Monte Carlo Study of the Two-Dimensional Quadratic Ising Ferromagnet with Spins $S = 1/2$ and $S = 1$ with Crystal-Field Interactions. *Phys. Rev. B*, 48, 9452-9455.

Žukovič, M. ve Bobák, A., (2009). Critical and Compensation phenomena in a mixed-spin ternary alloy: A Monte Carlo study. *J. Magn. Magn. Mater.*, 322, 2868.